

1-1-2012

Spray characterization of flex-fuel gasoline di injectors and spray interaction with charge motion in a variable valve actuation engine

Atsushi Matsumoto
Wayne State University,

Follow this and additional works at: http://digitalcommons.wayne.edu/oa_dissertations

Recommended Citation

Matsumoto, Atsushi, "Spray characterization of flex-fuel gasoline di injectors and spray interaction with charge motion in a variable valve actuation engine" (2012). *Wayne State University Dissertations*. Paper 457.

This Open Access Dissertation is brought to you for free and open access by DigitalCommons@WayneState. It has been accepted for inclusion in Wayne State University Dissertations by an authorized administrator of DigitalCommons@WayneState.

**SPRAY CHARACTERIZATION OF FLEX-FUEL GASOLINE DI INJECTORS
AND SPRAY INTERACTION WITH CHARGE MOTION
IN A VARIABLE VALVE ACTUATION ENGINE**

by

ATSUSHI MATSUMOTO

DISSERTATION

Submitted to the Graduate School

of Wayne State University,

Detroit, Michigan

in partial fulfillment for the requirements

for the degree of

DOCTOR OF PHILOSOPHY

2012

MAJOR: MECHANICAL ENGINEERING

Approved by:

Advisor

Date

ACKNOWLEDGEMENTS

I am deeply thankful to my academic advisor, Dr. Ming-Chia Lai, whose support and guidance were essential for the progress of the study. I would also like to thank my other committee members, Dr. Trilochan Singh, Dr. Naeim Henein, and Dr. Tze-Chien Sun for their invaluable contributions. And I appreciate the help and advice from Mr. Eugene Snowden, Mr. Marvin Santure and other members of the Machine Shop. I would like to express my gratitude to Mr. Wayne Moore at Delphi Advanced Powertrain for his cooperation to the project. Lastly, I offer my regards to the lab colleagues who worked together throughout the research, especially to Dr. Xingbin Xie, Mr. Yi Zheng, and Mr. Po-I Lee who assisted me with their knowledge and experience in the field of study.

TABLE OF CONTENTS

Acknowledgements.....	ii
List of Tables.....	vi
List of Figures.....	vii
Chapter 1 “Introduction”	1
1.1 Background.....	1
1.2 Objective of the Study.....	3
Chapter 2 “Literature Review”	5
2.1 Gasoline Direct Injection Engine.....	5
2.2 GDi Injector and Spray.....	9
2.3 Advanced Valvetrain Strategy.....	12
2.4 Gasoline Direct Injection with Ethanol	17
2.5 Visualization Method.....	20
2.6 Optical Accessible Engine.....	22
2.7 Simulation.....	23
Chapter 3 “Study Methodology”	25
3.1 Experimental Apparatus.....	25
3.1.1 Injection System	
3.1.2 Spray Chamber	
3.1.3 Optical Accessible Engine	
3.2 Optical Measurement System.....	38
3.2.1 Mie Scattering Method	
3.2.2 Shadowgraph Method	

3.2.3 Schlieren Method	
3.3 Image Processing of Schlieren Result.....	41
3.4 Numerical Simulation Setup.....	47
Chapter 4 “Result of Chamber Testing”	50
4.1 General Discussion of Schlieren Image.....	50
4.1.1 Optical Method Comparison	
4.1.2 Interpretation of Schlieren Image	
4.1.3 Summary	
4.2 Multi-hole Spray Testing.....	55
4.2.1 Effect of Ambient Condition	
4.2.2 Effect of Fuel Composition	
4.2.3 Effect of Fuel Temperature	
4.2.4 Effect of Injector Nozzle Design	
4.2.5 Summary	
4.3 Piston Impingement Testing.....	86
4.4 PDI Spray Testing.....	90
4.4.1 Effect of Ambient Condition	
4.4.2 Effect of Pulse Width	
4.4.3 Summary	
Chapter 5 “Result of Optical Accessible Engine Testing”	98
5.1 CFD Validation.....	98
5.2 Homogeneous Operation.....	101
5.2.1 Effect of Injector Nozzle Design	

5.2.2 Effect of Injection Timing	
5.2.3 Summary	
5.3 Stratified Operation.....	114
5.4 Effect of Valve Strategy.....	118
5.4.1 Two-valve EIVC Result	
5.4.2 Deactivated EIVC Result	
5.4.3 LIVC Result	
5.4.4 Summary	
Chapter 6 “Conclusion”	142
6.1 Summary of the Work.....	142
6.2 Recommendation and Future Work.....	147
6.2.1 Recommendation	
6.2.2 Future Work	
References.....	153
Abstract.....	162
Autobiographical Statement.....	164

LIST OF TABLES

Table 3.1: Specifications of tested injectors.....	27
Table 3.2: Fuel properties of E100, E50, gasoline, and iso-Octane for the reference at standard state.....	30
Table 3.3: OAE specification.....	33
Table 3.4: Camera resolution and speed.....	38
Table 4.1: Boiling point of Alkane (C4-C8)	61

LIST OF FIGURES

Figure 2.1: Metal engine test results at 1000RPM, 1bar BMEP with EIVC.....	16
Figure 2.2: Distillation curves for gasoline and ethanol	19
Figure 2.3: Basic scheme of Schlieren visualization method.....	21
Figure 3.1: Schematic of the spray chamber setup.....	29
Figure 3.2: Photograph and the schematic of cross section of the OAE.....	32
Figure 3.3: Spray targeting and plume number of Injector A and B.....	35
Figure 3.4: Valve lift profiles and the resultant cylinder pressure with the tested injection timing window.....	37
Figure 3.5: Mie-scattering visualization setup for the chamber test.....	39
Figure 3.6: Shadowgraph visualization setup for the chamber test.....	40
Figure 3.7: Schlieren visualization setup for the chamber test.....	41
Figure 3.8: Process of noise reduction.....	43
Figure 3.9: Example of resultant image of a 2-step thresholding	45
Figure 3.10: Definition of penetration and spray angle.....	46
Figure 3.11: Simulation domain and the coordinate.....	49
Figure 3.12: Adaptive Mesh Refinement (AMR)	49
Figure 4.1: Visualization method comparison of Injector A with E100, T=150°C (200°C for Shadowgraph), P=1bar.....	52
Figure 4.2: Schlieren images and assumed liquid phase for Injector A with E100 (T=200°C, P=1bar, Mass=5mg)	54
Figure 4.3: Effect of ambient temperature and pressure at 1.0ms ASOI.....	58
Figure 4.4: Effect of ambient temperature and pressure on spray penetration.....	59
Figure 4.5: Saturation pressure curve of ethanol and flash boiling.....	59

Figure 4.6: Effect of fuel composition. $T_{ch}=200^{\circ}\text{C}$, $P_{ch}=1\text{bar}$, $T_{fuel}=60\text{C}$, $PW=1.5\text{m}$	62
Figure 4.7: Penetration of spray for different fuels with fixed PW of 1.5ms.....	64
Figure 4.8: Area of projected sprays for different fuels with fixed PW of 1.5ms.....	64
Figure 4.9: Spray angle at 5, 10, 20mm down from the tip for different fuels with fixed PW of 1.5ms.....	66
Figure 4.10: Progress of the position of the centroid for different fuels with fixed PW of 1.5ms.....	67
Figure 4.11: Effect of fuel composition. $T_{ch}=200^{\circ}\text{C}$, $P_{ch}=4\text{bar}$, $T_{fuel}=60\text{C}$, $PW=0.5\text{ms}$	68
Figure 4.12: Area of projected sprays for different fuels with fixed PW of 0.5ms.....	69
Figure 4.13: Position of the centroid for different fuels with fixed PW of 1.5ms.....	69
Figure 4.14: Effect of fuel composition. $T_{ch}=200\text{C}$, $P_{ch}=1\text{bar}$, $T_{fuel}=60\text{C}$, Energy content=5mg of gasoline.....	71
Figure 4.15: Averaged penetration of spray for different fuels with fixed energy input...72	72
Figure 4.16: Area of projected sprays for different fuels with fixed energy input.....73	73
Figure 4.17: Spray angle at 5, 10, 20mm down from the tip for different fuels with fixed energy input.....	74
Figure 4.18: Progress of the position of the centroid for different fuels with fixed energy input.....	75
Figure 4.19: Effect of fuel temperature on spray propagation at $25^{\circ}\text{C}/1\text{bar}$, 10mg of gasoline or equivalent in energy.....	77
Figure 4.20: Effect of fuel temperature on spray propagation at $200^{\circ}\text{C}/1\text{bar}$, 10mg of gasoline or equivalent in energy.....	78
Figure 4.21: Effect of fuel temperature on spray propagation at $200^{\circ}\text{C}/3\text{bar}$, 10mg of gasoline or equivalent in energy.....	79
Figure 4.22: Effect of injector design (A&B) on spray propagation at $25^{\circ}\text{C} /1\text{bar}$, injection duration=1.5ms.....	81

Figure 4.23: Effect of injector design (A&B) on spray penetration at 25°C /1bar, injection duration=1.5ms.....	81
Figure 4.24: Spray bending of injector B at 25°C /3.2bar. 0.24ms (Left) and 1.10ms (Right) ASOI.....	82
Figure 4.25: Effect of injector design (A&B) on spray propagation at 200°C /1bar, 10mg of gasoline.....	82
Figure 4.26: Schlieren spray images for injector A (upper) and C (bottom) (T=200C P=3bar Pinj=10MPa Mass=5mg)	83
Figure 4.27: Picture of pistons for Injector A (Right) and Injector C (Left)	87
Figure 4.28: Piston impingement, Injector C, 15mm, 0.5ms injection duration.....	88
Figure 4.29: Piston impingement, Injector A, TDC (T=200C P=3bar Duration=0.5ms)	89
Figure 4.30: PDI Injection at 200C/4bar, PW=0.3ms.....	91
Figure 4.31: PDI Injection at 200C/1bar, PW=0.5ms.....	91
Figure 4.32: Effect of ambient pressure and temperature.....	92
Figure 4.33: Effect of temperature on penetration curve at 1bar (upper) and 4bar (bottom)	94
Figure 4.34: Effect of pulse width (PW) at 200C/4bar ambient condition.....	95
Figure 4.35: Effect of PW on penetration curve at 25°C of at 1bar (upper) and 4bar (bottom)	97
Figure 5.1: CFD validation of Injector B with injection at 240CAD bTDC with normal valve configuration. Injection quantity was 16mg.....	100
Figure 5.2: CFD validation of Injector A with injection at 90CAD with LIVC deactivation configuration. Injection quantity was 9mg, side view (left) and bottom view (right)	100
Figure 5.3: Homogeneous injection at 60deg after intake TDC with different injector	105
Figure 5.4: Schematic image of spray-tumble motion interaction.....	105

Figure 5.5 Dynamic ratio and turbulent kinetic energy of homogeneous injection at 60CAD aTDC.....	106
Figure 5.6: Total wall film mass of homogeneous injection at 60CAD aTDC.....	107
Figure 5.7: Effect of injection timing on spray and mixing for the homogeneous operation.....	109
Figure 5.8: Effect of injection timing on mixing at 30CAD after start of injection.....	109
Figure 5.9: Dynamic ratio and turbulent kinetic energy of homogeneous injection at various timing (Injector B)	110
Figure 5.10: Equivalent ratio distribution of homogeneous injection at 60CAD aTDC with Injector A.....	112
Figure 5.11: Equivalent ratio distribution of homogeneous injection at 60CAD aTDC with Injector B.....	112
Figure 5.12: Piston wall wetting footprints and total liquid film mass evolution for homogeneous injection.....	113
Figure 5.13: Stratified injection at 70deg before compression TDC.....	116
Figure 5.14: Mixture accumulation of stratified injection at 15CAD ASOI.....	116
Figure 5.15: Dynamic ratio and turbulent kinetic energy of stratified injection at 70CAD bTDC.....	117
Figure 5.16: In-cylinder visualization of side and bottom views with the injection timing at 70CAD aTDC. Two-valve EIVC configuration.....	118
Figure 5.17: Piston/side wall impingement by early injections at 30/50CAD aTDC with two-valves EIVC.....	120
Figure 5.18: Spray stretch by later injections at 70/90CAD aTDC with two-valves EIVC.....	120
Figure 5.19: In-cylinder visualization of side and bottom views with the injection timing at 70CAD aTDC. One-valve EIVC configuration.....	122
Figure 5.20: Two-(red) and one-valve(green) comparison for EIVC with injection at 70CAD.....	122
Figure 5.21: EIVC penetration curves for injection timing sweep from 30-110CAD aTDC intake (330-250CAD bTDC firing)	123

Figure 5.22: Two-(red) and one-valve(green) comparison for EIVC with injection at 330CAD.....	124
Figure 5.23: Normalized spray area from bottom view, EIVC conditions.....	125
Figure 5.24: In-cylinder visualization of side and bottom views with the injection timing at 70CAD aTDC. LIVC configuration.....	127
Figure 5.25: EIVC(red) and LIVC(green) comparison for two-valve with injection at 70CAD.....	128
Figure 5.26: Normalized spray area from bottom view, two-valve conditions.....	129
Figure 5.27: Two-(red) and one-valve(green) comparison for LIVC with injection at 70CAD.....	130
Figure 5.28: Normalized spray area from bottom view, LIVC conditions.....	130
Figure 5.29: LIVC penetration curves for injection timing sweep from 30-110CAD aTDC intake (330-250CAD bTDC firing)	131
Figure 5.30: EIVC (red) and LIVC (green) comparison for deactivation with injection at 70CAD.....	132
Figure 5.31: Normalized spray area from bottom view, deactivation conditions.....	133
Figure 5.32: Dynamic ratios with injection at 60CAD.....	135
Figure 5.33: Mass averaged turbulent kinetic energy with injection at 60CAD.....	136
Figure 5.34: Total liquid film mass on the wall.....	136
Figure 5.35: Liquid/vapor fuel mass inside cylinder.....	137
Figure 5.36: Standard deviation of lambda.....	138
Figure 5.37: In-cylinder gas temperatures of LIVC configuration.....	139
Figure 6.1: Cylinder pressure curve of the preliminary combustion visualization testing.....	151
Figure 6.2: Visualization result of the preliminary combustion visualization testing.....	151

CHAPTER 1 "Introduction"

1.1 Background

Gasoline engine is an internal combustion (IC) engine which has been widely adopted for a power source of automotive powertrains. In many countries including the US and Japan, most of passenger cars are equipped with a gasoline engine because of its excellent power/weight ratio and noise level. Possibility of emitting larger amount of soot by diesel engines, the other type of major application of IC engine for an automobile, was a negative factor for automotive engine applications especially for use in city area. The automotive industries have been put a lot of effort to improve fuel efficiency of their gasoline engines in response to customer demands and business incentive. Meanwhile, as the environmental issues such as air pollution and the greenhouse effect draw attentions worldwide, the engine manufacturers are required to meet a regulation of the engine emission. Commonly carbon monoxide (CO), unburned hydrocarbon (UBHC or simply HC), nitrogen oxide (NO_x), and particulate matter (PM) in emission are regulated, and the regulation is getting strict over the years. Therefore engine research and development has been under a challenge to increase the fuel efficiency and decrease the engine emission simultaneously. The use of alternative fuel to minimize the petroleum dependency is also one of the major research areas of engine development.

Through the research and development, gasoline direct injection (GDI) engine has drawn an attention for a next generation gasoline engine. As its name indicates, a GDI engine injects fuel directly into the cylinder in order to manage fuel/air mixture formation more precisely. Detail of GDI engine is discussed in the reference [1] and in

Chapter 2. The first appearance of GDI engine was in middle of 20th century, but its feasibility for mass production had been in obscurity due to technical limitations. As the manufacturing and controlling technology developed, the first generation of mass-produced GDI engine was launched in 1996. Since the concept of first generation GDI was on the lean burn strategy to minimize the fuel consumption, serious NO_x emission due to excess oxygen obstructed its growth. In addition, aftertreatment by three-way catalyst did not work well because of excess oxygen in the exhaust gas. Soot and deposit formation caused by severe piston wetting was another concern for the first generation GDI engine.

Taking the problems of the first generation GDI engines, GDI strategy has been shifted to stoichiometric combustion. With stoichiometric operation, the emission can be compatible with a conventional three-way catalyst. Even with stoichiometric combustion, the advantages of direct injection is still attractive in terms of mixture preparation. Since the combustion initiation is limited at the spark plug in gasoline engines, importance of optimization of air/fuel mixture preparation is dominant for improved combustion. Direct injection can offer another control factors in fuel delivery of gasoline engine operation. In conventional port fuel injection (PFI) engines, the injection timing is limited to the time the intake valves open. In GDI engines, however, when and where the fuel is injected inside the cylinder can be under control by injection timing shifting and spray aiming design. Considering fuel injection takes place in the engine cylinder, the behavior of fuel spray must be influenced by the in-cylinder condition, temperature and pressure especially, which varies a lot corresponds to the injection timing. Therefore

understanding of GDI spray characteristics in various surrounding conditions is necessary in order to design and control the fuel delivery system precisely.

As the fuel delivery system develops, supply of air into the engine cylinder must be optimized either to achieve better combustion. Unlike diesel combustion by diffusion flame, gasoline engine's pre-mixed combustion requires complete air/fuel mixing before a spark ignites the mixture. It is easily imagined that the behavior of intake air can affect combustion quality especially for GDI engines in which the fuel and air are supplied separately. Some of the current GDI engines utilize the intake air motion to form desirable air/fuel mixture in the combustion chamber. Desirable air motion assists fuel/air mixing, and positioning of the mixture in case of stratified combustion. It is reasonable to control the intake air flow by valve strategy such as valve lift, duration, and phasing. Throttling is another big factor for intake air controlling. Therefore an advanced valvetrain coupled with direct injection is expected to provide an opportunity for better combustion and thus simultaneous reduction of fuel consumption and emissions. Understanding the effect of intake and in-cylinder flow on mixture formation is essential for further development of direct injection gasoline engines.

1.2 Objective of the Study

The objective of this study is to understand the characteristics of GDI sprays and behavior of in-cylinder charge motion in a GDI engine which is equipped with variable valve actuation. To meet the objectives, high-speed spray visualization utilizing Schlieren techniques was performed in the heated/pressurized chamber testing to characterize the spray behavior with different type of injectors under various injection

strategies and ambient conditions. The effect of ethanol in the fuel on the spray structure was also discussed in the chamber testing. This paper also presents high-speed Mie-scattering spray imaging results taken with an optical accessible engine (OAE) in order to study the effect of valvetrain and injection timing strategies on in-cylinder charge motion. Metal engine testing and three-dimensional Computation Fluid Dynamics (CFD) for simulating DI spray behaviors in the engine were carried out to support the optical engine work.

CHAPTER 2 “Literature Review”

2.1 Gasoline Direct Injection Engine

Gasoline Direct Injection (GDI) engine has great potential to be the next generation gasoline engine and replace the current Port Fuel Injection (PFI) engines [1]. Since its first mass production in 1996, a lot of effort in research and development of GDI engines have been conducted by automotive manufacturers and related research institutes. Many of automotive manufactures produce their own production GDI engines in the market already, but GDI engines have not been the majority of production gasoline engine yet because of compensation which they have to make as the following review claims.

PFI engines are equipped with the fuel injectors at the intake port. Fuel is injected in the port with relatively low fuel pressure in the range of 300-500kPa. The engine breaths fuel and air together during intake stroke to create homogeneous combustible mixture in the cylinder. Although low injection pressure increases the spray droplet diameter, longer mixing time until spark ignition and turbulent initiated by the intake air flow promote mixing and vaporization of the fuel for homogeneous combustion. Since the fuel and air are partially mixed already before they enter the combustion chamber, PFI engines must be operated with homogeneous combustion. Due to its nature, a PFI engine requires throttling to control the engine load, in other words, to control the amount of oxygen for combustion. Therefore PFI engines must be suffered by severe pumping loss. Fuel film and deposit formation on the intake valves and ports are another concerns of PFI engines because liquid fuel spray keeps hitting the surface of those area during the engine operation. Existence of liquid fuel during combustion

can result in unburned hydrocarbon emission and it becomes critical when the engine is cold [2]. These features of PFI engines limit the engine performance in terms of fuel economy and emission.

GDI engines, on the other hand, are equipped with the fuel injectors at the inside of cylinder. The injector can be mounted at the side or at the top of the cylinder depending on combustion strategy requirement. Since the air and fuel can be brought into the cylinder separately, GDI engines are able to manage the output torque easily by controlling the amount of fuel injected into the cylinder. Precise control of the amount of injection volume is critical for GDI engines, thus the realization of GDI engine must had waited for the development of the injection controlling technique. Due to the precise injection control, GDI engines can run with two different combustion modes; homogeneous and stratified. In homogeneous mode, homogeneous air/fuel mixture is prepared for premixed combustion, which is similar to the combustion takes place in PFI engines. Homogeneous operation typically runs with stoichiometric mixture achieved by combination of throttling and direct injection [3, 4]. Normally fuel injection takes place at the early intake stroke to ensure longer mixing time until spark ignites the mixture. One great advantage of GDI homogeneous operation is charge cooling effect. Since the vaporization process of the injected fuel occurs inside the cylinder, latent heat of vaporization decreases the mixture temperature. If the initial in-cylinder temperature at the beginning of compression is decreased, the temperature at the end of compression is also decreased. It suppresses the knocking tendency and makes possibility of higher compression ratio. Increased density of mixture by lower temperature can improve volumetric efficiency as well. By avoiding intake valve and port wall wetting by in-

cylinder spray direct injection, reduced emission can be expected comparing to PFI operation. However, small back pressure of in-cylinder injection with homogeneous operation could result in over penetration of the spray. The spray may hit the piston surface or the side wall, and fuel film formation and/or oil dilution may occur. In stratified combustion mode, the mixture distribution at the time of combustion must be "stratified". The air/fuel mixture should be near stoichiometric at the vicinity of the spark plug to ensure flame propagation. However, the overall equivalence ratio in the cylinder can be lean. This combustion strategy is also known as "lean burn". Severe throttling to limit the amount of air is not required and it helps reduce pumping loss, which is one of the major concerns of PFI engines. However, lean burn engines produce more NO_x emission due to increased availability of oxygen in the process of combustion. Increased NO_x emission is a major concern of lean burn operation and typically treated by adding extra NO_x catalyst in addition to a conventional three-way catalyst in the exhaust aftertreatment system. With stratified combustion mode, GDI engines breath only air during intake stroke and inject fuel during the compression stroke. In order to overcome the high cylinder pressure during the compression stroke, the fuel injecting pressure is in the order of 5-20MPa. High injection pressure contributes to smaller fuel spray droplets either. The compression is proceeded under higher specific heat ratio of pure air which results in higher engine efficiency. By the fuel injection into the high temperature air, charge cooling effect can be expected. Reduced mixture temperature can contribute to designing the compression ratio higher for better engine efficiency. In addition, lower combustion temperature can result in smaller amount of heat loss into the surroundings. Since a GDI engine typically injects fuel near the end of compression

stroke when it runs in the stratified mode, piston wetting and resultant unburned hydrocarbon and soot emission have been identified as issues [5-7]. Transient from one mode to the other in response to various engine load requirement has been a issue for GDI engines in terms of knocking, emission, and stability. Generally homogeneous mode takes charge in higher load because of its near stoichiometric operation, and stratified mode takes lower load by lean burn. GDI is able to handle this transient by split injection [8]. During transient, a part of required amount of fuel is injected in intake stroke to produce lean homogeneous mixture. And the secondary injection takes place near firing TDC for partially stratified charge. By optimizing the ratio of the amount of each injection, GDI engine is able to minimize the undesired effect of mode transient.

In summary, the major advantages of GDI engines over the PFI engines are summarized as follows:

- improved BSFC
 - less pumping loss (stratified operation)
 - less heat losses (stratified operation)
 - higher compression ratio
 - increased volumetric efficiency
- improved load control including transient response
- selective emission advantages
 - reduced CO₂ and UBHC emissions
 - more precise air/fuel ratio control for complete combustion

And the disadvantages are:

- complexity and difficulty in controlling the injection and combustion over the required operating range
- three-way catalysts cannot be utilized (stratified operation)
- higher NO_x emission (stratified operation)
- possible UBHC emissions by strong wall wetting

2.2 GDI Injector and Spray

A GDI engine with well optimized spray structure and injection strategies potentially meets the ever-tightening emission standards and fuel economy regulations [9, 10]. The previous section claims GDI engines are compatible to various operating modes to be optimized for various running conditions. Therefore, better understanding of the spray characteristics under different in-cylinder conditions is essential to optimize the GDI combustion system. Even though DI spray has been under investigation for decades in the area of diesel engine research, the knowledge and understanding of diesel DI spray cannot be simply transferred to GDI operations because of difference in fuel properties and injection strategies such as injection pressure and nozzle design.

It is well known that there are three major concepts of GDI for how fuel is delivered into the combustion chamber; wall-, air-, and spray-guided [11]. The wall-guided concept coupled with other techniques such as upright intake port and swirl injector was proposed with the first mass production GDI engine [12]. Wall-guided GDI engines inject fuel towards the hot piston surface to promote fuel vaporization. The direction of spray momentum is altered by the piston cavity curvature in order to deliver

the fuel vapor to the vicinity of the spark plug. Due to severe piston impingement, HC and soot formation has been a problem for this concept. In order to reduce the effect of wall wetting, air-guided concept was introduced. With this concept, in-cylinder flow (swirl and tumble) was utilized more effectively to deliver the air/fuel mixture towards the spark plug without severe piston impingement. Since the mixture preparation of wall-guided GDI engines are also assisted by in-cylinder flow to some extent, there is no clear difference in the definition of those two concepts. Some GDI engines were successfully designed under those concepts [13, 14]. Even in air-guided, however, the effect of wall wetting could not be completely removed. Combustion stability could be poorer due to less robustness of mixture behavior due to lack of solid guide. In order to improve GDI engines for less surface wetting and more robustness, the spray-guided concept has drawn attention [10, 15, 16]. In spray-guided GDI engines, the injector aims near spark plug for fuel delivery to reduce wall wetting. The key for the success of this concept is management of fuel vaporization. The spray must be well atomized and vaporized during the short time between injection and ignition to prevent misfire. Air- and spray-guided GDI are considered as practical because of less emission, therefore the characteristics of spray is getting even more important for assure the robustness of mixture behavior.

In GDI engines, spray development is critically related to mixture formation, therefore the injection strategies must be well-optimized to maximize the fuel economy and emission benefits. Although swirl injectors were widely studied for GDI engines [17-19], solenoid-driven multi-hole injectors are found to be more suitable because they offer advantages of more stability in spray pattern, and flexibility in spray plume

targeting [20]. Especially, lower sensitivity of spray cone angle to the ambient pressure under stratified operation is preferred for DI operation [21]. They also have flexibility to individualize the ratio of hole length and diameter (L/D) for each hole, the hole angle, and the hole distribution pattern for better match to the combustion chamber geometry. Multi-hole injectors have been under investigation in the area of diesel engines for decades. Therefore, multi-hole injectors have been identified as a preferred solution and are subject to intensive development by many fuel system and engine OEMs in recent years [21-23]. An empirical equation for spray penetration as a function of time derived by Hiroyasu and Arai [24] is well known as

$$L(t) = \begin{cases} 0.39 \cdot \left(\frac{2\Delta P}{\rho_l} \right)^{0.5} t & \text{for } t < t_b \\ 2.95 \cdot \left(\frac{\Delta P}{\rho_g} \right)^{0.25} (d_0 t)^{0.5} & \text{for } t > t_b \end{cases}$$

where t_b is breakup time and expressed as

$$t_b = 28.6 \frac{\rho_l d_0}{(\rho_g \Delta P)^{0.5}}$$

and ΔP is pressure drop, ρ_l and ρ_a are density of liquid and air respectively, and d_0 is orifice diameter. Although this equation has been widely accepted especially for spray simulation, advanced injector mechanism and higher injection pressure of recent injection strategy raise questions about its reliability. It is also known that better atomization and vaporization can be achievable if the fuel is injected through a smaller nozzle hole. Many researchers have reported that the Sauter Mean Diameter (SMD) of liquid droplets in the spray decreases for a smaller orifice, while penetration is sacrificed [25, 26]. Siebers has found that the length of liquid phase penetration in the spray is

linearly dependent on the orifice diameter [27]. Advantages of smaller nozzle holes have been reported for other aspects. Low PM and CO in emission are attributed to smaller SMD, which enhances vaporization and mixing [28]. One major concern of multi-hole injectors is injection failure by hole fouling. Since the nozzle tip may be exposed to high-temperature propagating flame front, small orifice (~0.2mm) of multi-hole injector is easily affected by fouling. The Piezoelectric Direct Injector (PDI) is designed for very fast and precise injection which is suitable for spray-guided GDI. Outward-opening pintle injector providing excellent stable spray for spray guided GDI engines. Generally, the shape of the spray is a very wide hollow cone with toroidal vortices at the side [29]. The body of the spray consists of number of strings rather than a sheet. The vortices at the side of the spray transport momentum of the initial direction of the spray into circular motion resulting in short spray penetration. Since the toroidal vortices consists of an ignitable mixture with strong rotating momentum, it is the preferred position for spark discharge in SI spray-guided operations. Management of the position of vortices which must be at spark plug gap is required for stabilized combustion [30].

2.3 Advanced Valvetrain Strategy

Although the amount of air is regulated by a throttle in conventional gasoline engines, advanced valvetrain is prospected to control the intake air behavior more effectively. Most of current IC engines are equipped with two intake and two exhaust valves because of availability of the center of the combustion chamber roof for a spark plug or an injector with keeping the total available valve opening gap large enough.

Valve overlapping, which opens intake valves before exhaust valves are completely closed, is a commonly used technique to improve intake flow dynamics for increased volumetric efficiency by taking the full advantage of inertia of the flow. Variable Valve Timing (VVT) is a technique that can solve the problem of obtaining optimal engine performance over a wide range of load and engine speed. VVT allows the intake and exhaust valves to open and close at varying crank angles, depending on the speed and load conditions [31].

Early Intake Valve Close (EIVC) and Later Intake Valve Close (LIVC) strategies have been introduced for the advanced valvetrain for a stoichiometric GDI engine [32, 33]. By their difference of the valve lift, EIVC and LIVC cams are also called Low Lift Cam (LLC) and High Lift Cam (HLC) respectively. Both cams are designed for Miller cycle engine, which effective compression ratio is smaller than expansion ratio. Miller cycle is able to reduce the peak pressure and knocking by less effective compression ratio and produce extra power by relatively longer power stroke [34]. EIVC has been studied in previous work and shown to offer fuel consumption reduction primarily at low loads due to reduced throttling. The use of LIVC is an alternative strategy that provides similar benefits of fuel consumption reduction at part loads. Deactivation of one of the intake valves is another approach for the advanced valvetrain. Moore et al. insisted that use of valve deactivation has shown to improve stability and reduce particulate emissions [35]. A significant reduction of pumping loss can be achieved under deactivation by reducing throttling, and increased stability of combustion was reported as well. Since this article is closely related to the optical engine work of this dissertation, the result of the deactivation work is summarized in the following sections.

ENGINE DESCRIPTION and SETUP

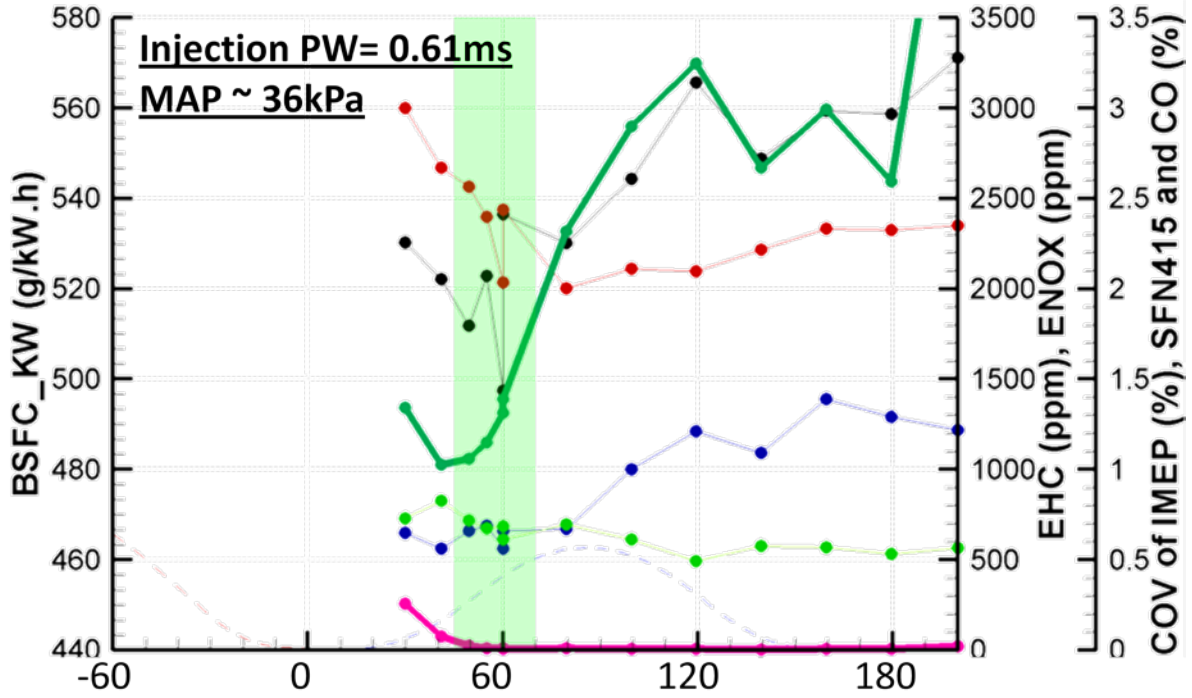
Metal engine testing was performed using a 2.0L 4-cylinder Spark Ignited DI turbocharged engine with Dual Independent Cam Phasing (DICP). Pure gasoline was used for the fuel although the engine had flex-fuel capability. The engine was modified to increase the Compression Ratio (CR) from 9.2 to 11.9 with remodeled pistons. A two-step Variable Valve Actuation (VVA) system was designed and installed to provide effective compression ratio management using LIVC and EIVC. These strategies allowed CR and load control by use of cam phasing. Evaluation of the hardware as a flexible fuel engine is reported in the reference [36].

The engine was tested at 1000RPM/1bar BMEP condition to compare the effect of valve deactivation on combustion stability, engine efficiency, emissions and allowable injection timing windows. The engine was operated with stoichiometric charge under throttling. The spark timing was chosen with minimum advance for the best torque (MBT). Only EIVC cam results are presented in this paper. Cam timing optimization was done at each case to maximize engine efficiency for both the conventional two-valve and the one-valve (valve deactivation) configurations. The cam timing optimization was conducted independently for the different strategies to allow comparison at an optimal performance point instead of comparing at the same cam settings which could bias the conclusions. Detail and other results of metal engine testing can be found in the reference [35].

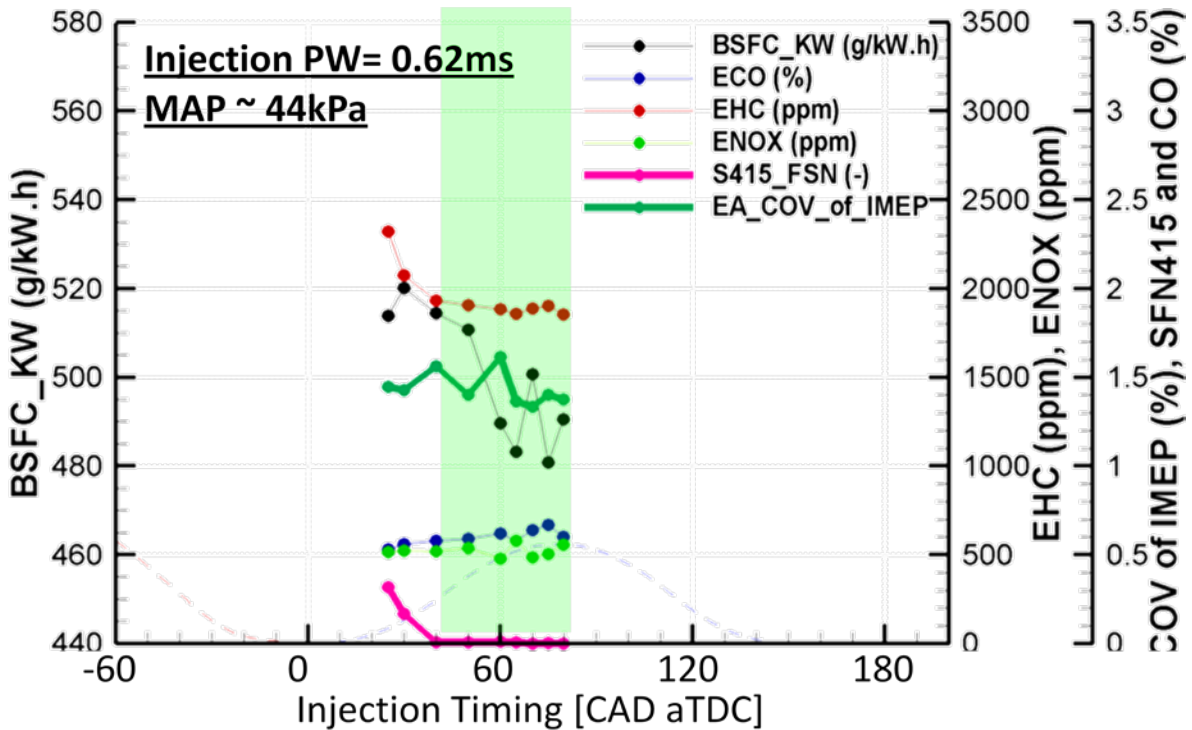
METAL ENGINE TEST RESULT

Fig. 2.1 (a) is the results of the metal engine testing with conventional two intake valves with EIVC configuration. Brake Specific Fuel Consumption (BSFC), emission data including CO, HC, NO_x, and soot, and coefficient of variation (COV) of IMEP are plotted. Valve lift curves and possible injection window are also shown in the figure. The criterion of the injection window was based on COV less than 3% and low soot to avoid the piston impingement region. Another constraint was BSFC less than 1% over minimum BSFC that was not soot constrained. The earlier side of the window was limited by soot generation started growing at 310CAD before firing Top Dead Center (TDC). This is believed to be the result of spray impingement to the piston which forms liquid film on the surface. As the injection timing retarded, there was no soot observed. However, COV of IMEP rapidly increased around 290CAD and this settled on the other side of the injection window.

Fig. 2.1 (b) shows the results of one valve deactivated EIVC. By deactivation, Manifold Absolute Pressure (MAP) was increased by reduced throttling. As a result, BSFC improved due to reduced pumping loss. Both soot and HC emissions were reduced at early injections, and the injection window could be expanded for 10 degrees approximately. The poor combustion stability with the later injection was not observed either. A significant improvement was not achieved because of low load which required severe throttling. The benefit of valve deactivation was more obvious at higher speed/load as reported in [35].



(a) Two intake valves (Conventional)



(b) One intake valve (Deactivation)

Fig. 2.1 Metal engine test results at 1000RPM, 1bar BMEP with EIVC [35]

2.4 Gasoline Direct Injection with Ethanol

Ethanol is of interest in the US market as a renewable source of oxygenated fuel for gasoline engines [11]. Currently ethanol produced in the US comes primarily from fermentation of corn starch, which energy balance is in question. If the production of ethanol is further developed and improved in terms of energy balance, ethanol can be a primary energy resource for IC engines.

Ethanol has been identified as a major type of fuel to displace gasoline in the automotive applications, and the combination of ethanol-gasoline blended fuel and GDI engine has been studied widely [37-39]. Some countries such as the US have encouraged the production of vehicles that are capable of operating on E85 (85% denatured ethanol and 15% gasoline in volume ratio). Production E85-compatible vehicles are normally equipped modified fuel delivery systems that can withstand the highly corrosive nature of the alcohol. However, these vehicles do not take full advantage of the properties of ethanol during the mixture formation and combustion processes. Significant advantages of ethanol on those processes are its high Octane number providing excellent knock resistance, and high latent heat of vaporization which promotes charge cooling for increased power density [40, 41]. Therefore an engine optimized for ethanol-gasoline blended fuel is able to run with higher compression ratio resulting in better engine efficiency. It should be noted that the heat of vaporization is not linear dependent to the ratio of gasoline-ethanol blend [42]. The heat of vaporization of the blend tends to increase as more ethanol is added up to 20%. Then it decreases until E30, and starts increasing again for the rest of range. Ethanol has a flat distillation curve which is different significantly from multi-component gasoline as Fig. 2.2 shows.

Gasoline contains multiple hydrocarbons and shows an increasing distillation curve which corresponds to multiple boiling points of each hydrocarbon. The difference of properties of phase change must affect the process of vaporization and the quality of combustion. It is known that the laminar flame speed of ethanol is faster than gasoline, and ethanol-gasoline blend contributes engine performance by faster combustion especially at high speed operation [43]. Positive results of ethanol fuel have been drawn at full load for the engine-out emissions as well [44]. Since alcohol contains oxygen atoms in its molecular structure, improved oxygen availability reduces soot emission. NO_x can be reduced due to lower combustion temperature by charge cooling effect. At part load, a regular gasoline engine produces more HC emission due to low combustion temperature. Ethanol fuel can suppress the HC emission greatly by lower concentration of aromatics and olefins which is believed to be the source of HC [45]. GDI engine will be capable of operation with variable ratio of ethanol-gasoline blends from E0 (pure gasoline) to E85 by employing variable effective compression ratio accomplished through cam phasing and variable valve actuation. Ethanol containing fuel can significantly reduce the development of injector hole fouling due to synergy effect of reduced injector tip temperature and lower amount of aromatics and sulfur contained in the fuel [39]. A negative impact of ethanol on engine operation is its 33% reduction in Lower Heating Value (LHV) on a volume basis in comparison with gasoline. HC emission may increase because larger volume of fuel injection is required, which could result in incomplete vaporization at the spark timing. Greater charge cooling and lower volatility of ethanol affects negatively in cold start conditions [41, 42]. Although lower vapor pressure of ethanol may suppress the process of vaporization, the vapor pressure

of gasoline-ethanol mixture does not show linear dependency to the ratio of mixing. Not much difference has been reported between ethanol and gasoline spray behavior [37], but detail study is needed for better understanding of the characteristics of those fuel to optimize the fuel system for flex-fuel GDI engines.

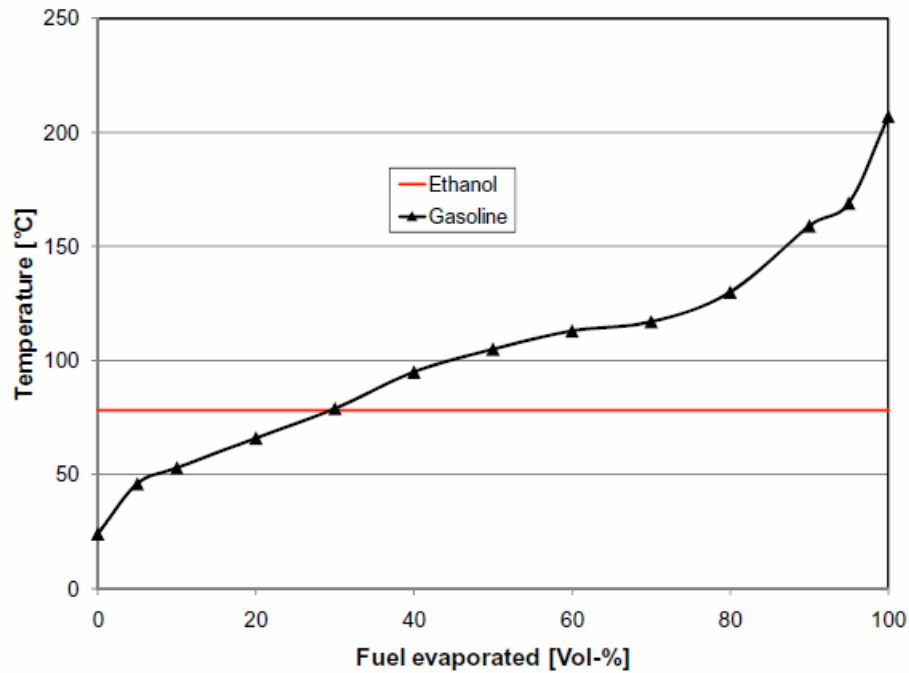


Fig. 2.2 Distillation curves for gasoline and ethanol [45]

It is well known that the physical properties of fuel also affect the spray and combustion behavior. Density directly affect the mass of fuel to be injected and thus the amount of heat release during combustion. Ethanol has higher density than regular gasoline, therefore more mass is injected with the same injection duration. The behavior of fuel spray and droplets are affected as well by density in terms of momentum and kinetic energy. Viscosity and surface tension of the fuel are related to atomization and fuel system tolerance. Especially the ratio of inertia force and surface tension is known

as Weber number and subject to study in spray breakup [46, 47]. Since ethanol has higher viscosity and surface tension than gasoline, it has more resistance against atomization.

2.5 Visualization Method

Mie-scattering technique has been often applied in spray visualization [48-50]. Mie-scattering is the elastic scattering of light from droplets which diameter is larger than the wavelength of the incident light. Typically spray droplets in automotive applications have diameter range of micrometers. Visible light has wavelength in the range of nanometer. If visible light is used as a light source, the incident light is reflected, refracted, and interfered in the droplets and scattered as Mie-scattering to make the droplets visible. It should be noted that the Mie-scattering technique can visualize liquid spray only.

Back-lit is another common technique for spray visualization [5, 51]. The light source is placed on the other side of the camera with respect to the object. If the incident light is parallel, it is called shadowgraph technique. On the contrary to the Mie-scattering, the incoming light is absorbed or attenuated by the object and make it visible as a shadow. Back-lit is supposed to visualize vapor phase as well due to refraction of the incident light traveling through the spray.

The Schlieren method is one of the most effective techniques to visualize non-homogeneous transparent flow fields, such as the vapor phase of sprays. Using the Schlieren technique, it is able to visualize the change of the refraction indexes and density gradient in the object caused by material and temperature difference [52]. Fig.

2.3 shows the basic principles of the Schlieren. Suppose parallel light is coming through the object. If the object is homogeneous, the light fluxes are accumulated at the focal point by the magnifying lens and project an image on the screen. However, if there is inhomogeneity in the object, light passing through the inhomogeneity area may be refracted and off the focus of the lens. Therefore the intensity change in the projected image can be observed, and its difference can be clearer by cutting the refracted light by a knife edge [53, 54]. The difference between Schlieren and shadowgraph is use of parallel light source and a knife edge. These two make the Schlieren method distinctive and offer clearer vapor phase visualization.

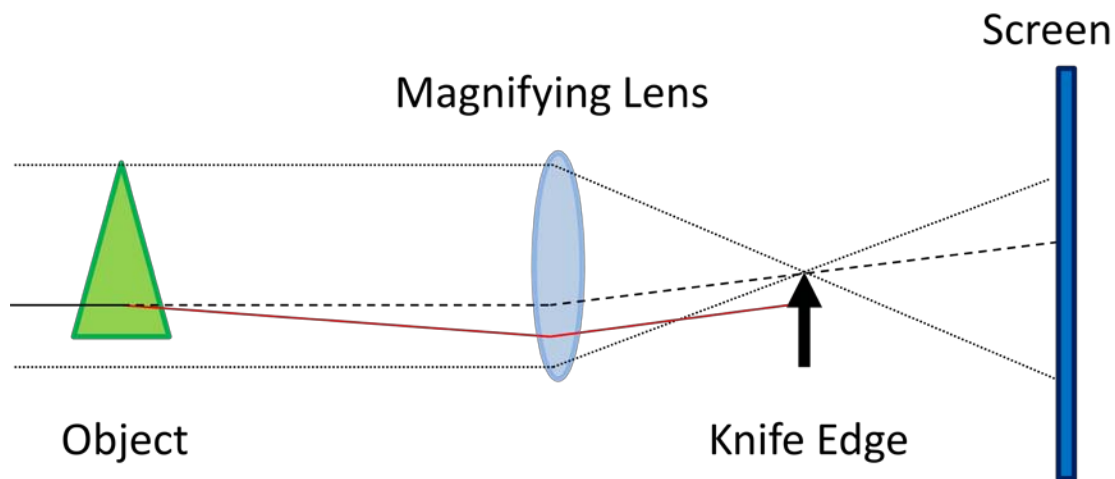


Fig. 2.3 Basic scheme of Schlieren visualization method

2.6 Optical Accessible Engine

Characterization of spray and its interaction with charge motion, and the liner and piston surfaces, in terms of the degree of vaporization and mixing are important R&D issues for the optimization of GDI spray. Even though spray is studied in a test chamber and understood for its behavior, the spray must act differently in a real engine operating condition because of difference in chamber geometry and existence of in-cylinder flow. Wall wetting is undesirable for any IC engine operation due to increase of soot and unburned hydrocarbon emissions. However, it may not be avoidable for DI operation at early homogeneous injection or late stratified injection. Commonly DI spray has massive momentum comparing to in-cylinder air flow to overcome the bulk air flow effect on the spray formation. Once the spray breaks up into droplets and its momentum is dissipated, the behavior of the air/fuel mixture is expected to be influenced strongly by the in-cylinder flow.

Optical Accessible Engine (OAE) offers dynamic and realistic in-cylinder charge motion with direct imaging capability, and it is widely used for spray and combustion research [55-57]. Most common type of OAE is equipped with a hollow piston with a optical window on the top of it to provide an optical path to the bottom of the piston, which is named Bowditch piston. An optical engine may have windows on the side of the cylinder. Comparisons of combustion and emission behavior in a metal single cylinder diesel engine and an optical engine with the same geometry has been performed, and reasonable similarity has been reported [58, 59]. Even though an OAE is able to simulate in-cylinder event occurs in a real engine, difference in the heat transfer characteristic caused by material difference of the combustion chamber wall

could affect the mixture behavior. Large amount of blow-by through the piston ring gaps, and big crevice volume due to the piston rings which commonly mounted at the lower position in optical engines may have an effect on the charge motion and combustion characteristics. In addition, operation of optical engine testing may be limited in few cycles in order to minimize fuel and combustion product deposit on optical windows to maintain the resultant image quality. Therefore obtaining stable condition in flow and temperature in the cylinder may be sacrificed and the similarity of in-cylinder and boundary condition of optical and real engine is compromised.

2.7 Simulation

Three dimensional CFD numerical simulation is universally used in order to make selections of injection strategy in the early period of engine design. Many studies have been done in numerical simulation of spray development and mixture formation, and it is under development to be more accurate to understand mixture formation of DI engine which is very critical for better fuel efficiency and emission [60-62].

Many 3D CFD simulations perform spray calculation based on Discrete Droplet Model (DDM) [63]. DDM applies drop “parcels” in the computational domain, which contains a number of identical particles with same radius, velocity, temperature, etc. Therefore one particle can represent all particles in the parcel, and calculation such as momentum and heat/mass transfer equations can be applied on the parcel. For spray breakup, droplet interaction and vaporization are calculated by sub-models. Those sub-modeling are normally based on empirical equations. In spray simulation, spray breakup is a critical event and studies have been conducted to model the discrete phase of

spray. The Taylor Analogy Breakup (TAB) model [64] is a classic method for calculating drop breakup. The Kelvin-Helmholtz (KH) model which represents the primary breakup, and Rayleigh-Taylor (RT) model representing the secondary breakup are presented by Ricart and Reitz [65] and suggested to adjust the model constant with respect to experimental data from spray bomb experiments [66]. The KH model and RT model are combined to simulate the spray [67, 68] which shows good agreement with the experiment results. O'Rourke model has been widely used for the collision and coalescence model [67]. An alternative to the O'Rourke numerical collision scheme is the No Time Counter (NTC) method presented by Schmidt and Rutland [69]. The NTC method is based on the techniques used in gas dynamics for Direct Simulation Monte Carlo (DSMC) calculations.

If sprays hit a piston bowl during stratified operation, this impingement should be studied more for better understanding of mixture formation. It has been reported that the piston impingement must be taken into account for a better simulation result [37]. Over-estimation of volumetric efficiency for ethanol fuel was found and a suggestion was presented to create a sub-routine to accurately simulate impingement, vaporization, and heat transfer on a piston surface. The previous work on wall impingement discovered that the wall temperature strongly affected the vapor phase propagation after the spray hit the surface [70].

CHAPTER 3 “Study Methodology”

In this chapter, the study methodology of the research is discussed. The research has been accomplished by both experiment and simulation. The experimental apparatus is introduced first followed by the optical system setup. Then the image processing technique used for examination of Schlieren images is presented. Finally, the setup of numerical simulation is discussed.

3.1 Experimental Apparatus

The main experiments were performed by using a high-speed digital camera to capture the process of spray development under typical fuel injection conditions for a Gasoline Direct Injection (GDI) engine. The spray visualization experiments consist of the spray chamber testing and the Optical Accessible Engine (OAE) testing. The spray chamber testing is suitable for detail study of the spray development. And OAE testing has a benefit in its realistic ambient condition which the spray is injected into, and thus it is used for spray-air interaction study.


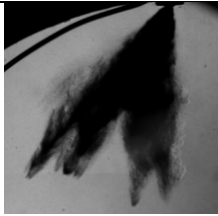
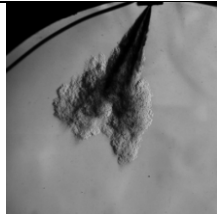
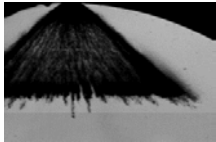
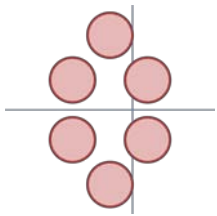
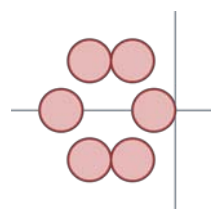
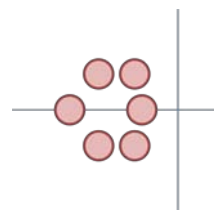
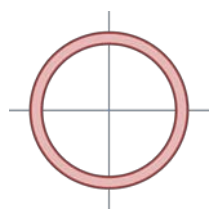
3.1.1 Injection System

The injection system had been shared in all the experiments. The fuel was stored in a stainless-steel fuel tank, which could be pressurized by compressed nitrogen up to 10MPa. An injection command signal, which was a negative TTL signal for the multi-hole injectors, was generated using a function generator or a customized Labview program. The signal was sent to a GDI driver to operate the injector. Since the injection is triggered at the falling edge of the negative TTL signal, and the injection duration

depends on the length of the command signal, changing the timing and the length of the pulse is able to control the fuel injection timing and quantity. The correlation between the length of injection command signal and resultant injected mass was provided by the injector manufacturer.

Four GDI injectors had tested in the experiments; three of them were multi-hole injector and the other one was an outward-opening pintle injector. Injector A is a production GDI injector which is designed for the production engine head used in this research, and also called “baseline” injector. Other injectors are prototype injectors. The spray pattern of Injector B is skewed with respect to the nozzle axis and rotated roughly 30degree. This makes only one plume penetrating towards the piston to reduce the possibility of piston wetting. And the diameter of the hole closest to the piston is less than the other five holes for less penetration of the plume which makes the amount of piston impingement even smaller. Injector B has larger hole diameter in average and thus larger flow rate compared to Injector A because it is designed for E85 compatible engines which requires more fuel injection during operation with high concentration of ethanol. Injector C has much smaller hole diameter with the spray targeting more accumulated. The last injector used in the testing is Piezoelectric Direct Injector (PDI). PDI has much larger flow rate, and its spray is in hollow cone shape. The specifications are summarized in Table 3.1. All four injectors have different hole geometries, mass flow rate, and spray targeting. The example pictures of the projected side view image and the spray footprint at 50mm down from the injector tip are presented for better understanding of the spray pattern.

Table 3.1 Specifications of tested injectors

	Injector A	Injector B	Injector C	PDI
Hole Diameter [mm]	0.23	0.225×1 0.259×5	0.104	-
Hole Length [mm]	0.31	~0.3	0.23	-
Averaged L/D	1.36	1.1	2.21	-
Number of holes	6	6	6	Hollow cone
Static mass flow with N-Heptane [g/s]	15.9	17.86	4.00	35
Example of spray image (side view)				
Downstream Footprint Crosshairs are on the injector tip.				

3.1.2 Spray Chamber

Fig. 3.1 shows the experimental setup for the spray chamber testing. The chamber is made of carbon steel and has a cylindrical shape which inner diameter and length are $\Phi 150\text{mm} \times 180\text{mm}$. It has two optical windows in parallel at both ends to allow straight view which is necessary for shadowgraph and Schlieren methods. The chamber has an additional small window at the middle perpendicular to the center of the chamber, which provide another optical access for the light source of the Mie-scattering visualization.

The injector is fixed at the middle of the test chamber. The specially designed injector holder has a built-in water jacket around the injector to insulate it from the hot chamber. It is capable to maintain the injector tip temperature from 25°C to 90°C . The water jacket may be used for heating up the injector either when the testing is under cold chamber conditions.

In case of the piston impingement testing, a dummy piston head is placed in the chamber with angle of 23° respect to the injector axis to replicate the relative position of the piston and the injector in the production side-mounted GDI engine.

An air supply system is required to produce environment of typical fuel injection conditions for GDI engines. For example, the ambient temperature and pressure must be high to simulate stratified in-cylinder condition. High temperature with low pressure represents a homogeneous injection condition with high Exhaust Gas Recirculation (EGR). The extreme ambient condition of the spray chamber is chosen to 200°C in temperature and 4bar in absolute pressure. In order to achieve the required condition, a 3kW electric circulation air heater has placed after the air reservoir, which can

pressurize shop air to 4bar. The outlet of the heater is connected to the chamber with a high-temperature resistant ball valve in between. The air supply line is divided into 4 branches at the inlet of the chamber to achieve uniform chamber temperature easily. And the position of the air inlet is the vicinity of the windows in order to enhance vaporization of fuel film from the surface of the window by hot and strong inlet air flow. The chamber outlet is connected to a vacuum pump which enable to provide the cylinder pressure as low as 0.7bar in absolute. At the time of injection, two valves upstream and downstream of the chamber were closed to produce quiescent ambient. Every time injection took place, the chamber was purged by the fresh air.

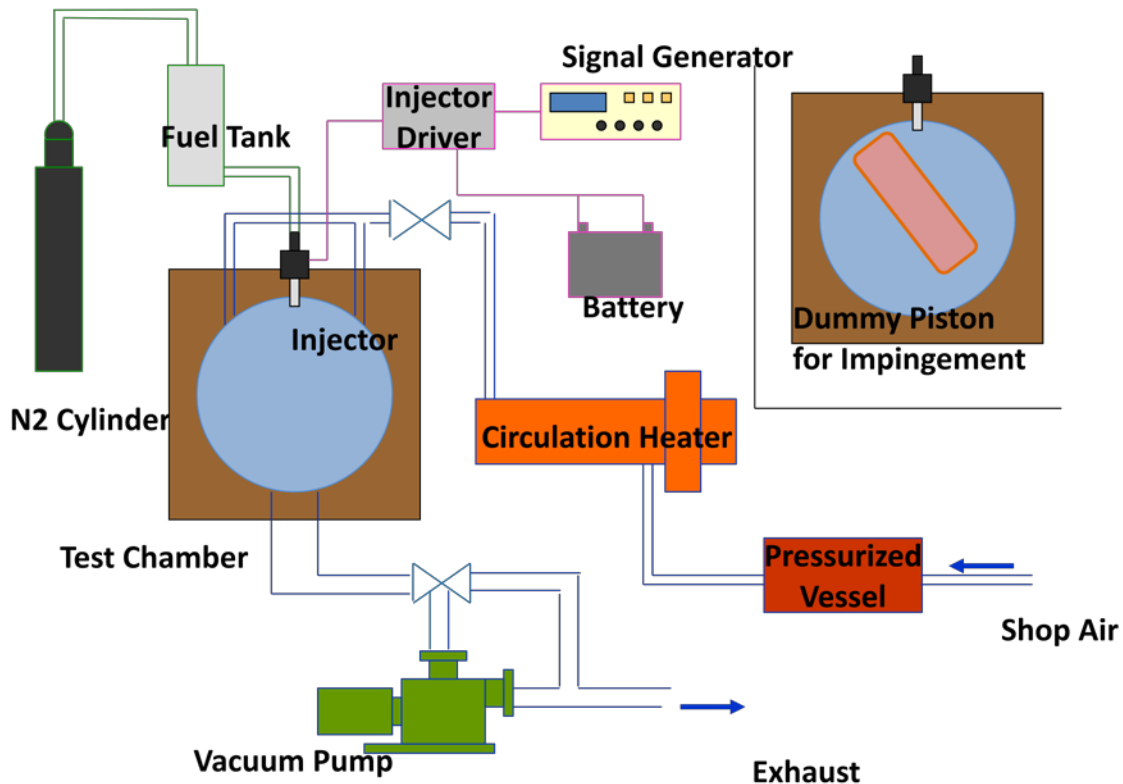


Fig. 3.1 Schematic of the spray chamber setup

Test Fuel

Three types of fuels were tested to examine the influence of ethanol content in gasoline fuel on spray formation. They are 100% pure ethanol (E100), RON-91 gasoline (E0), and the blend of two in 50% of volume ratio (E50). The specifications of the fuels are listed in Table 3.2. In the figure, the properties of iso-Octane is listed as well for a reference. The differentiating properties of ethanol are its lower heating value (LHV) and higher latent heat of vaporization. The stoichiometric air/fuel ratio is lower than gasoline because ethanol has oxygen in its molecular structure. Since ethanol is single component fuel, it has the constant boiling point of 78.4C at the standard state. Therefore the distillation curve of ethanol is nearly flat and very different from gasoline's as discussed in Chapter 2.4 (Fig 2.2). The viscosity and the surface tension of the tested gasoline is unknown.

Table 3.2 Fuel properties of E100, E50, gasoline, and iso-Octane for a reference at standard state

	E100	E50	Gasoline	Iso-Octane
Density [kg/m ³]	789	764	739	689
Lower Heating Value [MJ/kg]	26.8	34.7	43.1	43.9
Stoichiometric Air/Fuel ratio	9	13	14.7	15.1
Latent Heat of Vaporization [kJ/kg]	904	-	380-500	300
Boiling Temperature [C]	78.4	-	25-215	99.3
Viscosity [10 ³ Pa s]	1.07	-	-	0.466
Surface Tension [10 ³ N/m]	21.9	-	-	18.2
Research Octane Number	129	-	91	100

3.1.3 Optical Accessible Engine

A single cylinder optical accessible engine (OAE) was utilized for the study of in-cylinder charge motion. Fig. 3.2 shows a photograph and the schematic cross section of the OAE, and Table 3.3 summarizes the OAE specifications. The OAE operated with the same production cylinder head which was used in the fired metal engine testing as described in Chapter 2.3. The head is designed for side-mounted direct injection SI engine. Since the OAE allows single cylinder operation only, the cylinder number one was used for the testing. Other cylinders were deactivated by taking out the valve stems. The OAE was naturally aspirated without throttle. The bore and the stroke of the OAE is 86mm and 108mm respectively. The geometrical compression ratio is 12. It should be noted that the production engine has 86mm stroke, and the compression ratio is 11.8. The cylinder liner is made of quartz allowing full stroke visualization with the side view. The use of a Bowditch piston with a flat quartz window, which provided an optical path to the bottom of the combustion chamber, eliminated the similarity with respect to piston geometry; i.e. the optical piston does not have a piston cavity and valve recesses. These optical accesses were used either for lighting or imaging by the camera depending on the camera position at the side view or the bottom view. The piston have two piston rings and one piston rider made by filled PTFE for better sealing without lubricant. Because of the stroke and piston geometry difference, direct comparison of the results of OAE and metal engine are compromised. However, direct imaging of the interaction of the GDI spray and the air charge motion created by the tumble port of the head is still worth to study.

The optical engine was equipped with TDC and CAD encoders. The resolution of the CAD encoder is 400 signals per revolution. The signals were transferred to a Labview interface, and it provided definition of the injection timing pulses which were sent to an injector driver module to operate the injector. The signals were used to synchronize the high speed camera simultaneously. In-cylinder pressure was monitored via an in-cylinder pressure transducer through the spark plug access. Testing was limited to motored operation at 1000 RPM.

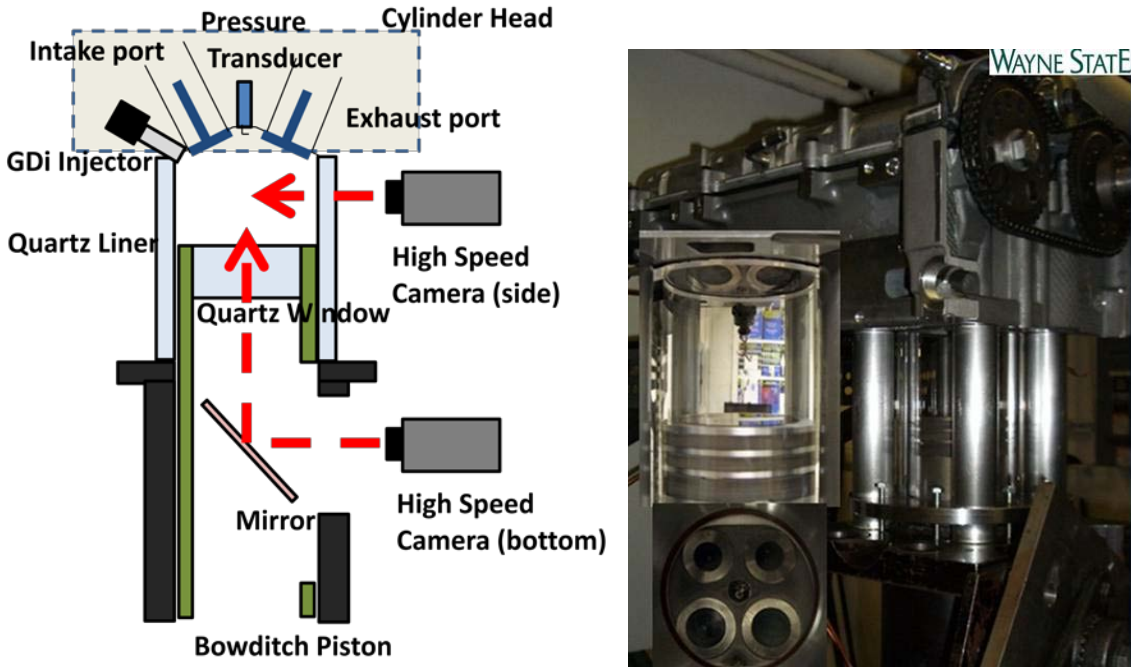


Fig. 3.2 Photograph and the schematic of cross section of the OAE

Table 3.3 OAE specification

General Configuration		Naturally aspirated Single cylinder Side-mounted direct injection	
Bore		86mm	
Stroke		108mm	
Compression Ratio		12	
Valves		2 intakes and 2 exhausts	
PROD	Intake Valve	Max Lift	10.3mm @104CAD aTDC
		Duration	263CAD
	Exhaust Valve	Max Lift	10.3mm @-84CAD aTDC
		Duration	253CAD
EIVC	Intake Valve	Max Lift	5.6mm @78CAD aTDC
		Duration	147CAD
	Exhaust Valve	Max Lift	10.3mm @-99CAD aTDC
		Duration	253CAD
LIVC	Intake Valve	Max Lift	10.3mm @129CAD aTDC
		Duration	302CAD
	Exhaust Valve	Max Lift	10.3mm @-79CAD aTDC
		Duration	253CAD
Injector		6-hole GDI Injector A & B	
Fuel		Ethanol (E100)	
Injection Pressure		10MPa	
Injection Mass		16, 32, or 9mg	
Injection Timing		30-180CAD aTDC for homogeneous 290CAD aTDC for stratified	
Motored Speed		1000RPM	

Injection Setup

The injector used in the testing was 6-hole GDI injector A and B with the spray targeting shown in Fig. 3.3. The major difference of these two injectors is the spray targeting. The injector B was designed to aim down to fill out the combustion chamber effectively. And the hole pattern is rotated 30 degree so that only one plume is injected towards the piston to attempt to reduce the amount of fuel hit the piston top. The symmetric spray pattern offered visibility of only three plumes for Injector A and four plumes for Injector B in the side view. The injector was mounted with the injector axis angle of 67 degree with respect to the cylinder axis. The injection pressure was fixed at 10MPa. The injection mass was 16 or 32mg for the injector comparison, and fixed at 9mg for the advanced valve strategy comparison which is same as the metal engine testing. Injections at 60, 120, 180, and 290CAD aTDC were tested for the study of the effect of injection timing. In addition, the tested injection timings for the advanced valve study were determined to cover the injection window of the metal engine testing which described in Chapter 2.3. It is reminded that the criterion of the injection window was based on COV less than 3% and low soot to avoid the piston impingement region. Another constraint was BSFC less than 1% over minimum BSFC that was not soot constrained. As a result, the tested injection timings were determined to 30-110CAD aTDC with every 20 degree step.

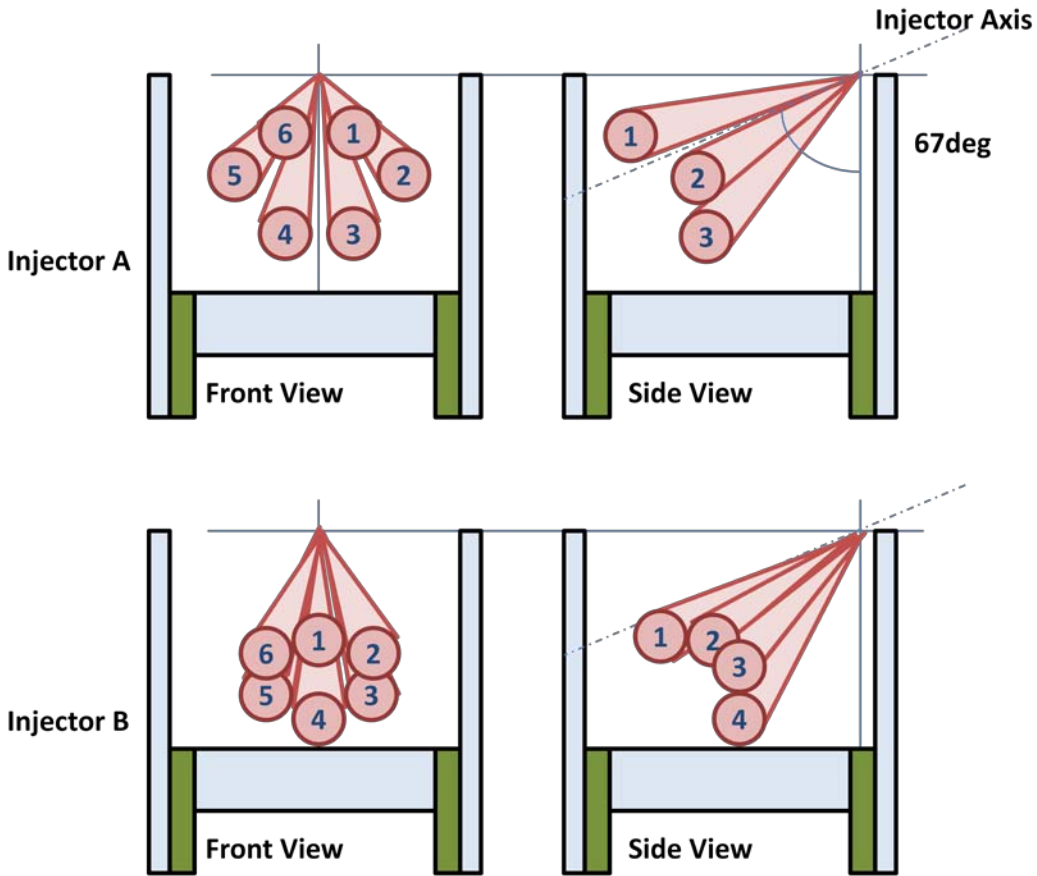


Fig. 3.3 Spray targeting and plume number of Injector A and B

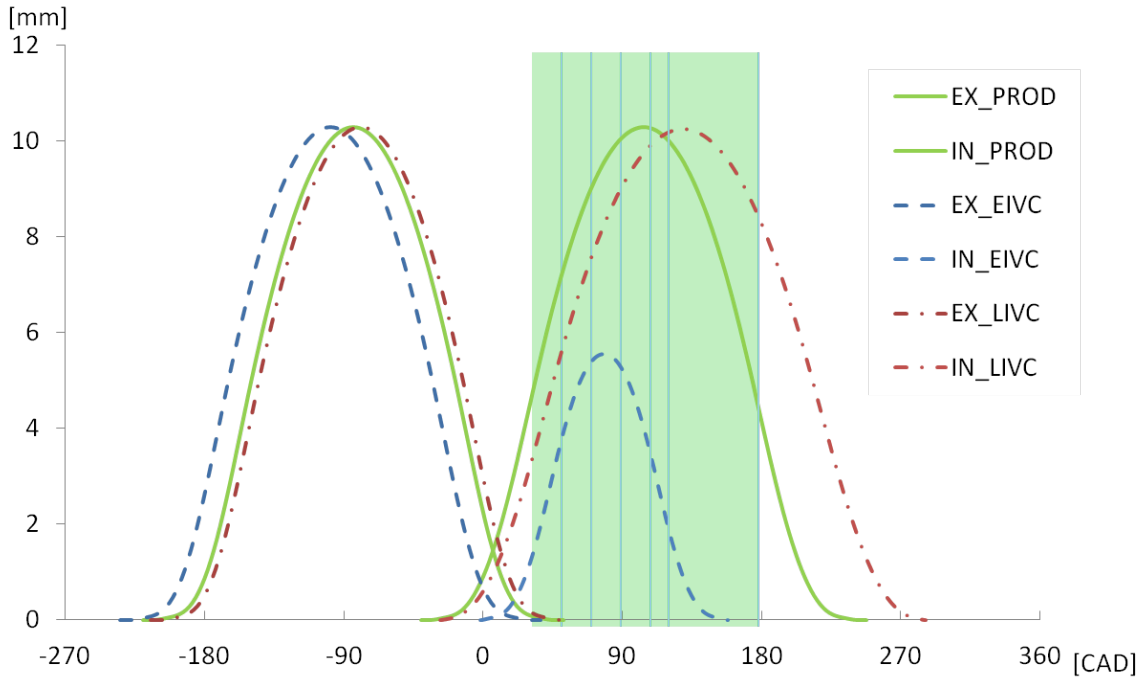
Cam Setup

Three types of intake cams, production cam, Early Intake Valve Close (EIVC) cam, and Late Intake Valve Close (LIVC) cam were tested to understand the effect of the advanced valve strategy. The exhaust cam was shared for all the testing. The cam timings of each cam are configured as Table 3.3 lists. The valve lift curve is plotted in Fig. 3.4. The production and LIVC cam configurations had sufficient valve overlap, while the EIVC cam had almost zero overlap because it was designed for low speed/load operation. The resultant pressure trace for EIVC and LIVC configurations are plotted in Fig. 4(b). The pressure drop of the EIVC configurations at the beginning of the intake

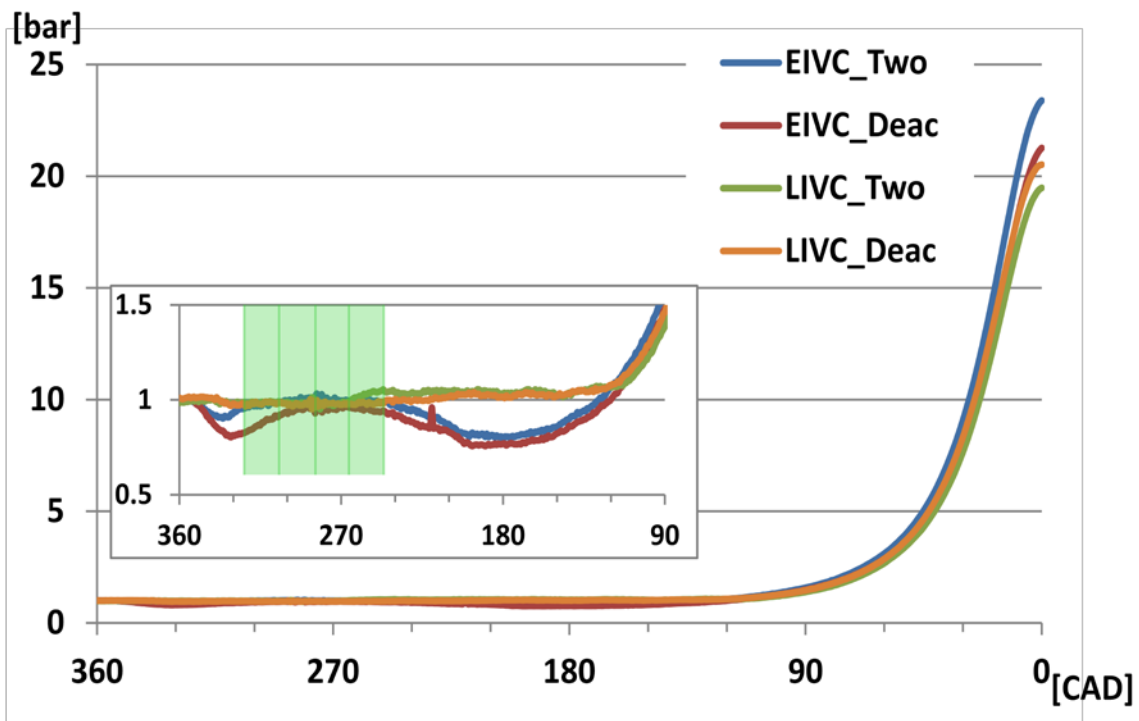
stroke indicated that low valve lift of EIVC (5.6mm at maximum) acted like a throttle by being a choke. The degree of pressure drop became approximately twice if one valve was deactivated. Since the EIVC valves closed before BDC, negative pressure by over expansion was observed again near BDC. Such pressure drops did not occur for LIVC due to its sufficient valve lift (10.3mm), but the start of compression was retarded until 120CAD bTDC firing (240CAD aTDC intake). This is how the effective compression ratio is managed in Miller cycle engines, and as a result of this setting, the peak pressure of two- and one-valve EIVC, two- and one-valve LIVC became 23.5, 21.4, 19.5, and 20.5bar respectively.

Test Fuel

For visualization purpose, 100% pure ethanol was used for fuel injection. Ethanol was favorable for minimization of film development on the liners and windows which degraded optical clarity. Results of the spray chamber reveals later that the spray behavior of the ethanol is almost identical with gasoline at low temperature condition such as in this optical engine work.



(a) Valve lift curve with injection window



(b) Pressure trace with zoomed plot of intake stroke

Fig. 3.4 Valve lift profiles and the resultant cylinder pressure with the tested injection timing window

3.2 Optical Measurement System

In order to capture the spray development, a high speed digital camera has been used. The camera speed was set for the best frequency with the chosen resolution for each testing, which is summarized in Table 3.4. The table also shows the corresponding interval between frames for each frame speed. The bottom view of the OAE testing employed lower rate than its maximum speed because of necessity of synchronization with the side view movies. The injection signal was used to trigger the high-speed camera to synchronize the camera to the injection. The lighting of OAE was simple as setting two 60W projection lamps at the position of minimum reflection interference. The optical setup of the chamber testing for three visualization methods, Mie-scattering, back-lit, and Schlieren are introduced as follows.

Table 3.4 Camera resolution and speed

	Spray Chamber	OAE Side View		OAE Bottom View
Resolution [px]	512 × 512 76mm×76mm	512 × 512 110mm×110mm	480 × 640 83mm×110mm	512 × 512 84mm×84mm
Frame Speed [FPS] (Interval [μs])	8281 (120.75)	8213 (121.75)	7207 (138.75)	7207 (138.75)

3.2.1 Mie-scattering Method

A 3W copper-vapor laser was used for the light source of Mie-scattering. A copper-vapor laser uses vapors of copper as the lasing medium. Since the laser is emitted as a sequence of pulses which duration is in the order of nanosecond, it is suitable for high speed imaging. The actual exposure time becomes equivalent to the pulse width of the laser, no matter what the camera setting is, when the frequencies of the laser and camera are synchronized. The top view of the Mie-scattering visualization setup for the chamber test is shown in Fig. 3.5. The incident light coming through the side window was perpendicular to the camera axis. The laser beam is expanded at the magnifying lens to illuminate the whole spray.

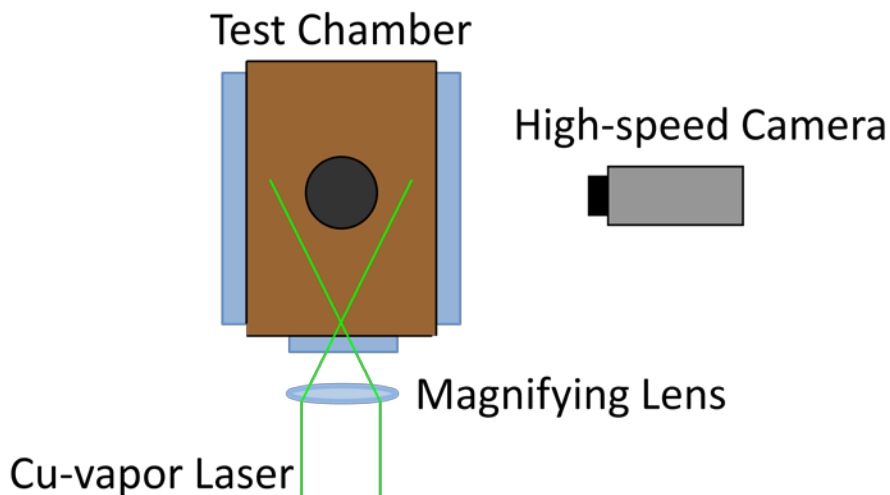


Fig. 3.5 Mie-scattering visualization setup for the chamber test

3.2.2 Back-lit Method

Back-lit requires light source on the other side of the camera as Fig. 3.6 illustrates. The light source was two 60W projection lamps. In order to eliminate the effect of un-uniformity of the light source on the image background, a light-scattering sheet was placed between the light source and the spray. The exposure time of the camera was set to $10\mu\text{s}$.

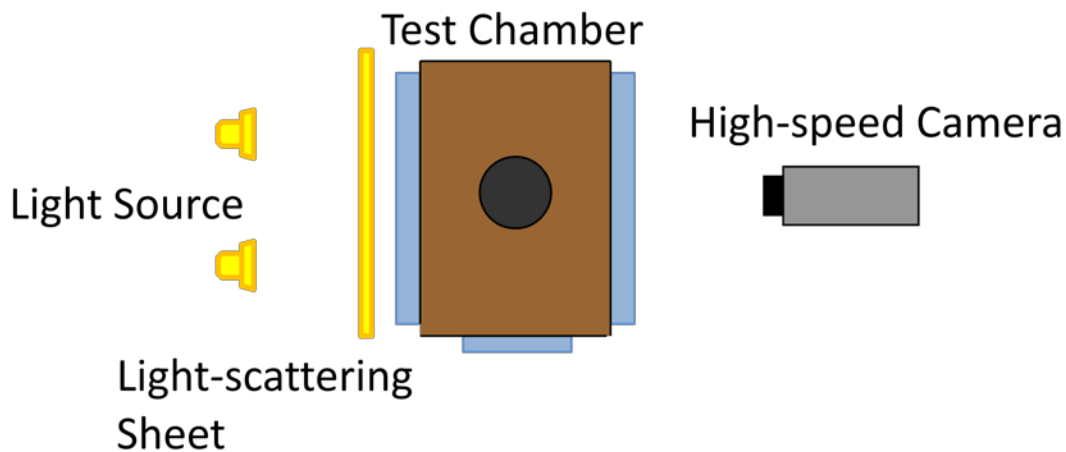


Fig. 3.6 Back-lit visualization setup for the chamber test

3.2.3 Schlieren Method

Fig. 3.7 illustrates the top view of the basic scheme of the Schlieren setup. The light source was a 60W projection lamp which was strong enough to set the exposure time of the camera $2\mu\text{s}$. The light coming from the source passed the pin hole, which was placed on the focal length of the first magnifying lens. As a result, the beam after the lens became parallel. Then the parallel light proceeded through the chamber where the injection events took place, and reached the other magnifying lens. On the focal point of second lens, there was a knife edge placed to cut the refracted light beam. And

finally, the beam came into the high speed camera. This "straight" layout of Schlieren takes large space to set up, but the simplest optical passage guarantees good quality of the resultant image.

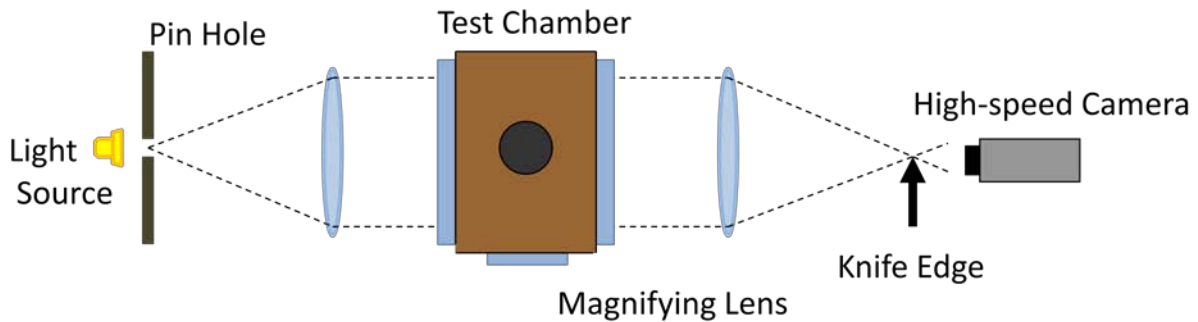


Fig. 3.7 Schlieren visualization setup for the chamber test

3.3 Image Processing of Schlieren Result

The Schlieren images taken by the high speed camera should be processed for better understanding of the captured event. Spray penetration, spray angle, area of projected image, and position of the centroid of the spray were measured with the spray chamber test results in order to represent the spray shape. The image processing of Mie-scattering and shadowgraph images is simple as adjusting image intensity or setting a threshold value to distinguish the spray and background. However, Schlieren images need more than that because the vapor area of the spray consists a gradation of black and white and it is difficult to resolve. All scripts introduced here were written and run with MATLAB.

First, a raw image was subtracted from a background image to reduce the effect of inhomogeneity of the light source. This also eliminated black spots caused by dusts

on the windows and the lens. The obtained image was filtered through a Low Pass Filter (LPF) by the Fourier Transform to make the background more uniform. The MATLAB built-in function of Fast Fourier Transform (FFT) was used for the calculation. The equations of FFT and inverse FFT are given by;

$$X(k) = \sum_{j=1}^N x(j) \omega_N^{(j-1)(k-1)}$$

$$x(j) = \frac{1}{N} \sum_{k=1}^N X(k) \omega_N^{-(j-1)(k-1)}$$

where $\omega_N = \exp(-2\pi i/N)$ is an Nth root of unity. And the filter was a disc which area is half the total area of the image. The process and the background intensity change are illustrated in Fig. 3.8.

Then a threshold was applied to convert the figure to a binary image. The discriminant analysis, as known as Otsu's method [71], was used to determine the threshold value. An optimal threshold is selected by the discriminant criterion so as to maximize the separation of the resultant classes in gray levels. The histogram of the spray image must have two peaks which represent spray body and background. Considering as the whole histogram is a mix of two classes, the threshold can be the value to maximize the inter-class variance. Variance indicates the degree of variety of the subjects, also known as a square root of the standard deviation, which is expressed as;

$$Var = \sigma^2 = \frac{1}{n} \sum_{i=1}^n (x_i - \bar{x})^2$$

where n is a number of subjects and \bar{x} is a mean value of the subjects. The inter-class variance with the threshold k is expressed as;

$$\sigma(k)^2 = \omega_0(\mu_0 - \mu_t)^2 + \omega_1(\mu_1 - \mu_t)^2$$

where ω_n is probability of occurrence for each class 0 and 1, and μ_n is an average for each class. μ_t represents the average of all pixels. The probability is given by;

$$\omega(k) = \sum_{i=1}^k \frac{n_i}{N}$$

where n_i denotes the number of pixels at gray level i . Since the classes are separated by the threshold value, the probability and class average are functions of the threshold.

The threshold value for maximum inter-class variance can be found by iteration.

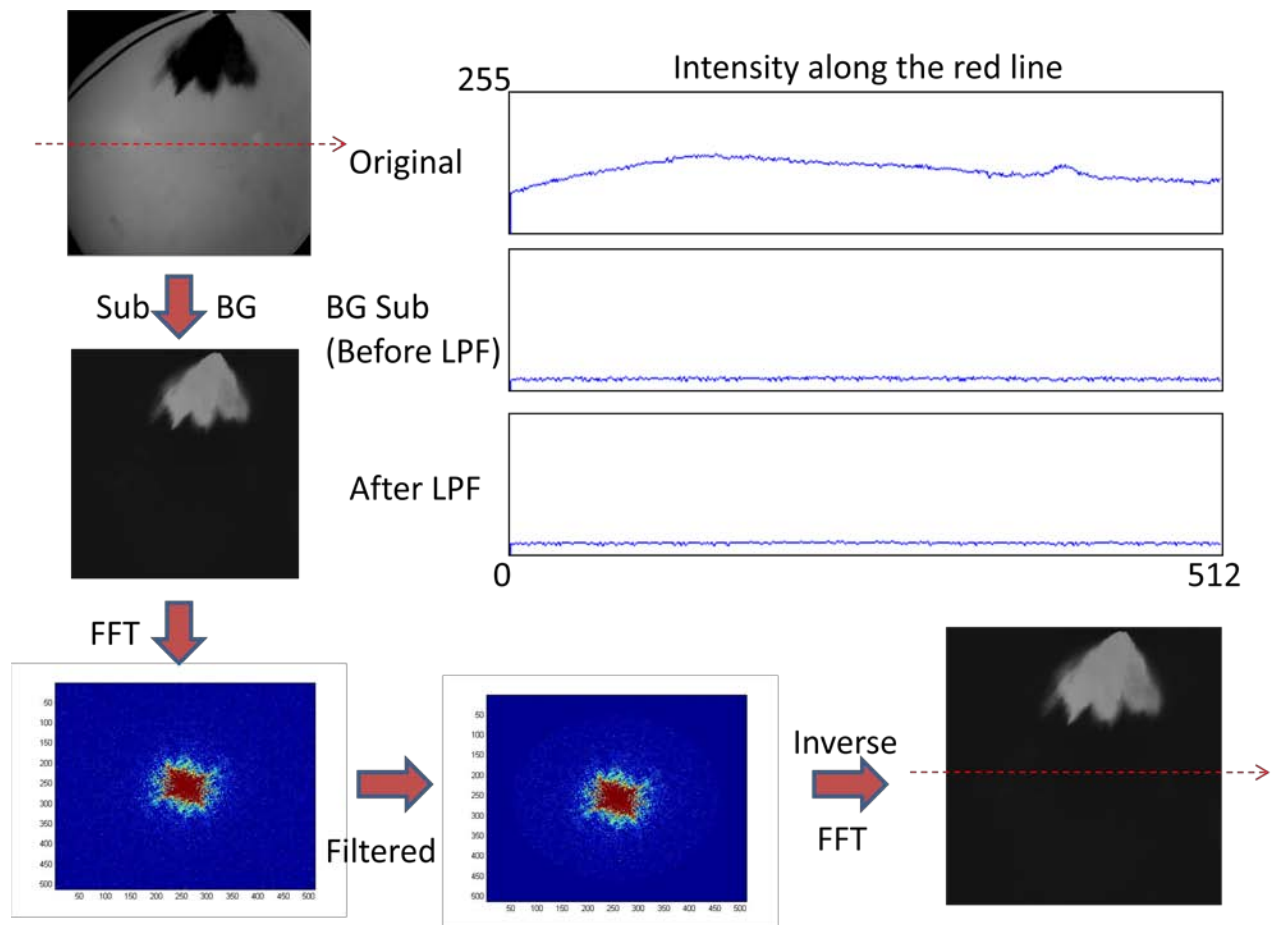


Fig. 3.8 Process of noise reduction

Although the threshold value found by the discriminant analysis can separate the dense spray from the background, simple thresholding could not pick up the vapor area for the most cases as shown in Fig 3.9. The red circles indicate the points of insufficiency of the spray area. In order to catch the vapor phase, 2-step thresholding is proposed which is a combination of simple thresholding and thresholded image of the variance of the image.

The idea is to consider the vapor area as a sort of wave motion of lean and rich (black and white) regions, where the variance of a partial section (5x5 pixels for example) must be larger than other relatively uniform areas of the spray center and the background. After calculation of partial variance, the value was returned in the center of the small square. And Otsu method was applied on it to make another binary image. As shown in Fig. 3.9, variance-based thresholded image was able to capture the vapor area. The center of the spray was filtered out because the thick spray cloud area had relatively uniform gray level. Then two binary images were added together and after applying Median filter to eliminate the isolating dots, the final binary image of spray was obtained.

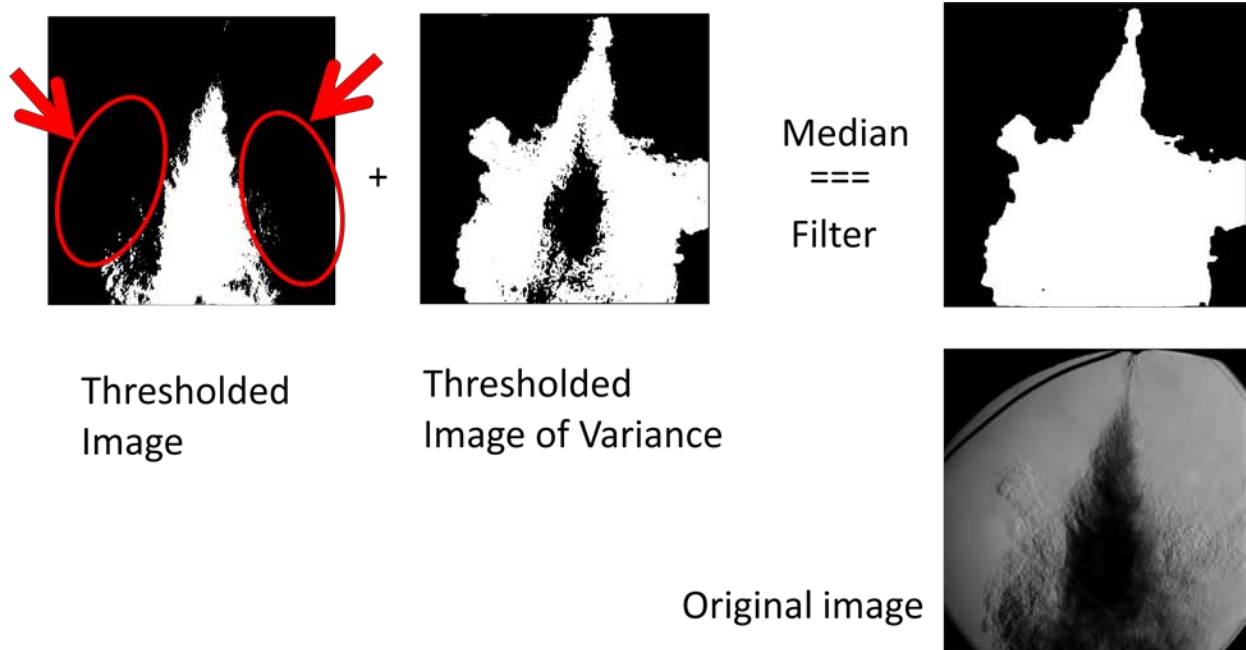


Fig. 3.9 Example of resultant image of a 2-step thresholding

The final binary images are processed to measure all four parameters; spray area, position of the centroid, penetration, and cone angle. The area of projected image was obtained simply counting the number of white pixels and converted to metric unit.

The position of the centroid of the spray was calculated by;

$$(X, Y) = \left(\frac{\sum_{i=1}^N \sqrt{(x_i - x_0)^2}}{N}, \frac{\sum_{i=1}^N \sqrt{(y_i - y_0)^2}}{N} \right)$$

where (x_0, y_0) is a reference point, and N is a number of white pixels. The gray level of the sprays was ignored because it did not represent the density of the spray directly due to superimposed plumes. Fig. 3.10 illustrates the definition of penetration and spray angle. Spray penetration was defined as a length from nozzle tip to the tip of the plumes. It indicates how far the spray travels with respect to time. In this paper, averaged

penetrations of all plumes are presented in the results chapters unless distinction of plumes is impossible. Three spray cone angles depending of the measured position were computed to quantify how the spray is widely distributed. Spray angle was defined as an angle between two lines (yellow lines in Fig. 6) which connect two intersections and the nozzle tip at 5, 10, and 20mm downward from the injector tip.

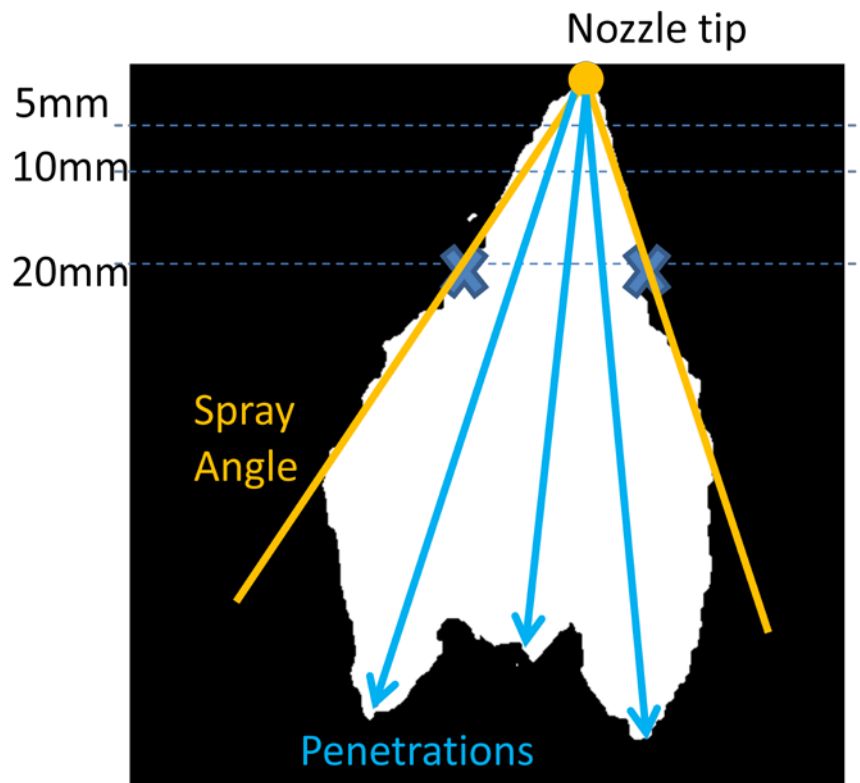


Fig. 3.10 Definition of penetration and spray angle

3.4 Numerical Simulation Setup

Simulations of multi-hole spray were carried out with CONVERGE, a commercial three dimensional CFD software [72] [70]. CONVERGE is a CFD code which is optimized for engine simulation. For example, it is equipped with automatic grid generation and mesh refinement, and easy setup of moving boundary helps simulate in-cylinder event as well as stationary spray chamber.

As many other CFD codes, CONVERGE relies on assumptions and empirical models for its calculation. In CONVERGE, spray calculation is based on Discrete Droplet Model (DDM). The droplet drag coefficient was determined by the dynamic drag model for accurate spray modeling [73]. No Time Counter (NTC) method were chosen for and collision model. The time rate of change of droplet radius due to ethanol vaporization is calculated from the Frossling correlation [74]. The turbulence model was the rapid distortion renormalization group (RNG) k - ϵ model, which is one of the Reynolds-averaged Navier-Stokes equation models [75]. This model is designed for rapid compression or expansion and therefore well suited for engine simulations. In addition, the Han and Reitz heat transfer wall model is used for the simulation. Kelvin-Helmholtz and Rayleigh-Taylor models, known as the KH-RT model developed by Reitz was chosen for the break-up model. KH model simulated the primary aerodynamic instabilities breakup and the RT model calculated the secondary decelerative instabilities breakup. Only KH instabilities are responsible for drop breakup inside of the breakup length, while both KH and RT mechanisms are activated beyond the breakup length [72][70]. In the KH breakup model, the initial parcel diameters were set equal to the nozzle hole diameter.

The calculation domain included the cylinder and the intake and exhaust ports as shown in Fig. 3.11. The coordinate (XYZ) is also shown in the figure. The piston crown represents the geometry of the fired metal engine discussed in Chapter 2 instead of the flat crown geometry of the OAE. Although the base grid size was 8mm, the embedded mesh refinements made the mesh finer at critical areas near the injector and the intake valves. The finest mesh size was 0.5mm at the injector tip area. In addition to the embedded grid control, CONVERGE is able to use Adaptive Mesh Refinement (AMR) automatically to enhance the mesh around the spray edge as shown in Fig. 3.12. The level of embedding for velocity, temperature, and mass fraction in this study was set to 3, which made the mesh size 1mm where AMR was turned on.

In the simulation, the effect of injector design, injection timing, and valve strategies of EIVC and LIVC cams were evaluated at 1000RPM. Fuel properties were specified to represent 100% pure ethanol. The injection timing of advanced valvetrain testing was at 60CAD aTDC for all the cases except the validation, in which 90CAD was chosen. The calculation time step was set to 1 μ s.

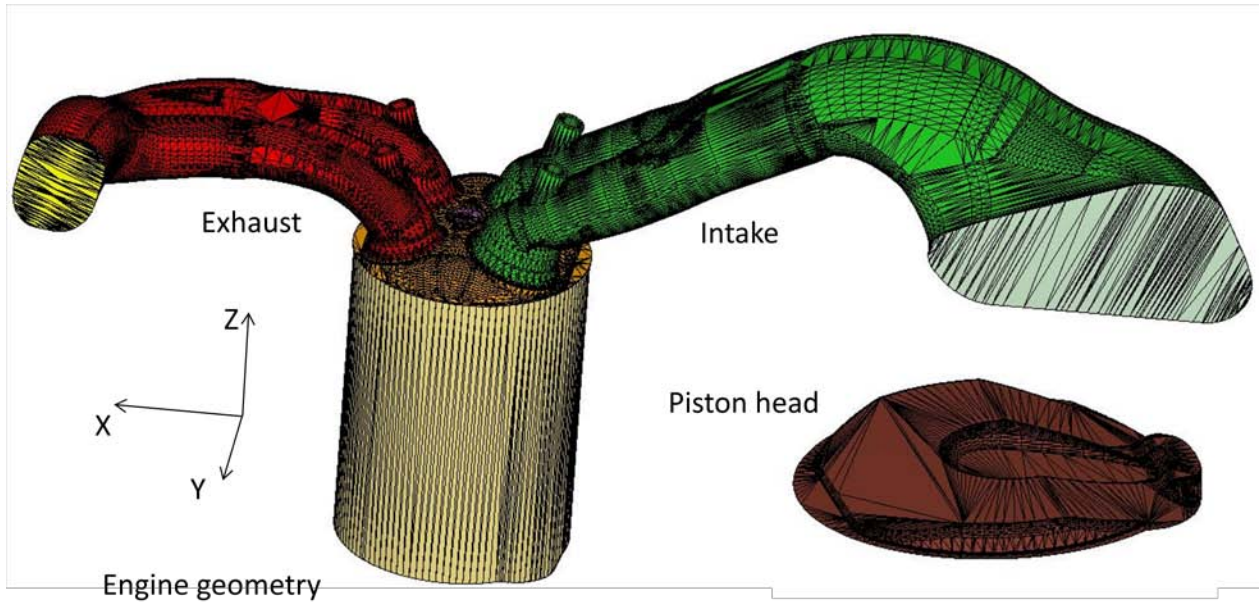


Fig. 3.11 Simulation domain and the coordinate

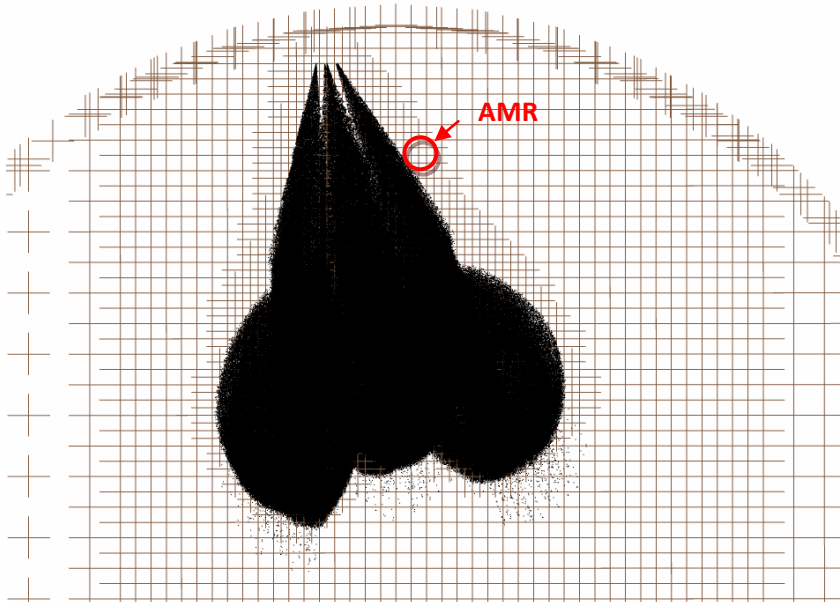


Fig. 3.12 Adaptive Mesh Refinement (AMR)

CHAPTER 4 “Result of Chamber Testing”

In this chapter, the result of high-speed spray visualization performed in the spray chamber is discussed. At first, different visualization techniques are compared for understanding and interpretation of the resultant images. And the sample Schlieren images are investigated. Then the Schlieren imaging results of multi-hole spray testing is studied. The effect of different conditions including ambient conditions (temperature, pressure) and injection conditions (fuel type, fuel temperature, nozzle design) on spray formation is discussed in both qualitative and quantitative methods. Then the spray behavior after piston impingement is examined briefly. The spray of outward-opening pintle injector is evaluated as well by Schlieren imaging.

4.1 General Discussion of Schlieren Image

4.1.1 Optical Method Comparison

Three different imaging techniques were compared for better understanding of spray visualization and interpretation of the images. Only Injector A and pure ethanol (E100) as fuel were used through this test. The injection command pulse width was 1.5ms for all the cases. Mie scattering and back-lit (shadowgraph) photography have been widely adopted for spray visualization. It has been reported that good resultant image can be obtained for liquid spray visualization though, these techniques are not suitable for vapor visualization due to their optical feature.

Samples of raw images for three visualization methods are shown in Fig 4.1. The left two columns are comparison of Mie-scattering and Schlieren with 5MPa injection pressure, and the right two columns are comparison of Schlieren and back-lit with

10MPa injection pressure. In order to have the best comparison in terms of vapor visualization, the ambient condition was set to high temperature (200°C for back-lit and 150°C for the rest) with low pressure (1bar) to maximize the degree of vaporization. Mie-scattering result showed good contrast of bright spray and black background indicating clearly where liquid spray exists. On the other hand, the images of Schlieren was able to visualize the vapor cloud around the black spray core, which could not be seen at all in Mie scattering images. It was observed that the shape of the black region at the center of the spray of the Schlieren images were almost identical to the shape of Mie-scattering spray images at the same condition especially at 1.5ms after start of injection (ASOI). This indicates that the Schlieren method was able to capture the behavior of the liquid phase as well. It should be noted that this black region could contain not only liquid, but also very dense or thick vapor phase. The back-lit images showed some dark blur area where the vapor was supposed to exist, but they were not clear enough to insist existence of the vapor phase as the Schlieren images. It is confirmed here that the Schlieren visualization is very effective to observe a vapor envelope of a spray as well as a dense core. Therefore Schlieren visualization was adopted for spray chamber testing. As seen at the background in the sample figure, the uniformity of the light source is critically related to the quality of Schlieren images. Use of strong and uniform light source is recommended to improve the image quality.

Comparison of Mie-scattering and Schlieren result notifies that the Mie-scattering results had slightly faster penetration at 1.5ms ASOI. This must be caused by injector tip temperature difference. Throughout the Schlieren testing in this comparison, the fuel temperature was maintained at 90°C, while it was set to 60°C for the back-lit testing.

Since the fuel temperature was not controlled during the Mie scattering visualization testing, it is assumed to be heated up more than 90°C. The higher injector tip temperature of Mie-scattering case enhanced flash boiling and resulted in faster penetration. Detail of flash boiling is discussed later in Chapter 4.2.

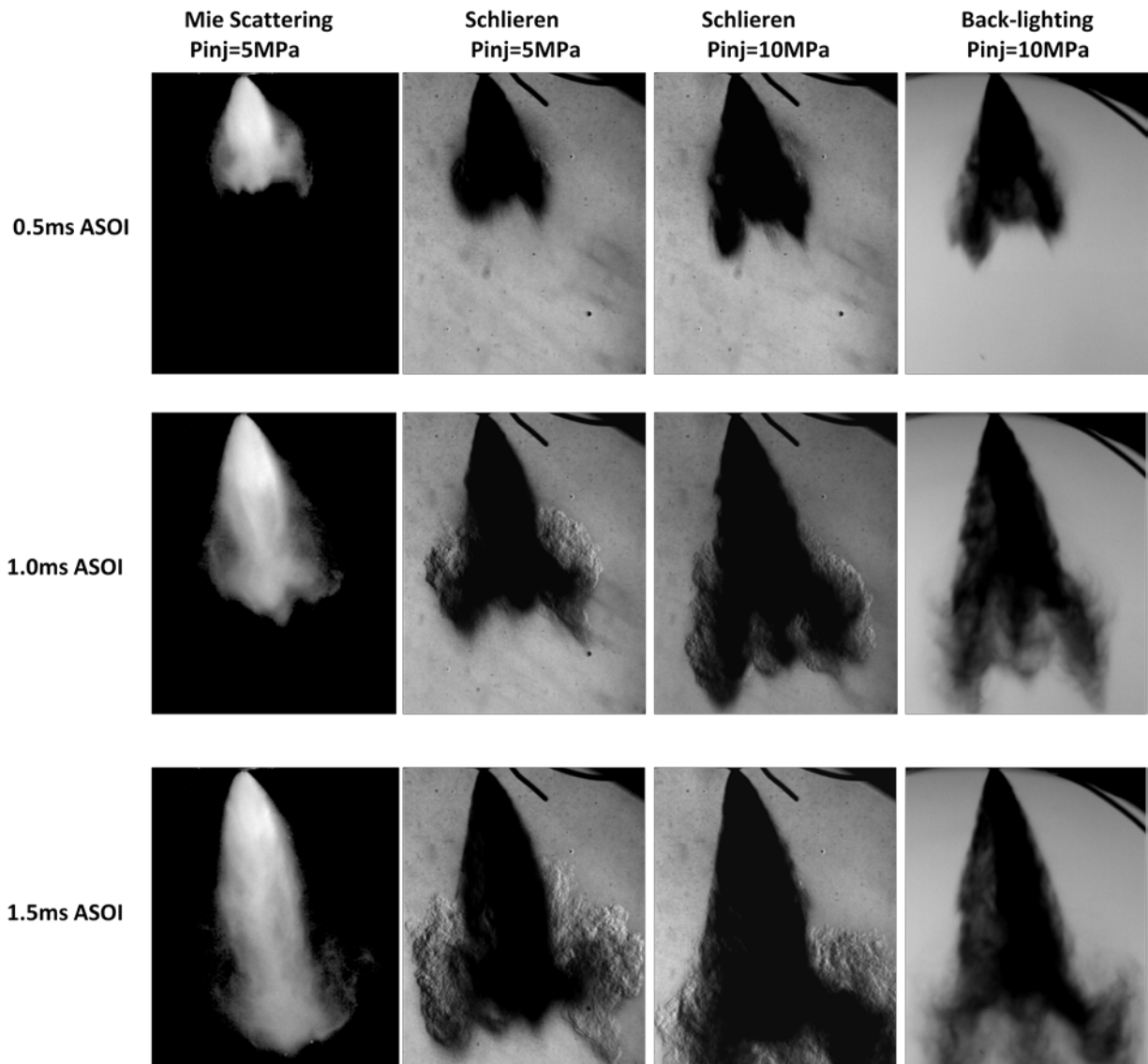


Fig. 4.1 Visualization method comparison of Injector A with E100, T=150°C (200°C for Shadowgraph), P=1bar

4.1.2 Interpretation of Schlieren Image

Schlieren images were examined to evaluate the process of vaporization. The sample Schlieren image shown in Fig. 4.2 was captured with the ambient temperature/pressure condition of 200°C/1bar and the injected fuel quantity was 5mg. The injected fuel was E100. Assumed liquid phase by image processing is also shown in the figure. The injected fuel started vaporizing from the spray surface after a few hundred microsecond delay in which spray breakup occurred. Once the fuel was vaporized, the vapor phase expanded and lost its momentum by energy exchange. And the vapor phase seems overtaken by the in-coming liquid spray. Therefore most of vapor was observed at the side of sprays at the early stage of the injection event up to 0.8ms ASOI. At the later stage, slower liquid penetration as well as accelerated vaporization due to continuing heat/mass transfer resulted in no more overtake. Vaporization proceeded from the peripheral of the plumes and completed around 1.6ms ASOI. Due to expansion of the vapor cloud and mixing by air entrainment, the resultant vapor phase after 1.5ms ASOI seems "evenly inhomogeneous" and the plumes are hardly distinguishable. It should be noted that the spray was keep penetrating even after the complete vaporization. The liquid phase penetration did not represent actual fuel distribution after vaporization. Therefore a research of vapor phase is necessary to understand the spray behavior.

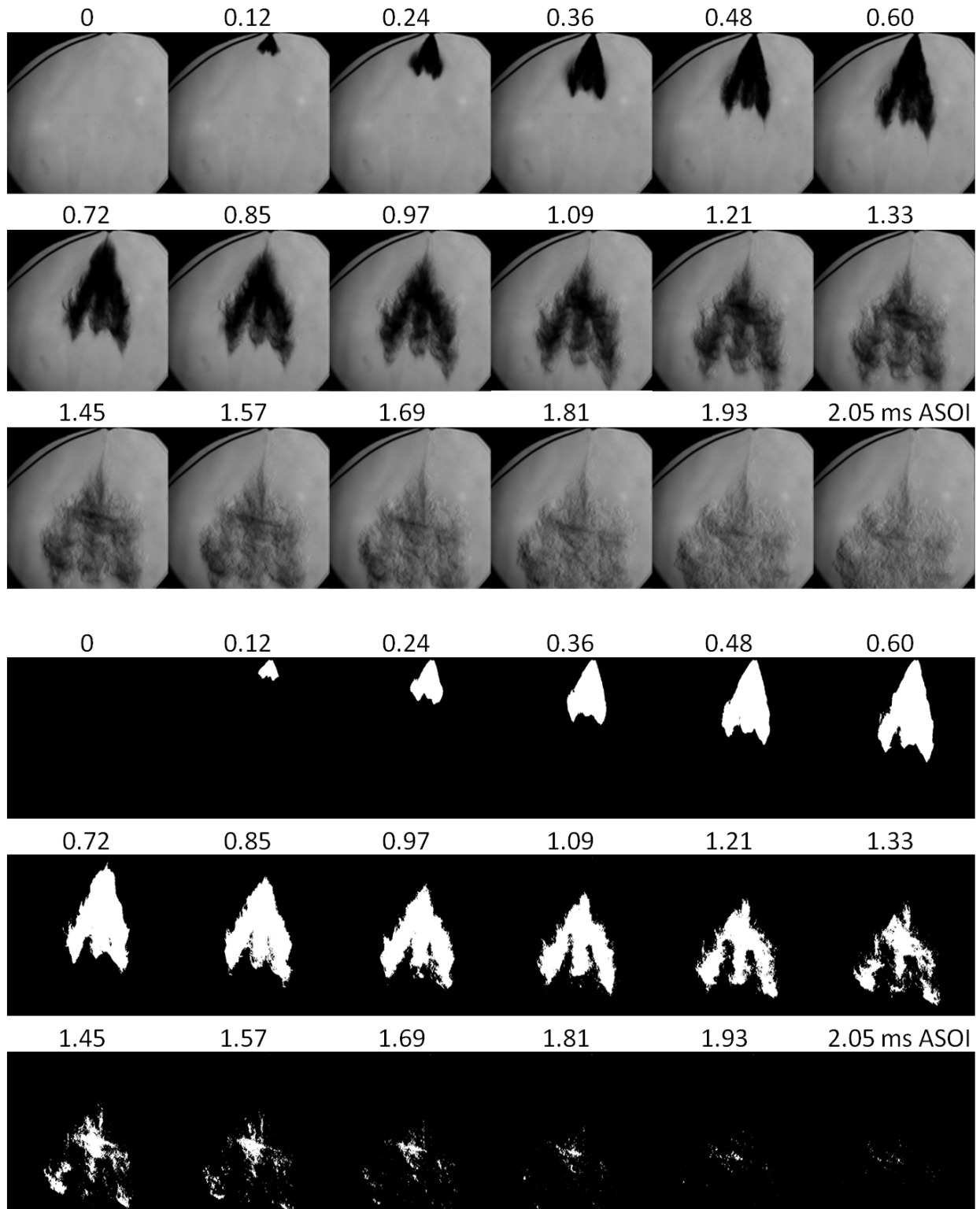


Fig. 4.2 Schlieren images and assumed liquid phase for Injector A with E100 ($T=200^{\circ}\text{C}$, $P=1\text{bar}$, $\text{Mass}=5\text{mg}$)

By comparing 5MPa and 10MPa injection pressures in Fig. 4.1, enhanced vaporization at the spray tip region and between the plumes was observed by Schlieren for higher injection pressure. This is believed to be caused by better mixing due to smaller droplets and larger amount of air entrainment that higher injection pressure could produce.

4.1.3 Summary

Three different visualization methods were compared in this section. Mie-scattering was better in liquid phase visualization because of good spray-background contrast in the resultant image. Back-lit imaging was not clear enough to evaluate the vapor phase. On the other hand, Schlieren visualization was very effective to observe the vapor phase of the spray as well as the dense core. By evaluating Schlieren images, process of fuel vaporization and fuel distribution even after the complete vaporization could be observed.

4.2 Multi-hole Spray Testing

The high-speed spray visualization by Schlieren technique was conducted using the spray chamber. First, effect of ambient condition, i.e. temperature and pressure, was examined with Injector A. The injected fuel was E100 with 1.5ms of the injection command pulse width. The fuel temperature was fixed at 60°C. Then the effect of fuel composition on the spray structure was examined with injector A again. Three types of fuel were used, 100% pure ethanol (E100), 100% pure gasoline (E0), and the blend of those two in 50% volume ratio (E50). The ambient temperature and pressure were

200°C and 1bar or 3bar to discuss the behavior of the vapor phase. The fuel temperature was fixed at 60°C. In addition, the effect of fuel temperature is discussed. Injector B was used for this testing. The fuel temperature varied from 25°C to 80°C to understand the effect of fuel temperature on the spray structure. The ambient condition was a combination of 25°C/200°C of temperature and 1bar/3bar of pressure. The influence of fuel (gasoline and E100) on the spray development is discussed as well. The energy content of the total injected fuels is kept constant; 10mg of gasoline or equivalent. Finally, three injectors are compared in terms of spray behavior. The fuel temperature was fixed at 60°C. Injector A and B are evaluated first with ambient conditions and fuel type changing. And Injector A and C are compared briefly.

4.2.1 Effect of Ambient Condition

High-speed Schlieren visualization of spray of Injector A was conducted to evaluate the effect of ambient condition, and the result is shown in Fig. 4.3. Those are the spray images for each condition at 1.0ms ASOI. Comparing 25°C and 100°C of chamber temperature at 1bar of ambient pressure, the degree of vaporization increased with the ambient temperature due to enhancement of heat transfer. However, the overall spray shape did not change much. When the temperature exceeded 150°C, more vapor was formed and the spray shape changed significantly. Penetration of the spray became shorter with the higher temperature due to energy dissipation by vaporization by enhanced mass/heat transfer (Fig. 4.4). By comparing penetration curves of 25°C and 200°C, the spray at 200°C had roughly 10% decreased at 1.0ms ASOI. With the higher ambient pressure, the spray shape change did not occur even at

the higher temperature. Image comparison of higher pressure cases just shows enhanced vaporization with the higher ambient temperature. Spray penetration was suppressed due to stronger resistance by increased air density, and the effect of ambient temperature was negligible.

The spray shape change observed in higher chamber temperature can be explained by flash boiling. It should be reminded that the boiling temperature of ethanol is 78°C. When the ambient temperature was far above the boiling temperature of the injected fuel, flash boiling instantly increased the volume of the spray and could collapse the multiple-hole plumes into a coherent spray, with a resultant spray image resembling that of an air-assisted DI spray. Once fuel is injected into high temperature and low pressure environment, the injected liquid is exposed to huge pressure drop as well as incoming heat transfer. Flash boiling occurs when the pressure of fuel drops instantly below the saturation pressure at certain temperature as Fig. 4.5 schematically explains. The saturation pressure and temperature data were taken from the reference [76]. It is believed that the flash boiling was not observed at higher ambient pressure because the pressure drop was not large enough to end up with fuel pressure less than the saturation pressure. The complexity of flash boiling sprays includes effects not only of ambient temperature and pressure, but of fuel temperature and pressure, and a combination of other effects, including injector nozzle design. For example in Fig. 4.1, the reason of longer penetration of Mie-scattering spray at 1.5ms ASOI than the 5MPa Schlieren spray can be the existence of flash boiling due to its higher fuel temperature. If the injection pressure increases, the flash boiling effect was less noticeable because larger initial momentum of the spray overcame the effect of the flash boiling which was

induced by sudden volume increase. The effect of fuel temperature and nozzle design is discussed later in this chapter.

It should be noted that the effect of flash boiling is not preferable for regular GDI multi-hole injector because it can destroy the well-designed spray targeting. Instant vaporization itself is attractive for engine operation. However, the local equivalence ratio could vary a lot inside the combustion chamber by the merged spray even though the fuel is well vaporized. As a result, uneven local equivalence ratio at the time of ignition can cause poor combustion stability.

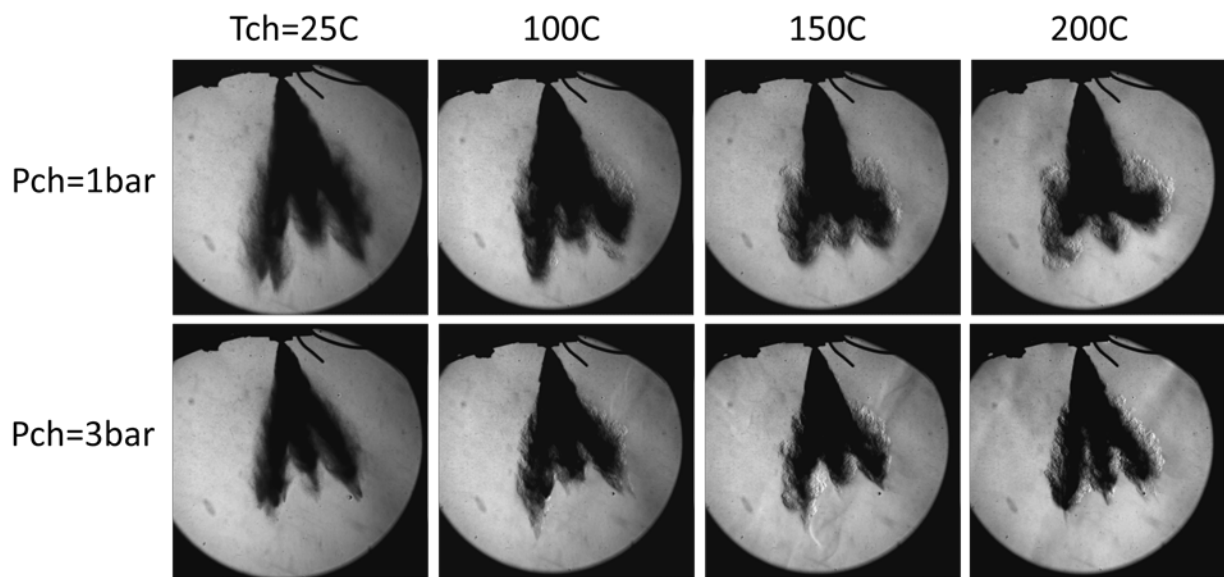


Fig. 4.3 Effect of ambient temperature and pressure at 1.0ms ASOI

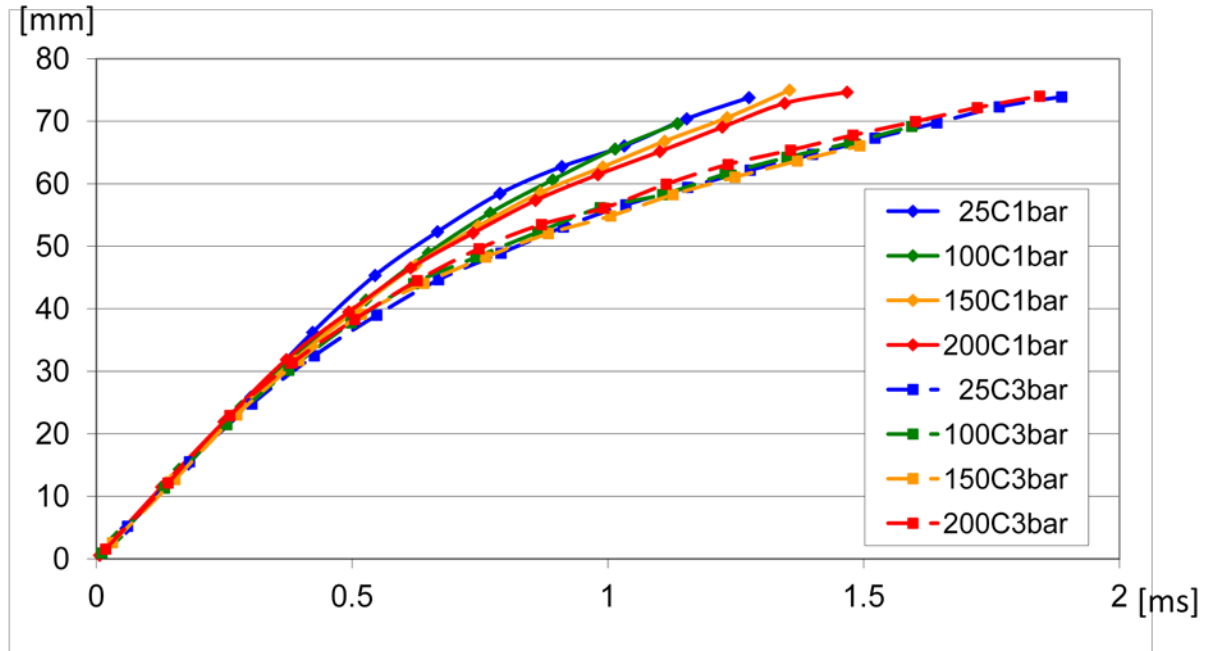


Fig. 4.4 Effect of ambient temperature and pressure on E100 spray penetration

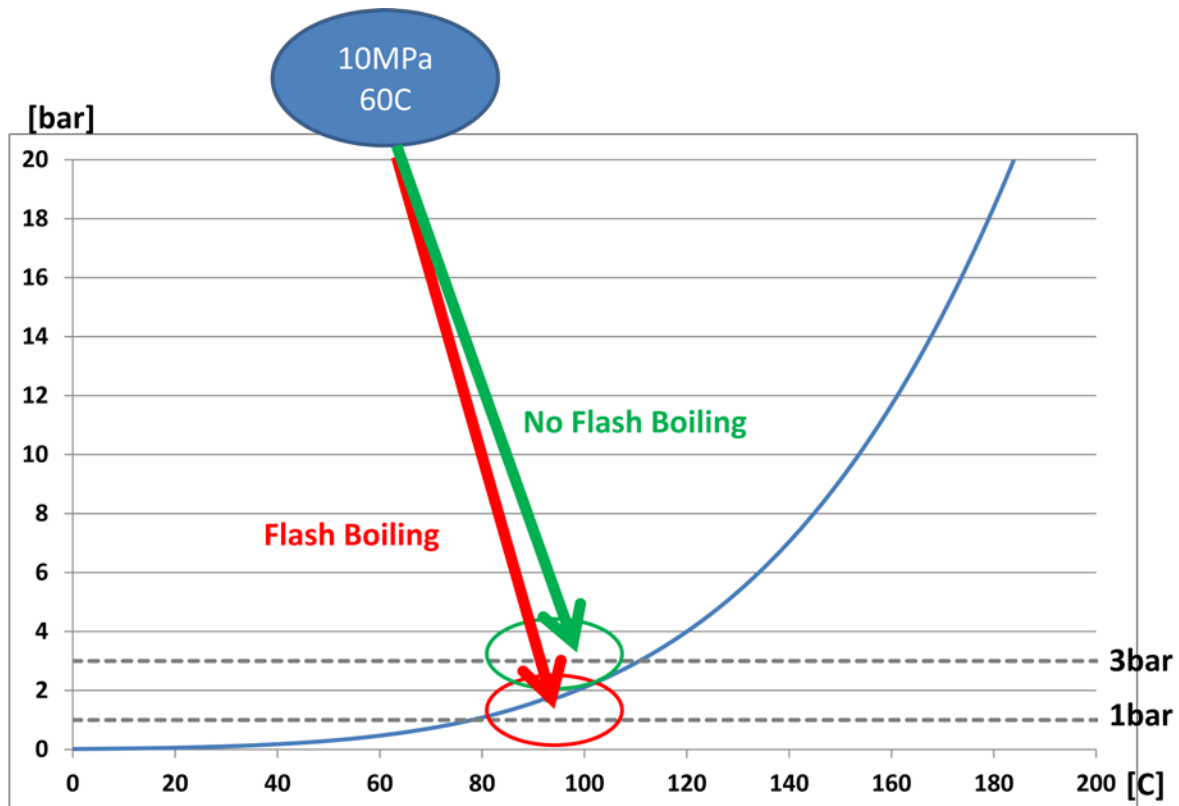


Fig. 4.5 Saturation pressure curve of ethanol and flash boiling

4.2.2 Effect of Fuel Composition

In this section, the effect of fuel composition on spray formation is examined. E0 (pure gasoline), E50 (50% gasoline and 50% ethanol), and E100 (pure ethanol) were tested. The injection quantity was determined based on two criteria. First criterion was constant injection volume by fixing the injection command pulse width (PW). The objective of this test is to evaluate the effect of fuel composition with the same injection condition. The other criterion was constant injected energy by fixing total heating value of each fuel. This is considered as more realistic flex-fuel operation, because the required energy is constant for a certain load condition.

Constant Injected Volume

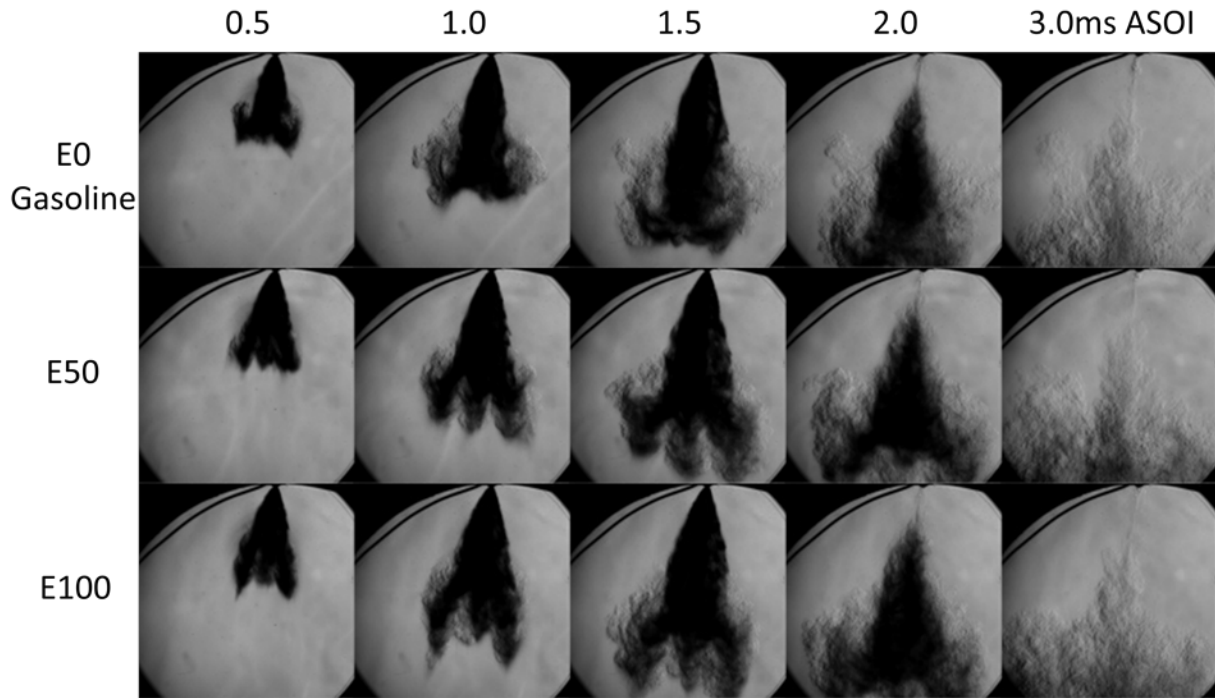
Pulse width of 1.5ms was chosen with the ambient condition of 200°C/1bar. The corresponding injected mass was 24.9mg for gasoline. The resultant images of the effect of fuel composition with constant injected volume are summarized in Fig. 4.6. At the early stage of injection, separation of plumes in E50 and E100 spray was observed, while the plumes of gasoline collapsed by flash boiling. At 0.5ms ASOI, the gasoline spray already showed some vapor at the surface of the spray. And more vapor cloud could be observed at the side of the spray jet with gasoline fuel at 1.0ms due to side plume bending by flash boiling. The instant vaporization by flash boiling must contribute for development of the side vapor too. The effect of flash boiling was stronger with pure gasoline because it contained hydrocarbons which had lower boiling point than ethanol. Commonly gasoline contains C4-C12 hydrocarbons, and C4 to C6 hydrocarbons has less boiling point than ethanol (Table 4.1). The fuel was vaporized as the time elapsed,

and the liquid core of the spray disappeared at 3ms ASOI. Although the vapor of gasoline was found to be widely distributed in the area from middle to bottom of the image, E100 vapor was detected mainly at the bottom of the image already at 2ms ASOI as the binary image shows. The sprays had vapor "wings" at the side of the sprays, and the position of the "wing" became lower with increased ethanol in the fuel. These results indicate that slow vaporization of E100 fuel at the beginning. The liquid fuel kept penetrating and traveled farther while the vaporized fuel lost its momentum and slowed down. The slow vaporization of ethanol can be considered as a result of relatively higher initial boiling point, which is 78°C at 1bar. On the other hand, gasoline generally contains lighter hydrocarbons which boiling points are lower than ethanol.

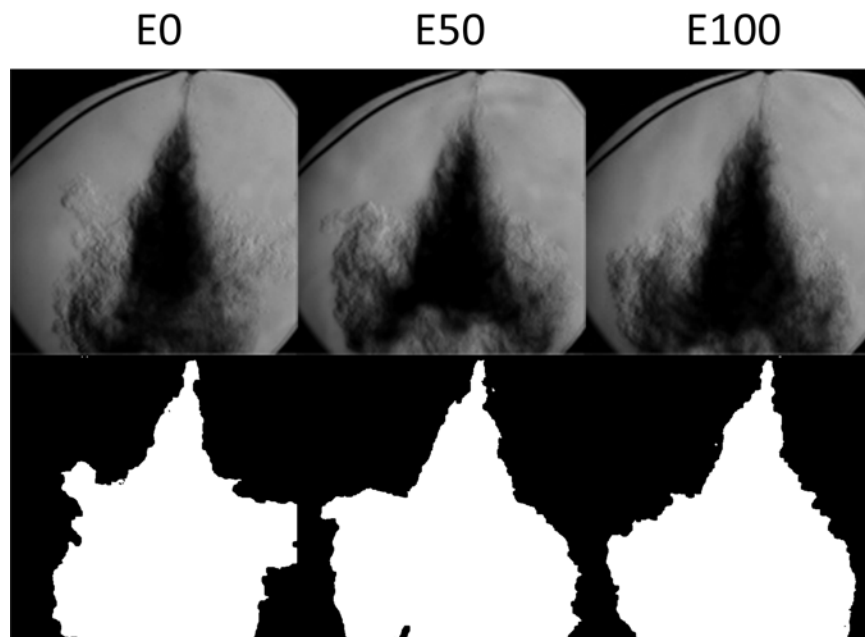
The position change of vapor could be critical especially if this injector is used for a spray-guided GDI engine, in which the ignition takes place right after the injection. The location of the "vapor wing" could be the position of spark discharge. The vapor location change by fuel composition must be taken into consideration if the engine is designed for flex-fuel operation.

Table 4.1 Boiling point of Alkane (C4-C8) [76]

	Formula	Boiling Point [°C]
Butane	C ₄ H ₁₀	0 ±1
Pentane	C ₅ H ₁₂	36.1 ±0.2
Hexane	C ₆ H ₁₄	68.8 ±0.3
Heptane	C ₇ H ₁₆	98.4 ±0.3
Octane	C ₈ H ₁₈	125.6 ±0.5



(a) Raw image comparison



(b) Binary image comparison at 2ms ASOI.

Fig. 4.6 Effect of fuel composition. $T_{ch}=200^{\circ}\text{C}$, $P_{ch}=1\text{bar}$, $T_{fuel}=60\text{C}$, $PW=1.5\text{ms}$

The effect of fuel was studied quantitatively. Fig. 4.7 shows penetration of the plumes of the spray with different fuels. The figure shows the results from three identical testing for each fuel, and the results demonstrate good consistency. Stable sprays are supposed to be an advantage of multi-hole injector, and it is confirmed experimentally. Up to 0.3ms ASOI, spray penetration was identical for all fuels. After that, gasoline spray was under influence of flash boiling, and started vaporizing and dissipated its momentum to slow down. Although the penetration of gasoline was slower at the middle of the figure from 0.8-1.6ms ASOI, it decelerated slower than ethanol sprays as time elapsed. The heavier components of gasoline must have more resistance to complete vaporization and kept penetrating more than the single component ethanol spray. The shape of E50 penetration resembled E100, but it was slightly slower because of vaporization of gasoline portion. As a result, penetration of E100 and E50 spray was 12.3% and 7.1% longer respectively than gasoline spray at 1.0ms ASOI.

The total areas of vapor and liquid phases of the projected spray were almost same for all fuels (Fig 4.8). The spray projection area was calculated up to 1.5ms since the spray reached at the bottom of the image at that time. The liquid spray of E0 shows less area because of liquid phase accumulation by plume collapse. In Fig. 4.6, more vapor fuel distribution at the middle of the image was observed with the pure gasoline fuel. This vapor cloud lead to almost identical total spray projection area for all three fuels even though the gasoline spray plumes collapsed into one jet due to flash boiling for smaller liquid area.

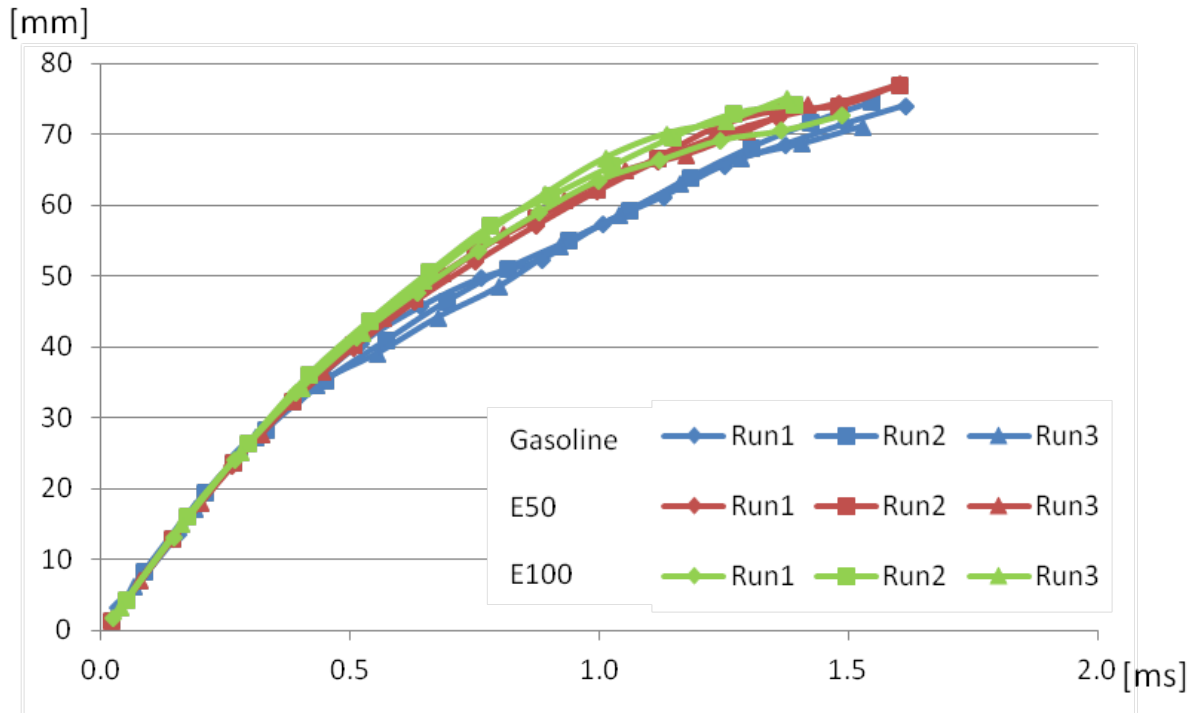


Fig.4.7 Penetration of spray for different fuels with fixed PW of 1.5ms

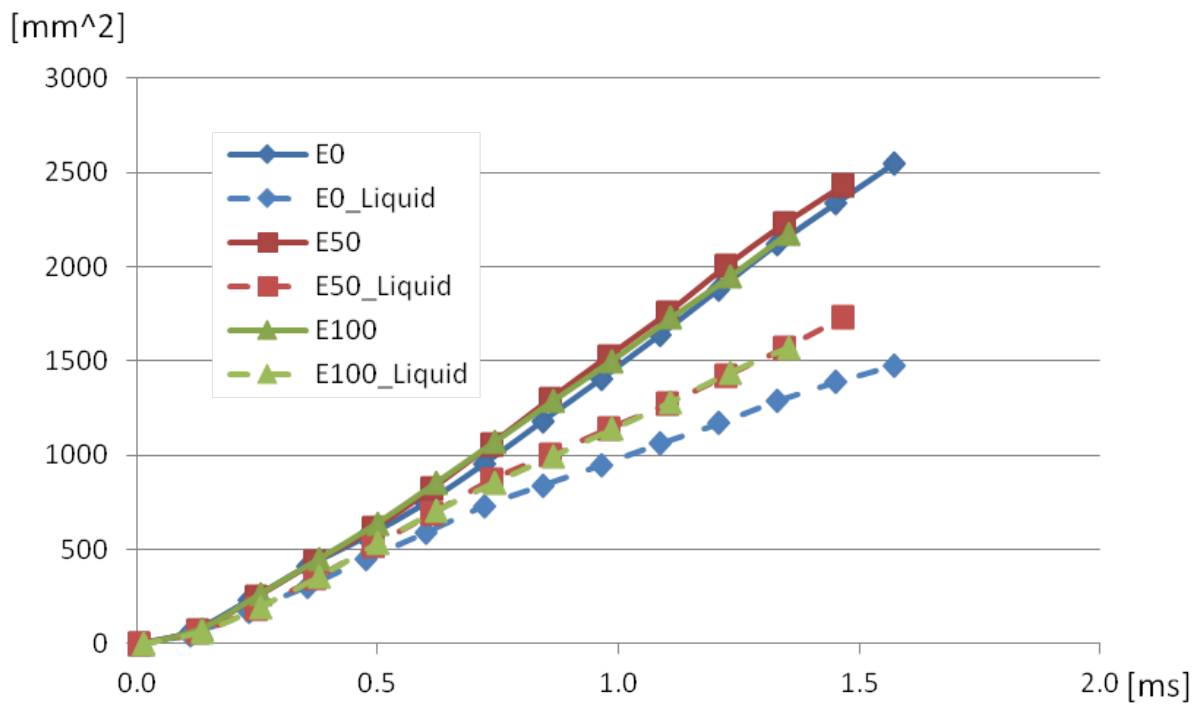


Fig. 4.8 Area of projected sprays for different fuels with fixed PW of 1.5ms

The spray angle were measured and the result is plotted in Fig, 4.9. The spray angle at 5, 10, 20mm down from the injector tip were almost identical for all the fuel except the beginning. At 5mm, gasoline spray had larger spray angle right after the start of injection. Instant expansion of fuels at the hole exit by flash boiling can explain this phenomena.

The position of the centroid of the sprays could indicate the influence of different fuels in Fig 4.10. At 1.0ms ASOI, the position of the centroid of E100 and E50 were 6.8% and 4.4% farther from the tip compared to the gasoline spray. Large differences of the position of the centroid was expected because of faster vaporization of gasoline fuel. However, it was not observed by image processing because it was impossible to calculate the position of the centroid after 1.5ms ASOI due to sprays exiting the field of view as shown in Fig. 4.6. However, the distance of the centroid from the nozzle tip indicates the same tendency as spray penetration and can be a substitute for penetration; gasoline spray's deceleration at the middle followed by ethanol spray's pursuit later.

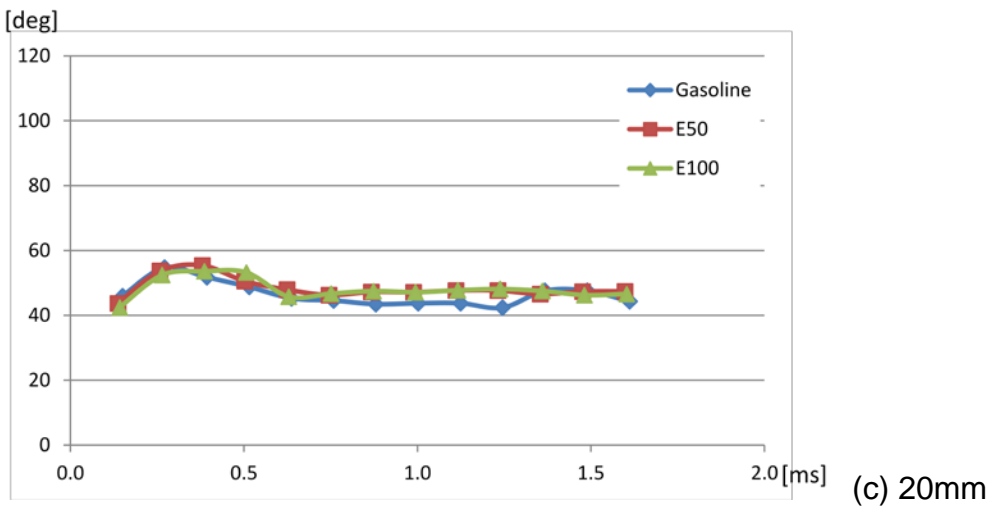
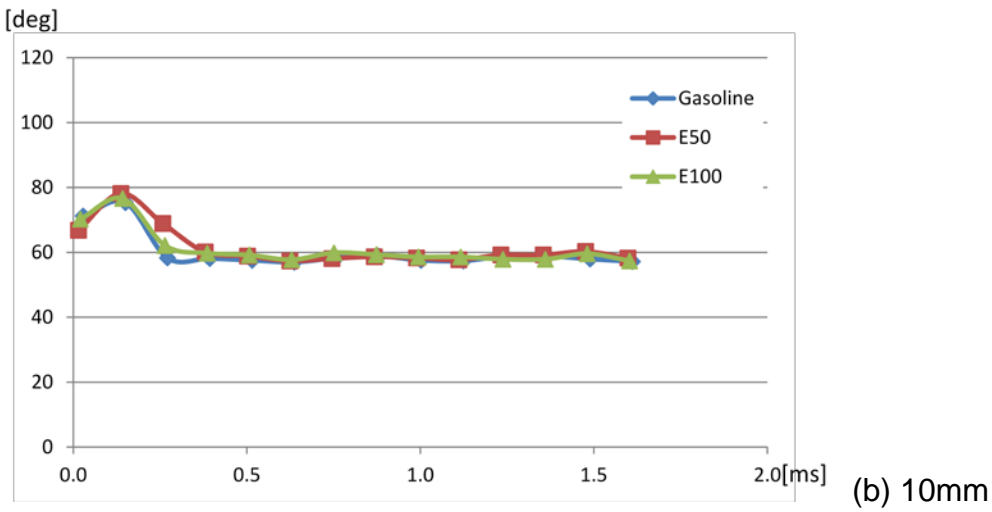
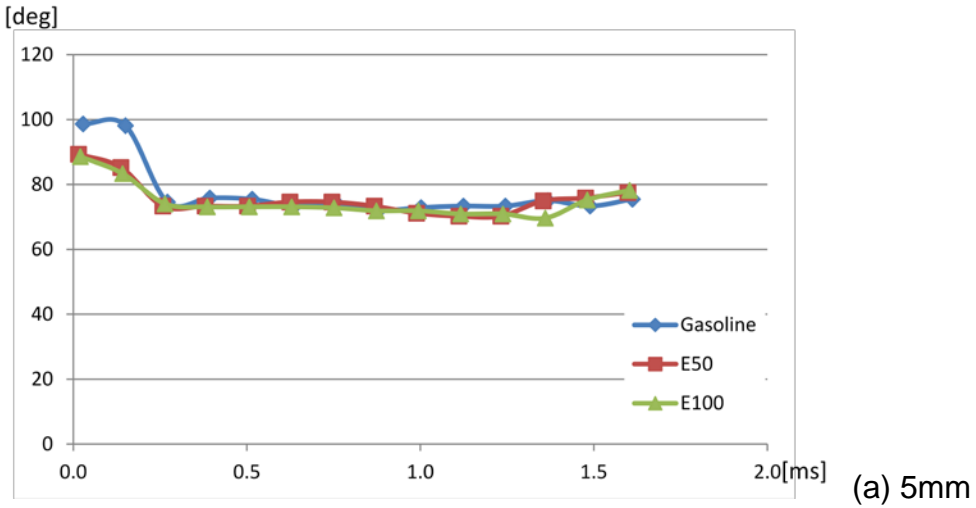
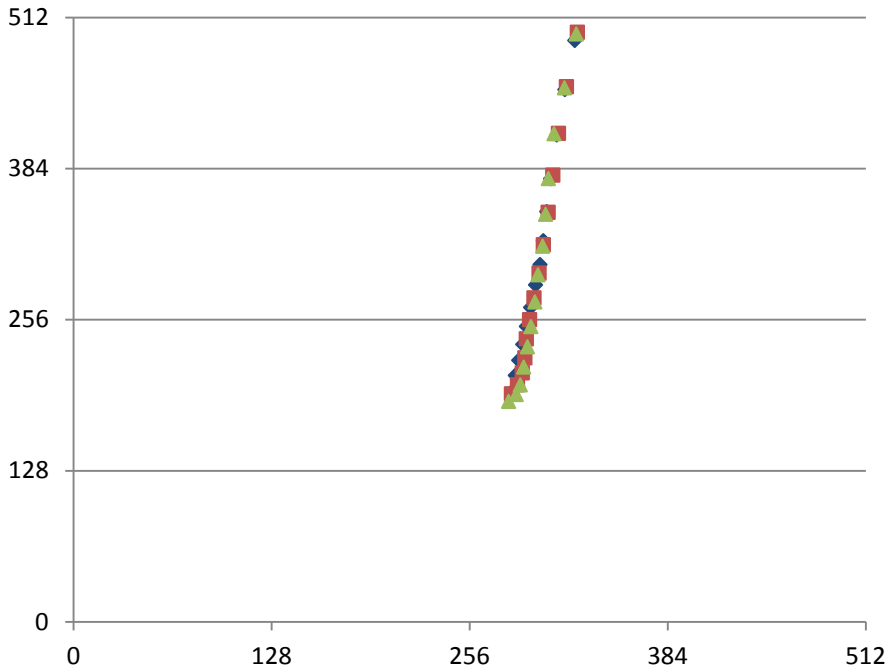
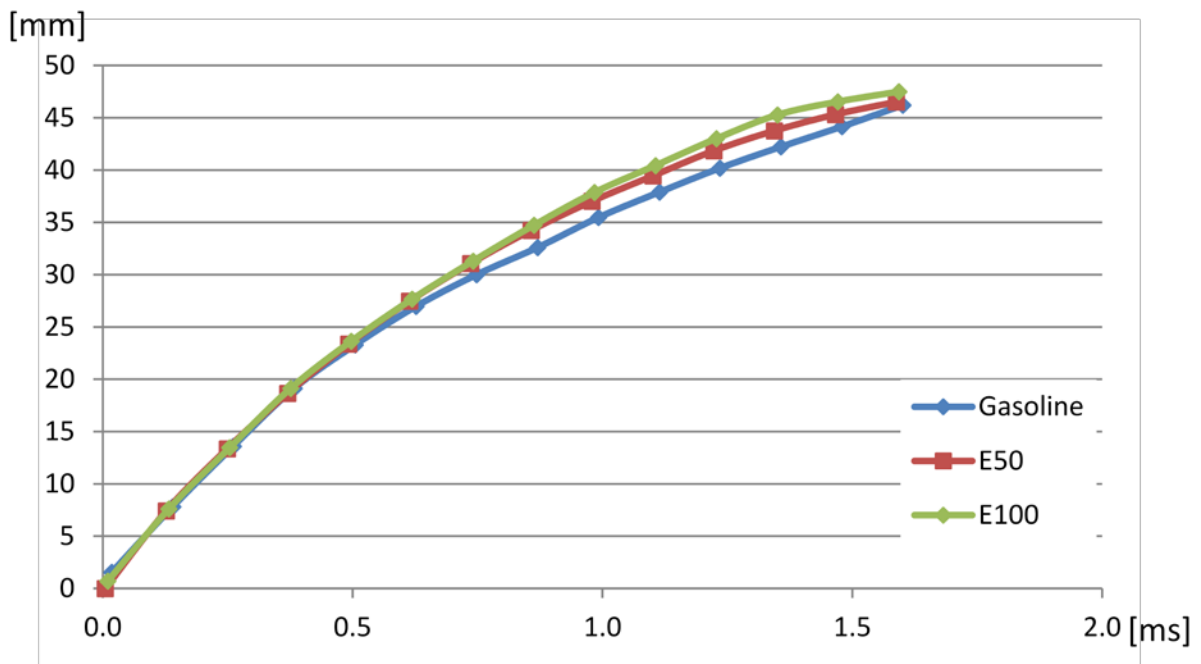


Fig. 4.9 Spray angle at 5, 10, 20mm down from the tip for different fuels with fixed PW of 1.5ms



(a) Position



(b) Distance from the nozzle tip

Fig. 4.10 Progress of the position of the centroid for different fuels with fixed PW of 1.5ms

In order to eliminate the effect of flash boiling, the chamber pressure was increased and the ambient condition of 200°C/4bar was tested. The injection pulse width was shortened to 0.5ms, which injected 9.7mg of gasoline, not to over-penetrate out of the image frame. As the image comparison shows in Fig. 4.11, the sprays of all three fuels behaved very similarly. There was no flash boiling effect observed, and higher back pressure suppressed the development of the sprays to the same level. The image processing revealed that the process of vaporization as well as the fuel location indicated by the position of the centroid of the spray were nearly identical for all three fuels (Figs. 4.12-13).

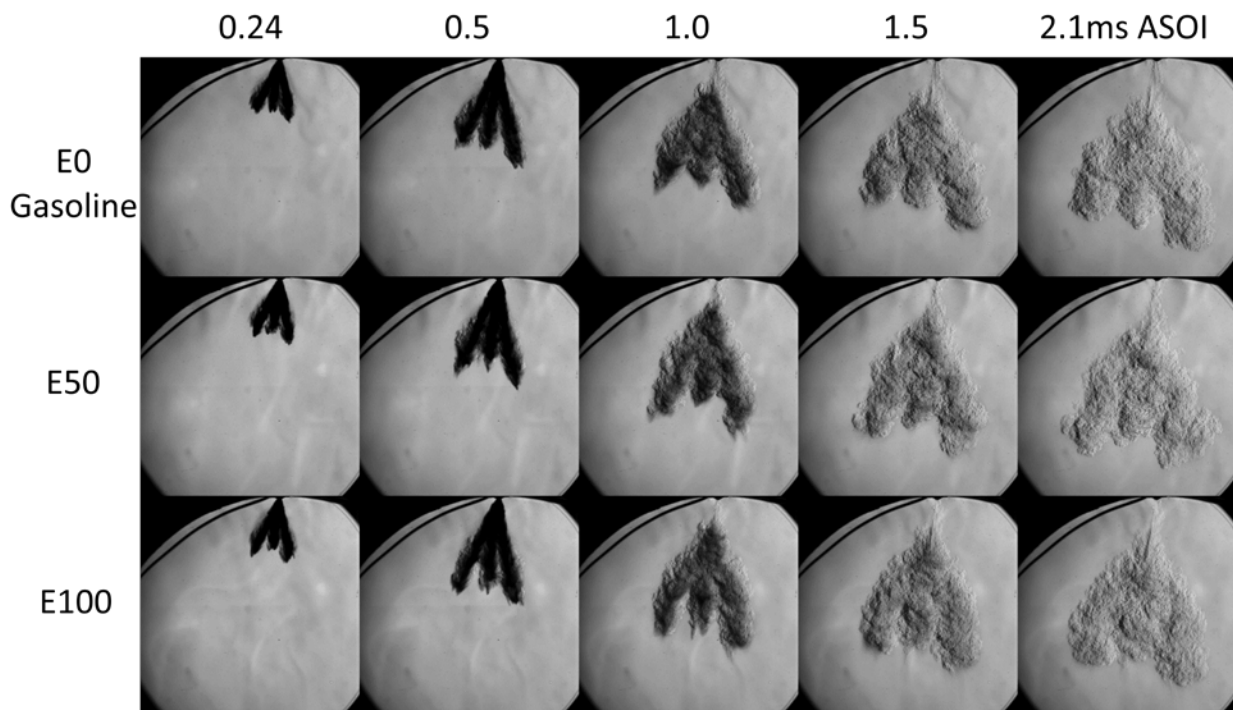


Fig. 4.11 Effect of fuel composition. $T_{ch}=200^{\circ}\text{C}$, $P_{ch}=4\text{bar}$, $T_{fuel}=60\text{C}$, $PW=0.5\text{ms}$

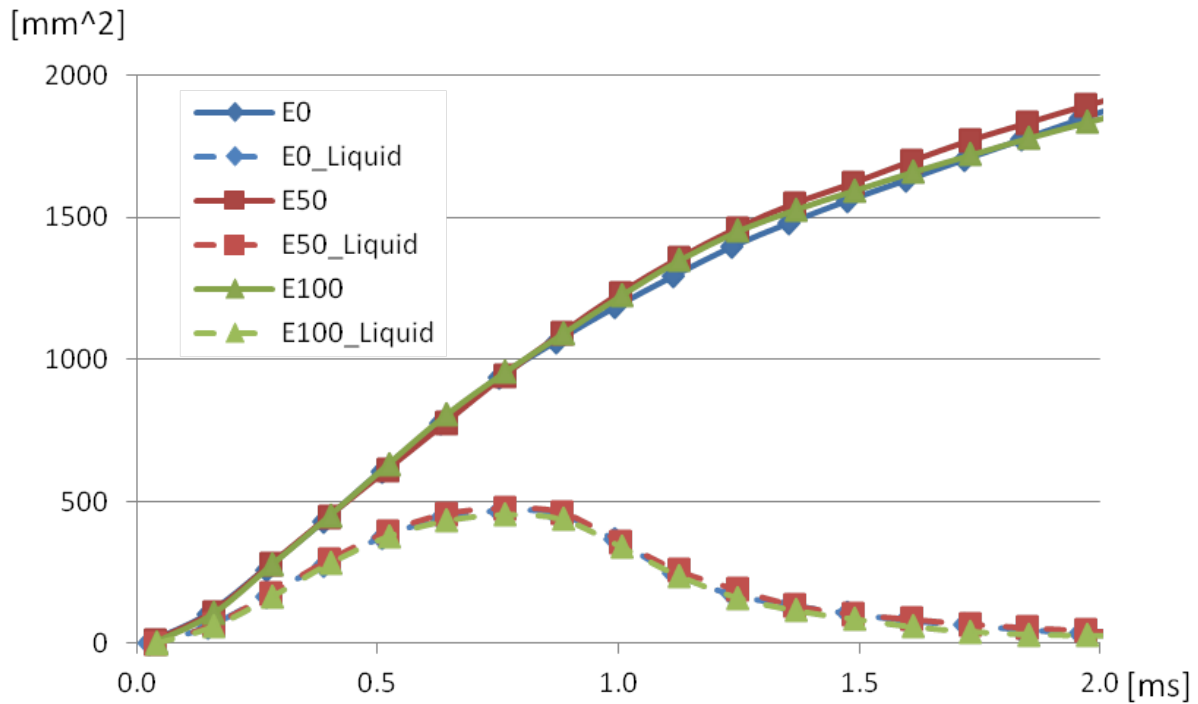


Fig. 4.12 Area of projected sprays for different fuels with fixed PW of 0.5ms

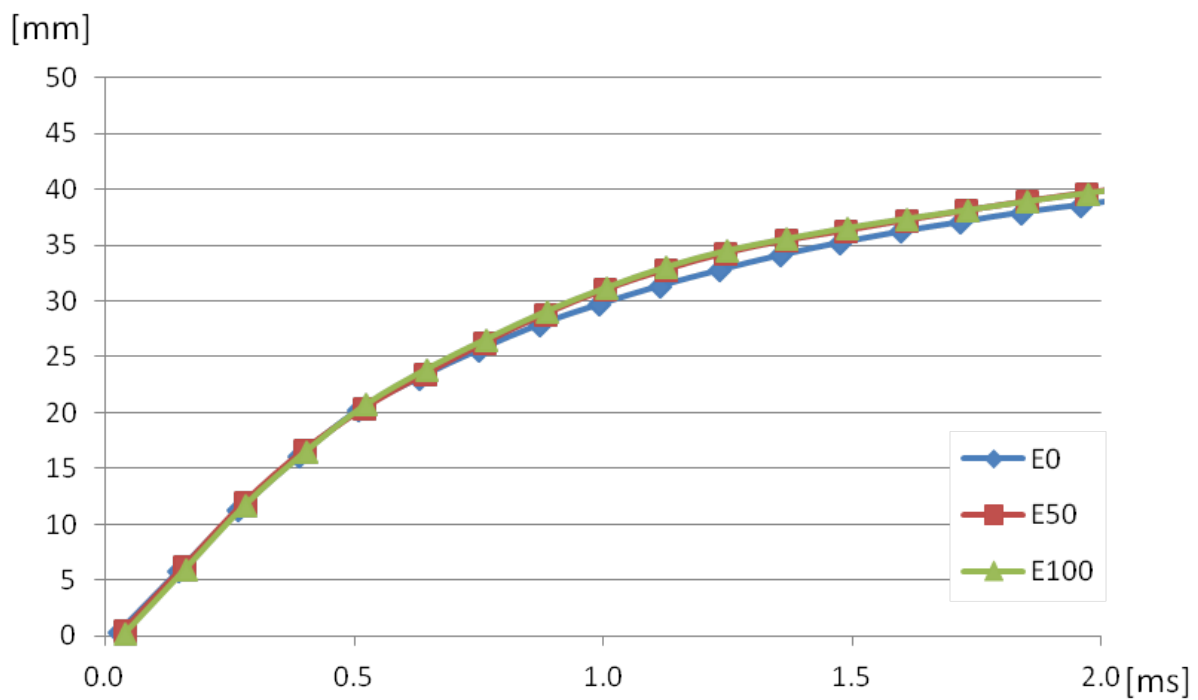


Fig. 4.13 Position of the centroid for different fuels with fixed PW of 1.5ms

Constant Injected Energy

In order to evaluate the effect of fuels in realistic flex-fuel engine operation, the total energy content of injected fuel was kept constant to be equivalent to 5mg of gasoline. The injected mass for each fuel was different, but that was required amount for the same output energy if the fuel is completely burned in a real engine. The total energy of 5mg of gasoline is 215.5J, calculating from the lower heating value (LHV) of gasoline which is 43.1MJ/kg. The LHV of E50 and E100 are 35.0 and 26.8MJ/kg respectively. Therefore the injected mass and corresponding pulse width of the injection command signal for gasoline, E50 and E100 were 5mg (0.38ms), 6.2mg (0.46ms), and 8.0mg (0.59ms) respectively.

Fig. 4.14 shows the resultant images of the testing. As a result of varying injection durations, spray shapes of different fuels would be expected to change dramatically. Actually, the influence of different fuels was clearly seen in the figure qualitatively. The shape of gasoline spray was strongly affected by flash boiling. The plumes collapsed and formed a one big jet. Therefore the center of the spray became dense and it must require more time to vaporize completely. However, it almost finished vaporizing at 1.5ms ASOI because of less injected mass. On the other hand, spray pattern of E100 spray was kept consistent. It started vaporizing from the surroundings of the each plumes. At 1.5ms ASOI, E100 spray still shows black area in the spray structure where some liquid could exist. The behavior of E50 was mix of those two fuels. At the early stage of injection, the spray shape was similar to E100. At the later stage of injection, the spray shape of E50 became closer to the gasoline spray.

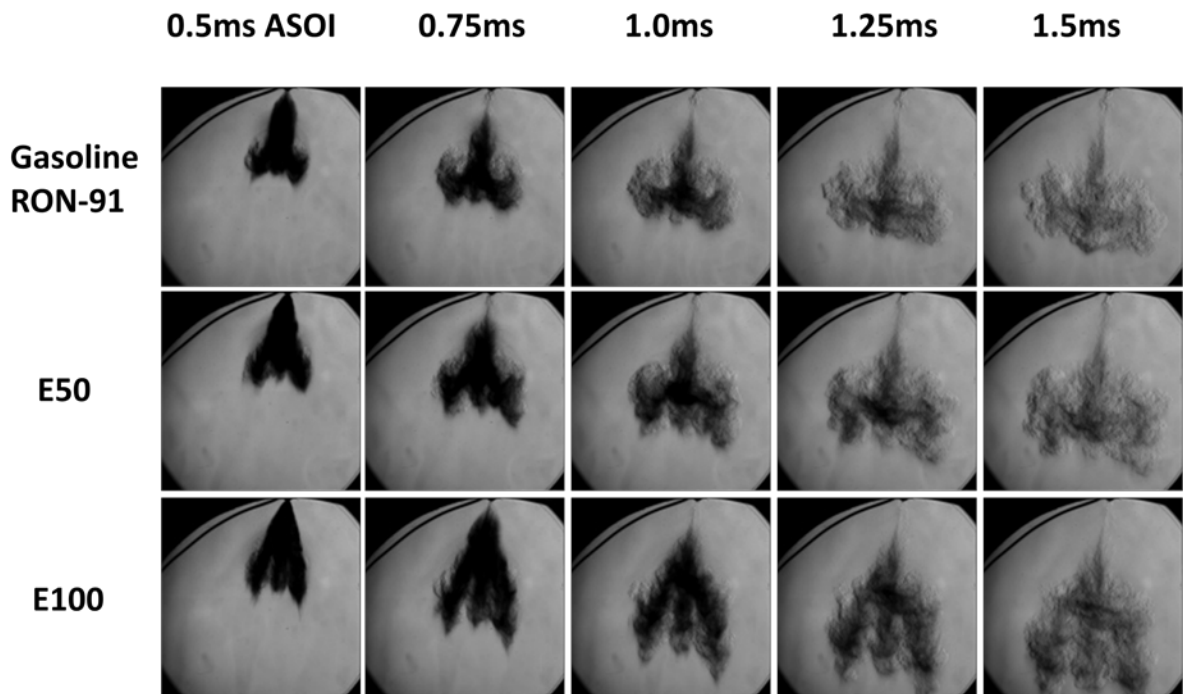


Fig. 4.14 Effect of fuel composition. $T_{ch}=200C$, $P_{ch}=1bar$, $T_{fuel}=60C$, Energy content=5mg of gasoline

Figs. 4.15-18 show the measured spray data; penetration, projection area, spray angle, and centroid position. The penetration of E50 was greater than gasoline, and E100 was even greater than E50 all the time because of longer injection duration and slower initial vaporization of ethanol. At 1.0ms ASOI, E50 spray had 8.1% longer penetration and E100 spray had 22.9% longer than gasoline spray. It should be noted that increased penetration may lead to piston impingement and side wall wetting resulting in increased hydrocarbon emissions and soot formation during engine operation. The injection strategy must be revised to minimize wall wetting, for example, injection timing shift or multiple injection to reduce the penetration is required. The same trend can be observed with the projected area shown in Fig. 4.16. The total spray area illustrates 14.4% and 27.8% of increase for E50 and E100 with respect to gasoline at

1.0ms ASOI. Ethanol spray had larger projection area all the time because of greater injected mass. Gradual slope of E0 liquid area decrease after 1ms indicates slower vaporization of the heavier gasoline components. There are no significant difference in the spray angle and the position of the centroid. The trend of the distance of the centroid from the injector tip was consistent with the penetration result.

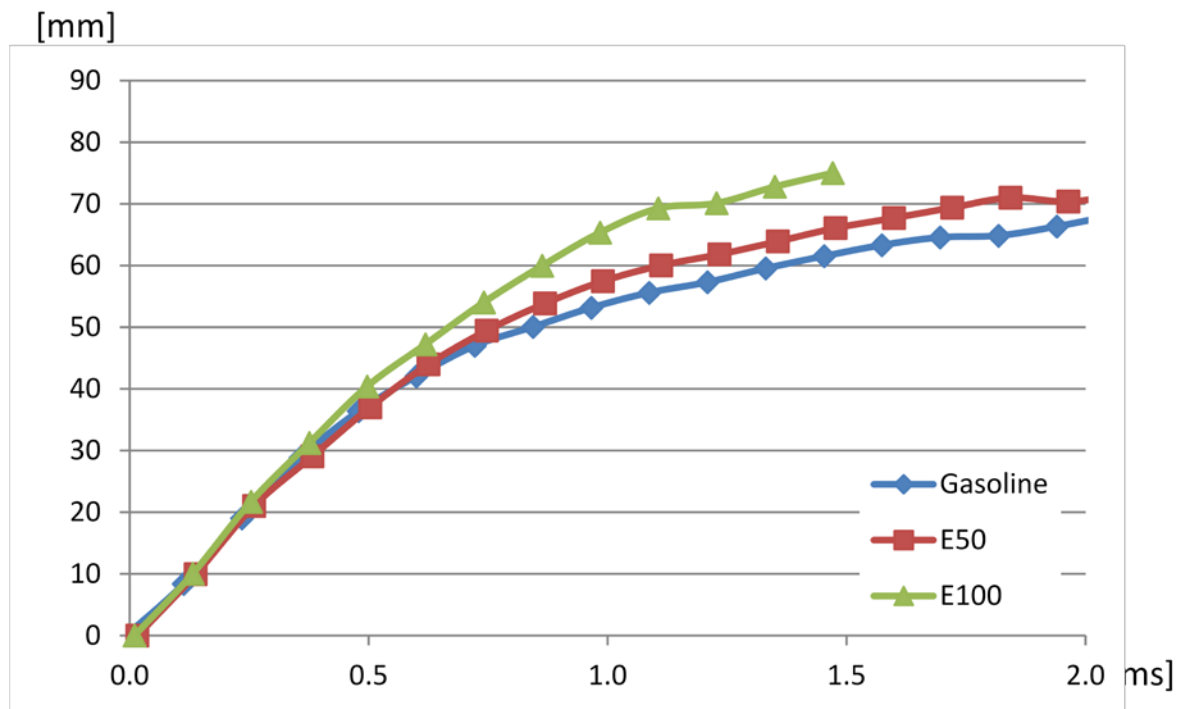


Fig. 4.15 Averaged penetration of spray for different fuels with fixed energy input

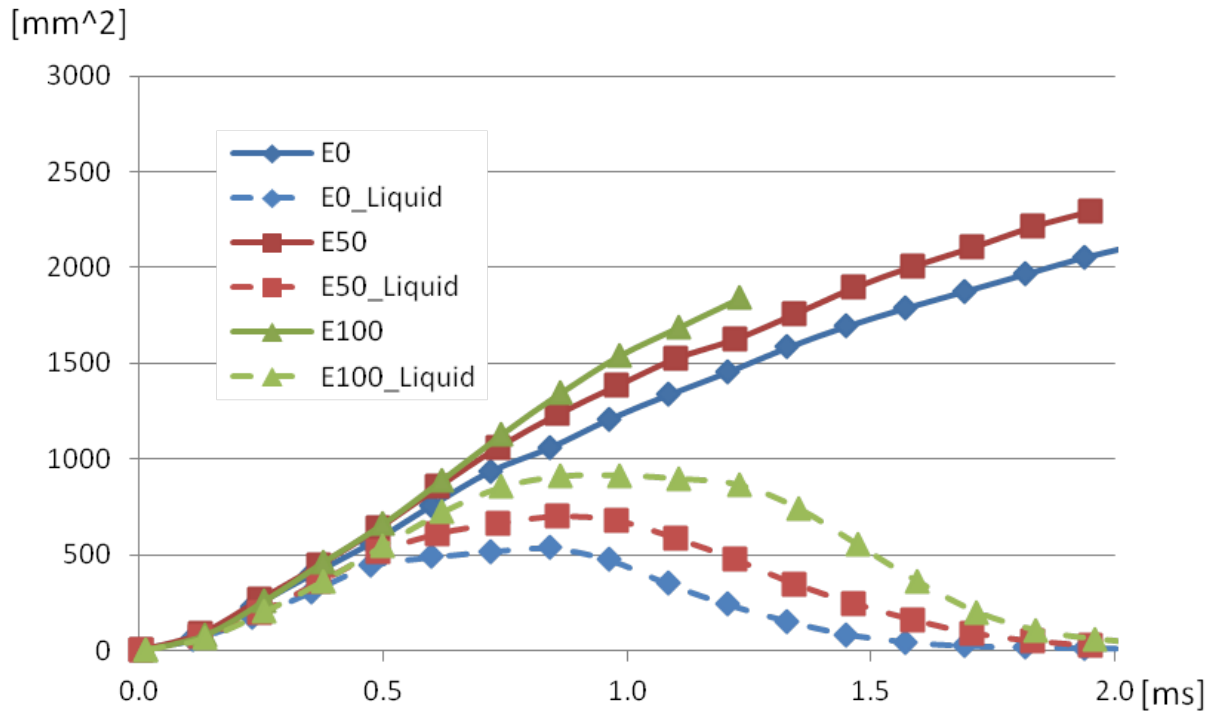
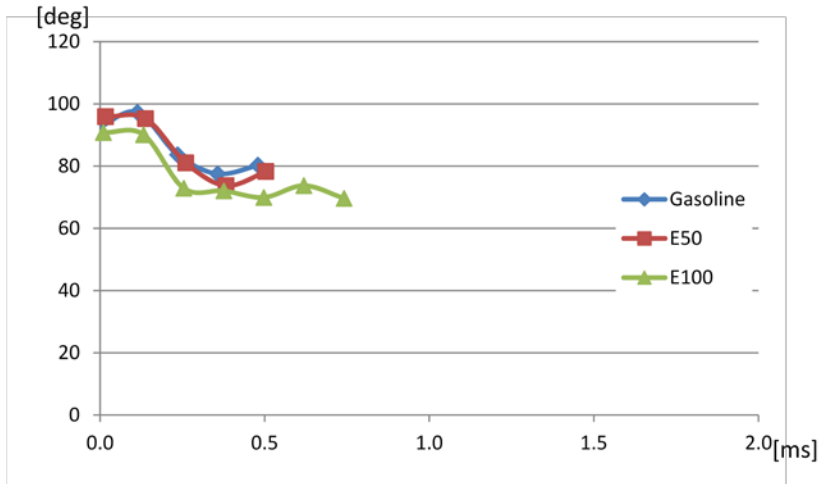
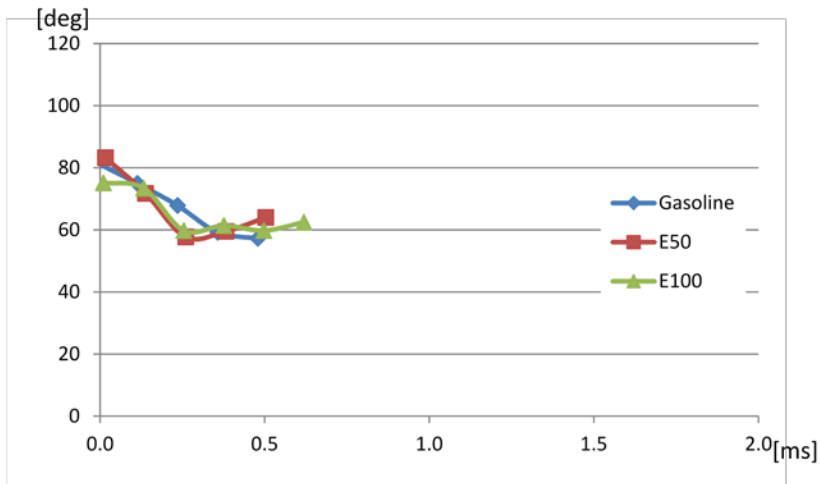


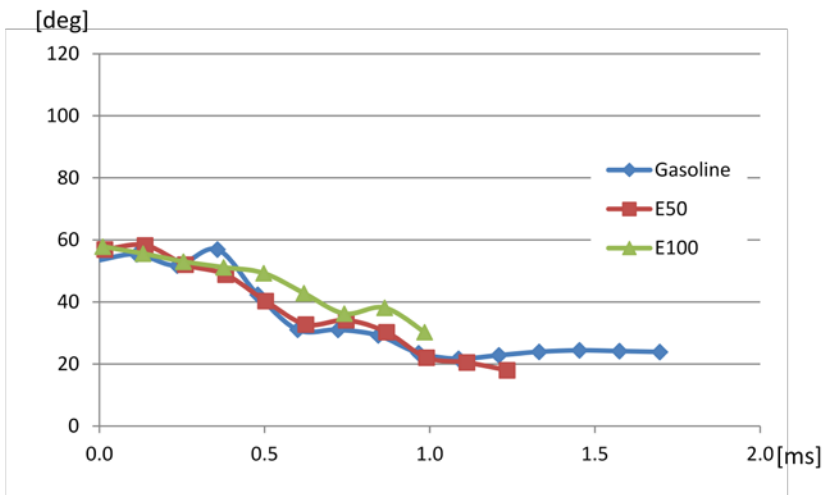
Fig. 4.16 Area of projected sprays for different fuels with fixed energy input



(a) 5mm

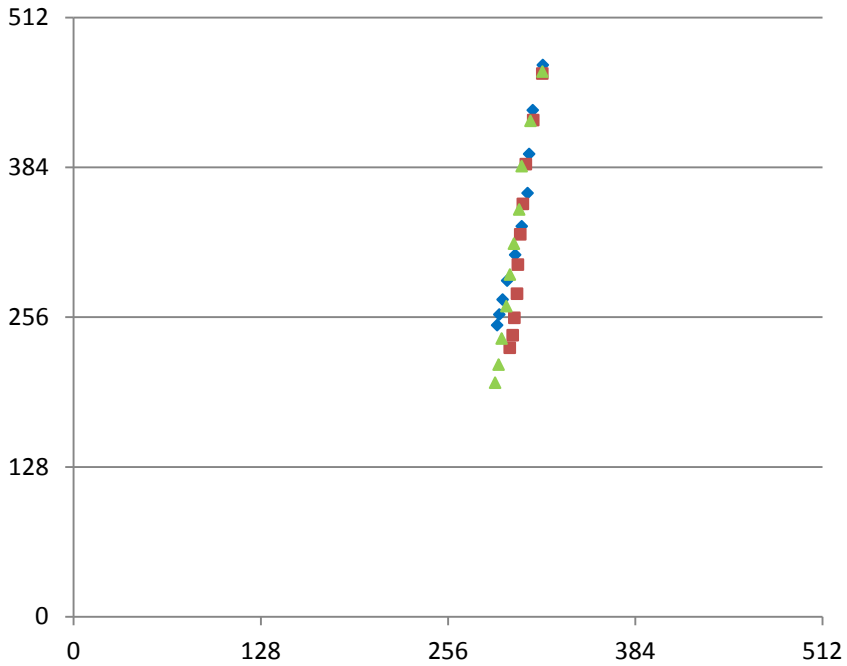


(b) 10mm

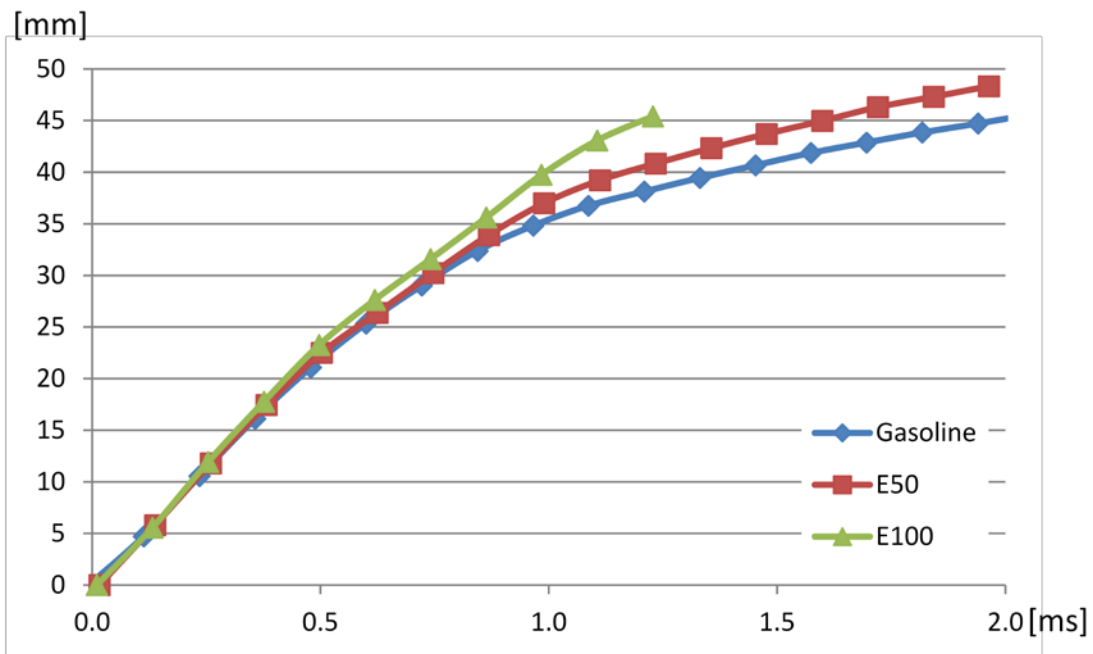


(c) 20mm

Fig. 4.17 Spray angle at 5, 10, 20mm down from the tip for different fuels with fixed energy input



(a) Position



(b) Distance from the nozzle tip

Fig. 4.18 Progress of the position of the centroid for different fuels with fixed energy input

4.2.3 Effect of Fuel Temperature

In this experiment, the effect of fuel temperature was examined for two types of fuels, pure gasoline and E100. The injection duration was determined to keep the total energy content of the injected fuel as 10mg of gasoline. Considering the difference of the heating value, the injected mass and injection command pulse width for gasoline and E100 were 10mg (0.54ms) and 16.1mg (0.87ms) respectively. Since Injector B was used in this testing, the flow rate was increased comparing to Injector A. The static flow rate of Injector B was approximately 30% greater.

The effect of fuel temperature under atmospheric ambient pressure is shown in Figs. 4.19 and 20. The surrounding temperature for each condition was 25°C and 200°C respectively. At low ambient temperature, only little enhancement of vaporization was observed with higher fuel temperature for both ethanol and gasoline spray in existence of vapor at the side of the spray. The same tendency was captured with ethanol spray at higher ambient temperature of 200°C with low fuel temperature up to 60°C. More and more vapor was observed up to 60°C of fuel temperature, while overall distribution of the fuel did not change much. However the plumes collapsed at 80°C of fuel temperature and changed its appearance significantly. Again, this is due to the flash boiling as the boiling point of ethanol at 1bar is 78°C. In contrast, the spray of gasoline was found to be almost independent on the fuel temperature even at the higher ambient temperature condition, slightly enhanced vaporization was observed for higher fuel temperature though. This can be explained by a gradient in the boiling point of multi-component of gasoline. According to Table 4.1, Alkane hydrocarbons C4-C6 have less boiling point than ethanol. Therefore those components, and possibly C7, were the

vaporized portion at 80°C of fuel temperature where ethanol experienced flash boiling. But the condition did not meet to vaporize the rest of the gasoline components. Multi-component gasoline was less sensitive to fuel temperature in the range of 25-80°C in terms of vaporization process and the resultant spray shape because of multiple boiling point corresponding to each hydrocarbon.

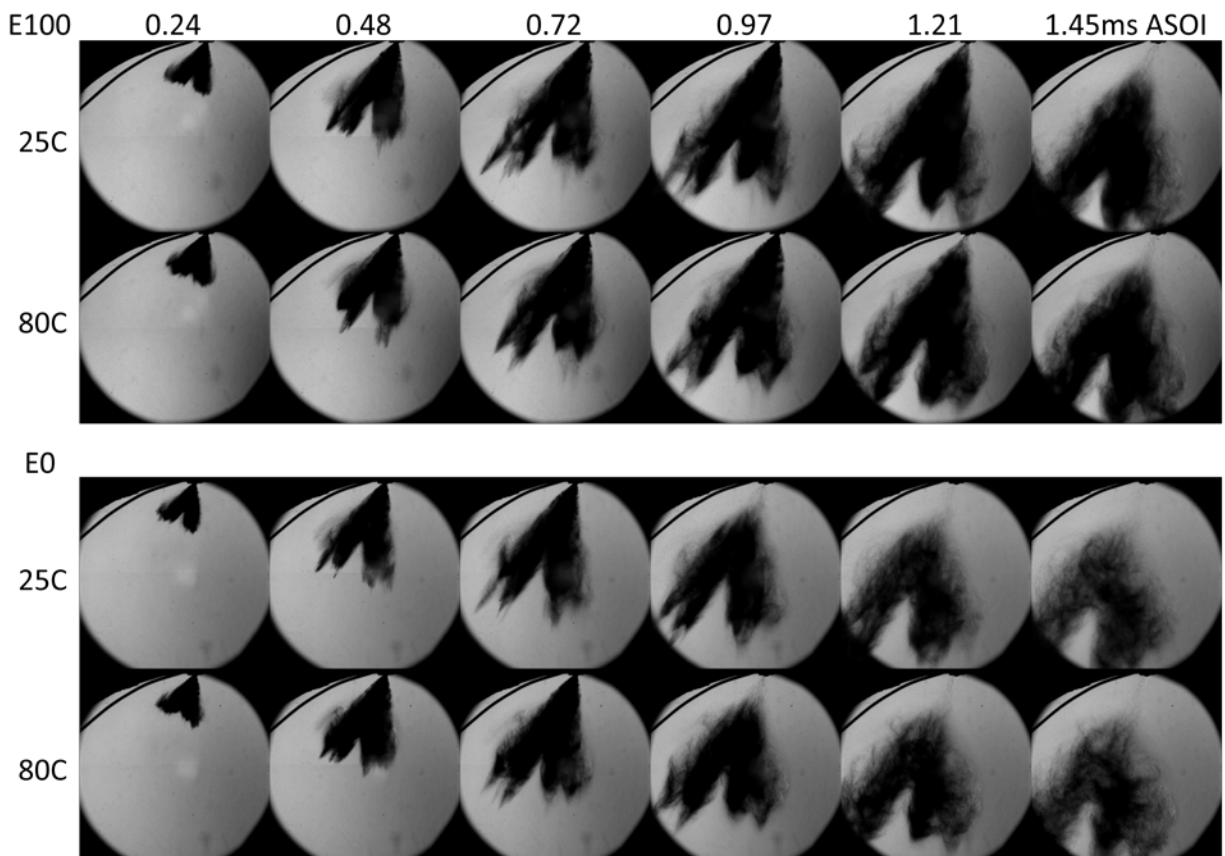


Fig. 4.19 Effect of fuel temperature on spray propagation at 25°C/1bar, 10mg of gasoline or equivalent in energy

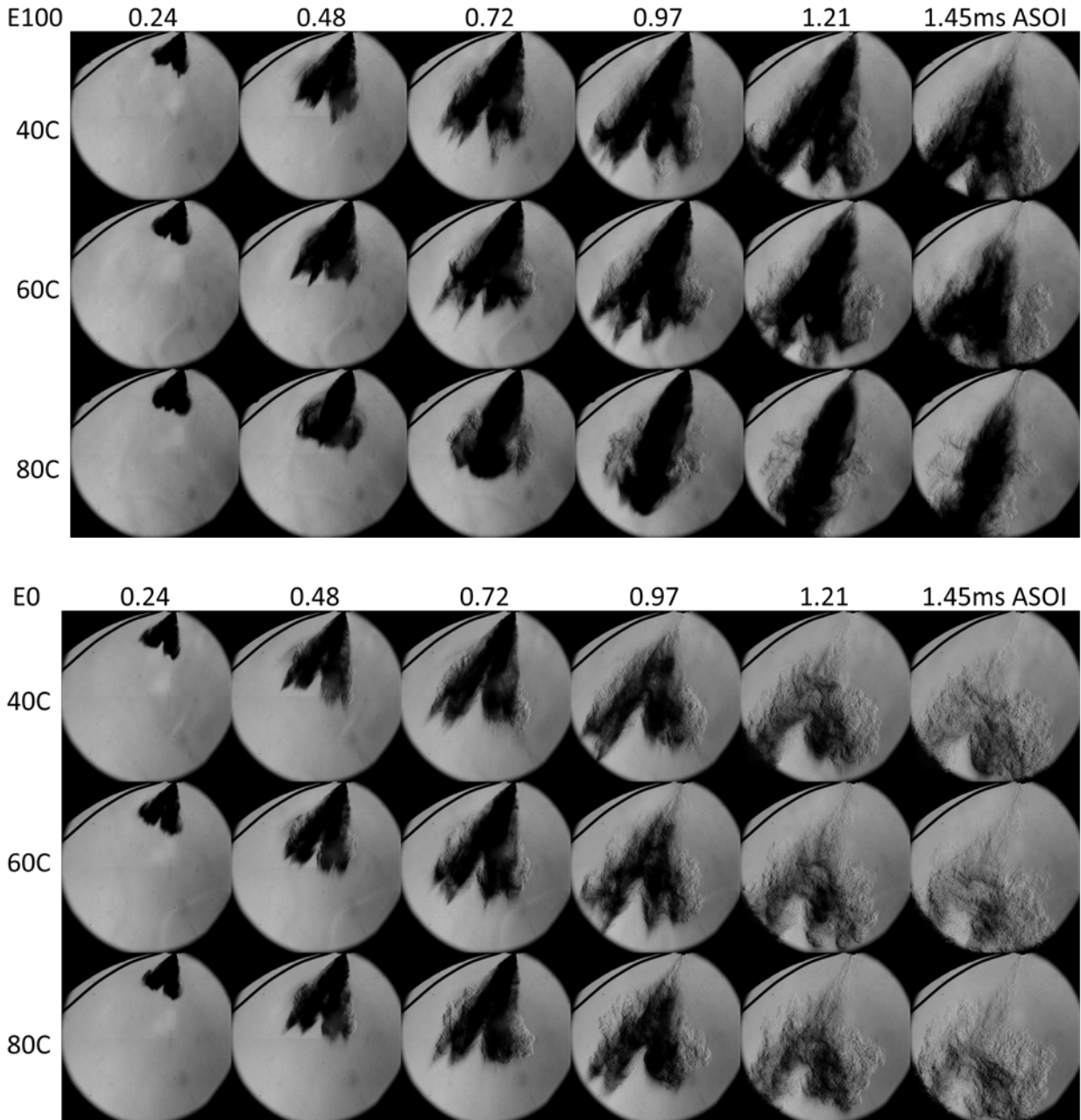


Fig. 4.20 Effect of fuel temperature on spray propagation at 200°C/1bar, 10mg of gasoline or equivalent in energy

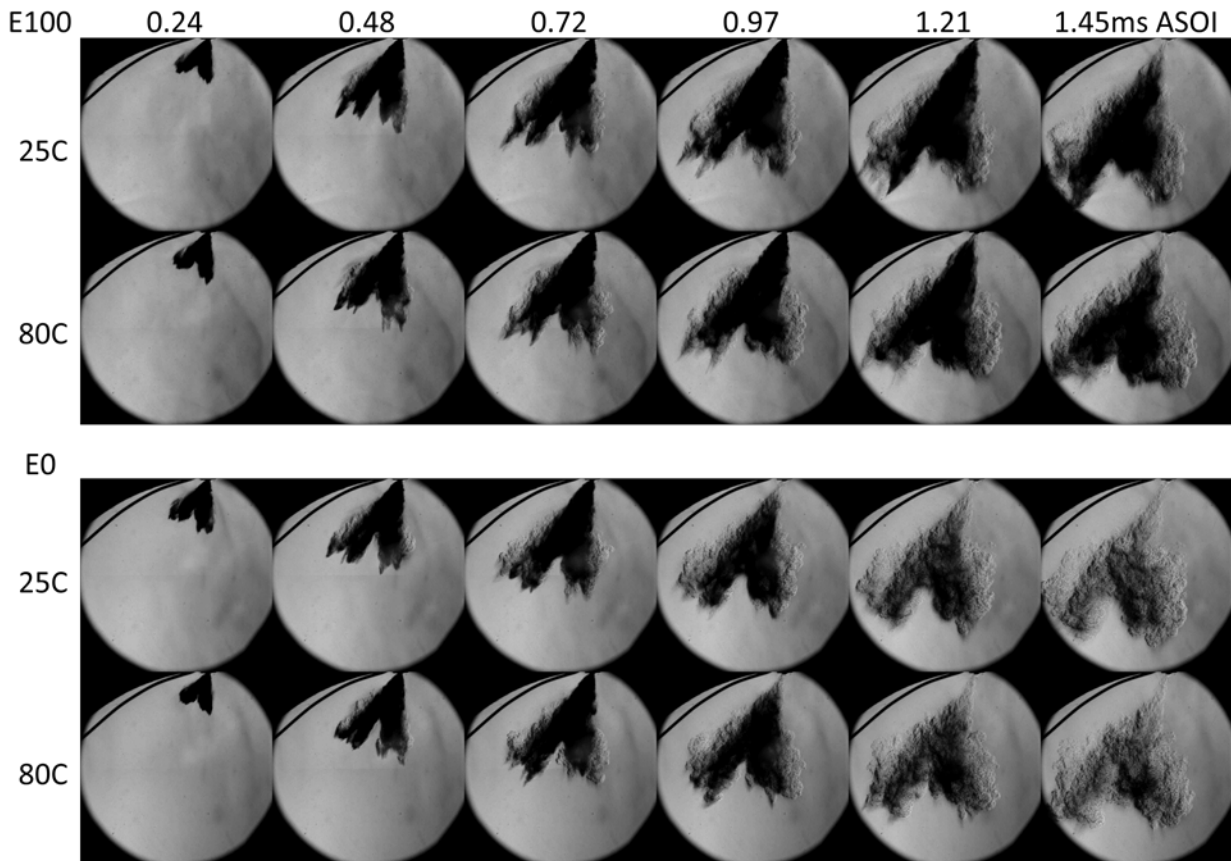


Fig. 4.21 Effect of fuel temperature on spray propagation at 200°C/3bar, 10mg of gasoline or equivalent in energy

Then the chamber pressure was increased to 3bar with high ambient temperature at 200°C. Once the ambient pressure became higher than the saturation pressure, no plume collapse existed even for the ethanol spray (Fig. 4.21). And the sprays of different fuel temperature were almost identical no matter what the ambient temperature was. Even though the effect of fuel temperature was negligible at the ambient condition of 200°C/3bar, enhanced vaporization must be seen if the chamber temperature increased more.

4.2.4 Effect of Injector Nozzle Design

Injector A and B were compared to evaluate the effect of nozzle design. Injector B has 30% more static flow rate than Injector A due to larger hole diameter. The injection duration was 1.5ms. Figs. 4.22 and 23 show spray propagation and penetration of both injectors at room temperature with atmospheric pressure. Even Injector B has larger hole diameter (0.263mm vs. 0.23mm) and thus larger flow rate (20.5 vs. 15.9 g/s), its penetration was comparable with Injector A at the early stage of injection. At later part of injection, the spray of Injector B traveled farther. One noticeable feature of Injector B was its strong spray bending as Fig. 4.24 illustrates. Left image was captured at 0.24ms and right image was at 1.10ms ASOI. The initial directions of “outside” sprays are indicated in the red arrows while actual spray directions at 1.10ms ASOI are green. Since this spray bending was observed in both ambient (Fig. 4.22) and 3bar (Fig. 4.24) chamber pressure, the effect of flash boiling is excluded from the reason. This behavior can be considered as a result of uneven air entrainment. As the spray footprint of Injector B shows in Fig. 4.24, the pairs of center plumes in the figure are close to each other and the “outside” plumes are isolated. It is possible that the air entrainment inside the "spray cage" caused drag force to pull the outside plumes into the center of the cage. Other possible reason for the spray bending is internal flow dynamics of the injector sac. Further study should be conducted because spray targeting is very critical for GDI engines.

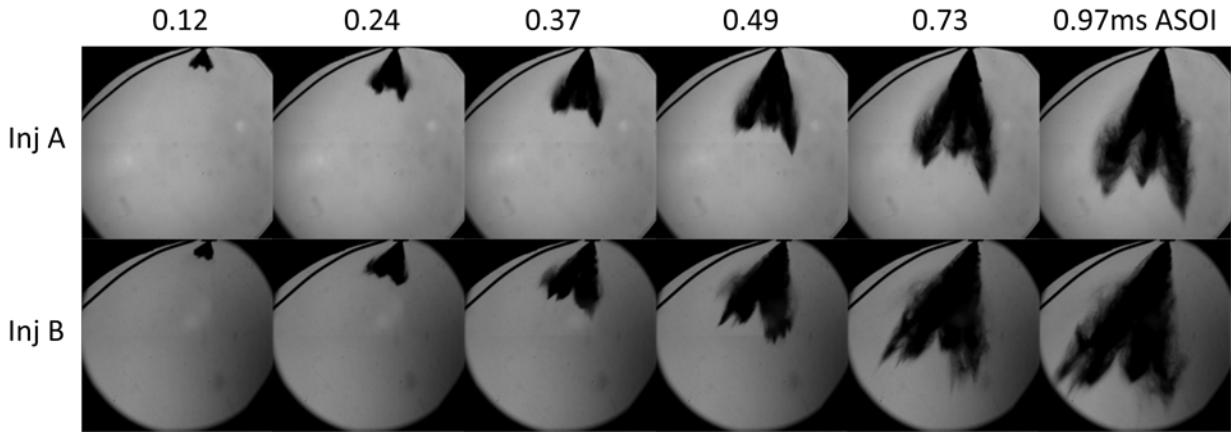


Fig. 4.22 Effect of injector design (A&B) on spray propagation at 25°C /1bar, injection duration=1.5ms

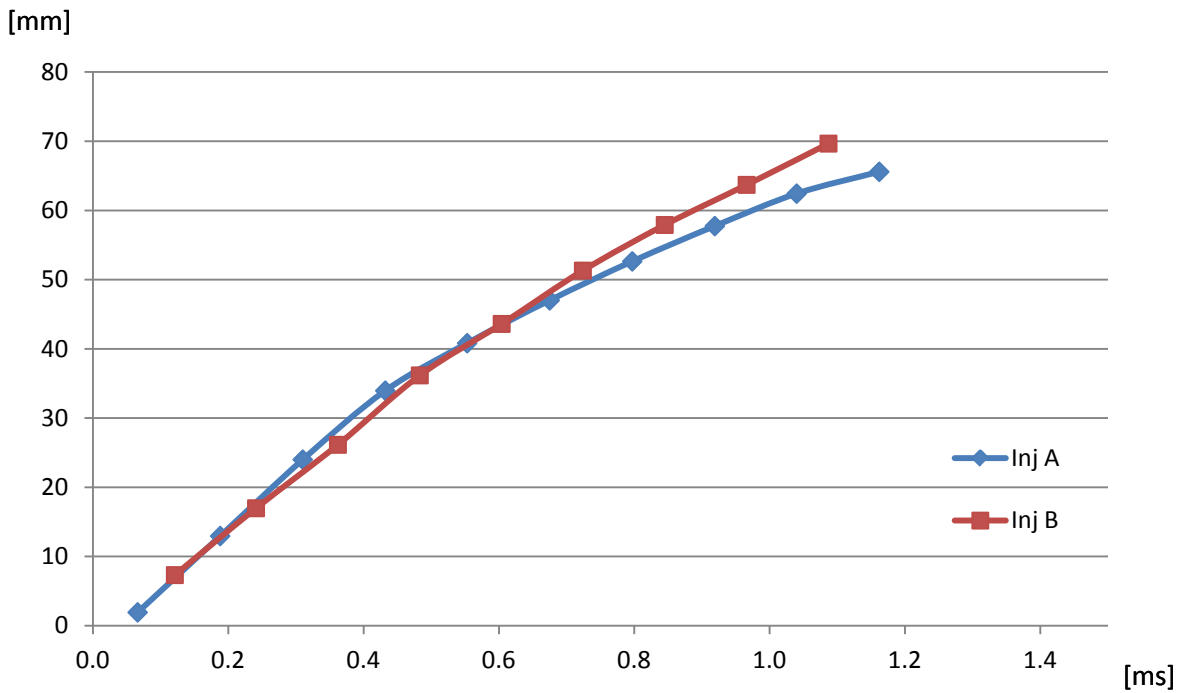


Fig. 4.23 Effect of injector design (A&B) on spray penetration at 25°C /1bar, injection duration=1.5ms

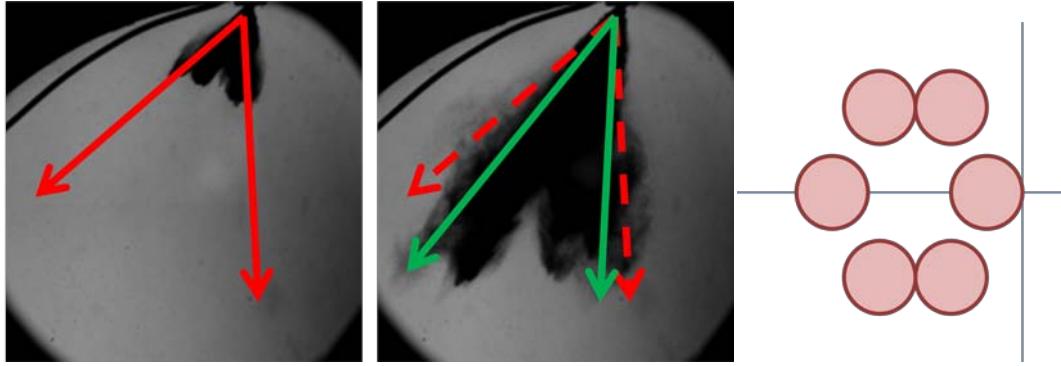


Fig. 4.24 Spray bending of injector B at 25°C / 3.2bar. 0.24ms (Left) and 1.10ms (Right) ASOI

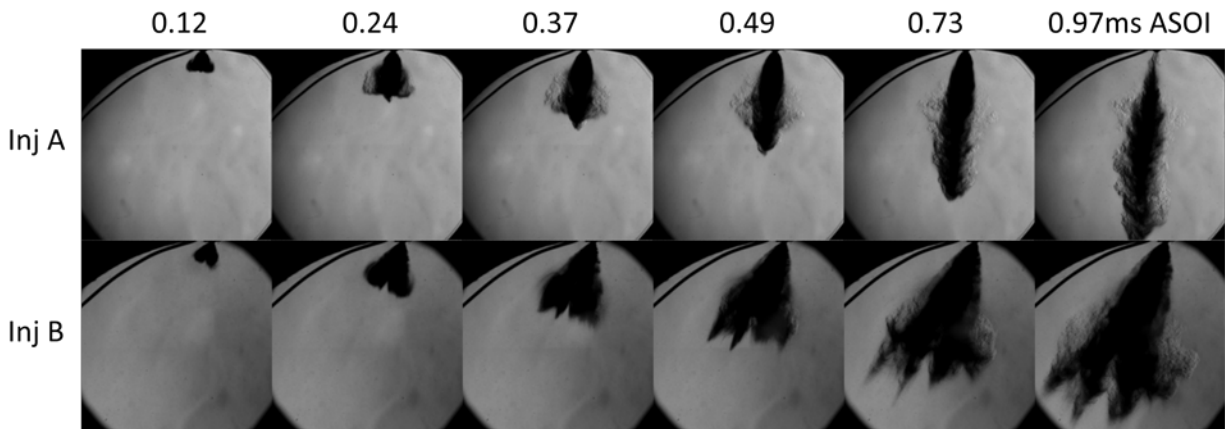


Fig. 4.25 Effect of injector design (A&B) on spray propagation at 200°C / 1bar, 10mg of gasoline

The spray images at higher ambient temperature at 200°C are shown in Fig. 4.25. In the figure, significant spray collapse of Injector A resulting in poor spatial fuel distribution was observed. As the previous section pointed out, this was caused by flash boiling. The dark core in the spray of Injector A indicates existence of liquid in the center of the merged jet, thus enhanced penetration caused by flash boiling will result in large amount of wall wetting. Even though Injector B has relatively narrower spray targeting (Table 3.1), the plumes were able to resist merging and maintained the spray targeting

better even in a flash boiling condition. This can be explained by larger flow rate of Injector B overcame the effect of flash boiling.

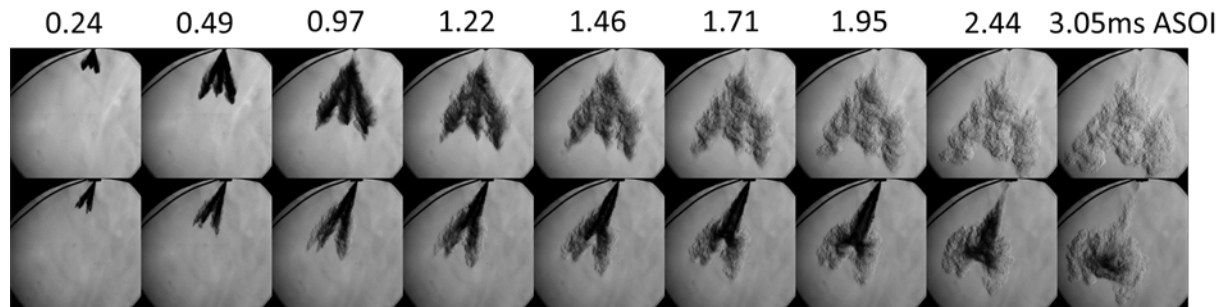


Fig. 4.26 Schlieren spray images for injector A (upper) and C (bottom) ($T=200^{\circ}\text{C}$ $P=3\text{bar}$ $P_{inj}=10\text{MPa}$ $\text{Mass}=5\text{mg}$)

For Injector A and C, Schlieren imaging was performed (Fig. 4.26) to evaluate the difference in the spray development. Temperature and pressure of the chamber were set to 200°C and 3bar respectively, and the injected fuel was ethanol with 5mg of mass. The corresponding injection command pulse width was 0.59 and 2.09ms respectively for Injector A and C. It was obvious that the individual plumes of smaller L/D (Injector A) penetrated faster and wider during the injection. Even though its individual plume had wider cone angle, the sprays of the injector A remain separated from each other better than injector C due to its larger spray targeting angle. The plumes of Injector C was able to be isolated at the beginning due to its narrower individual spray angle, but they merged later because of closer spray targeting. Flash boiling should not be counted for the reason because this testing was performed under higher ambient pressure. Injector A had wider spray cone angle with wider spray targeting angle, and this enlarged the available surface of the sprays and made the vaporization faster. At 3ms ASOI, the spray of Injector A was completely vaporized, but

Injector C still contained liquid phase at the center of the spray which was still penetrating further. Because of the faster vaporization and required shorter injection duration, Injector A was able to keep the mixture cloud near the nozzle exit, which is important to avoid excess wall wetting during GDI engine operation.

4.2.5 Summary

High-speed Schlieren visualization of multi-hole DI spray was conducted to evaluate the effect of ambient condition. High ambient temperature promoted vaporization and vaporized fuel dissipated its momentum for less penetration. High ambient pressure suppressed the spray development and made the effect of temperature negligible. Once fuel was injected into high temperature and low pressure environment, flash boiling could occur and changed the spray shape drastically by plume collapse. Flash boiling occurs when the pressure of fuel drops instantly below the saturation pressure. The effect of flash boiling is not preferable for regular GDI multi-hole injector because it can destroy the spray targeting.

Comparison of spray behavior with different fuels in flash boiling condition revealed that the gasoline spray showed faster vaporization and more flash boiling effect than the ethanol spray because of higher saturation pressure of lighter components of hydrocarbons. Although the initial penetrations of gasoline and ethanol spray were identical, gasoline spray slowed down at the middle of injection. Decelerating of the gasoline spray at the later stage of injection was also slower than ethanol spray because the heavier components remained in liquid. The total projection area and spray angle were almost identical for all the test fuels. The liquid spray of E0 had less area because of liquid phase accumulation by plume collapse. The position of

the centroid indicated the same tendency as spray penetration; gasoline spray's deceleration at the middle and ethanol's pursuit later. When the ambient pressure was increased to prevent flash boiling, the spray behavior became nearly identical for all fuels. To evaluate the effect of fuels in realistic flex-fuel engine operation, the spray visualization with constant energy content of injected fuel was performed. The difference caused by fuel variation was more noticeable. Gasoline spray had faster complete vaporization due to flash boiling and less injection quantity. The spatial distribution of E0 fuel was poorer than ethanol spray because of spray collapse and less quantity. Slower vaporization of the heavier gasoline components was observed by image processing. There are no significant difference in the spray angle and the position of the centroid.

Vaporization was promoted as the fuel temperature increased. Under atmospheric pressure with high ambient temperature, the ethanol spray collapsed by flash boiling and changed its shape drastically when the fuel temperature exceeded 80°C. Multi-component gasoline was found to be less sensitive to fuel temperature in the range of 25-80°C in terms of vaporization process and the resultant spray shape because of multiple boiling point corresponding to each component. At higher ambient pressure, such effect was not observed and the sprays were almost independent on fuel temperature.

The penetration was comparable with Injector A and B at the early stage of injection even though Injector B was designed for larger flow rate. At later part of injection, Injector B showed further penetration. One noticeable feature of Injector B was its strong spray bending possibly due to uneven air entrainment caused by spray

targeting design. Even though the spray targeting of Injector B was narrower, it could resist against spray collapse by flash boiling because of larger flow rate. The comparison of Injector A and C confirmed that the spray of a multi-hole injector with smaller L/D penetrated faster and wider during the injection. Injector A had wider spray cone angle with wider spray targeting angle, and this enlarged the available surface of the sprays to accelerate the vaporization faster. Because of the faster vaporization and required shorter injection duration, Injector A was able to keep the mixture cloud near the nozzle exit.

4.3 Piston Impingement Testing

Piston impingement testing was carried out for simulating spray-piston interference in a GDI engine. The testing neglected the effect of charge motion. Since spray velocity of GDI injection is significantly higher than typical in-cylinder charge flows, it is a reasonable compromise for spray-piston interactions. The state of the vapor cloud however will be influenced by the induced charge motion during intake and compression strokes. It should be reminded that delivery of slightly rich mixture around the spark plug is desirable when the stratified combustion takes place. The injector and the piston were mounted in the pressurized chamber with a capability of adjusting the relative position of the injector and the piston to simulate the relative position of the piston top respect to the injector in a real engine. The piston can be moved from TDC position up to 15mm down along with the cylindrical axis to observe the effect of the change of the spray timing. Injector-piston distance of 15mm represents roughly 40 degree crank angle rotation from TDC and approximately 6.7ms apart from TDC at

1000rpm engine speed. The production Injector A utilized the production piston crown, and the Injector C was tested with the prototype piston crown which was specially designed for the prototype injector. The picture of the pistons with different bowl design is shown in Fig. 4.27. The depth of the piston bowl is shallower for the prototype piston. For the piston impingement testing, the injection duration was set to 0.5ms. The injected fuel was E100.



Fig.4.27 Picture of pistons for Injector A (Right) and Injector C (Left)

Fig. 4.28 shows the results for the piston position 15mm down from the TDC position. The injector was placed on the right side of the images with the injector axis angle of 23 deg from the horizontal axis. The yellow line on the piston shows the bottom edge of the piston bowl. The imaginary combustion chamber roof and the spark plug were superposed on the images. The tested ambient temperature was 25°C and 150°C. The chamber pressure was atmospheric to simulate early injection for homogeneous operation mode. Fig. 4.29 shows the test result of Injector A with TDC piston position. The ambient condition was 200°C/3bar.

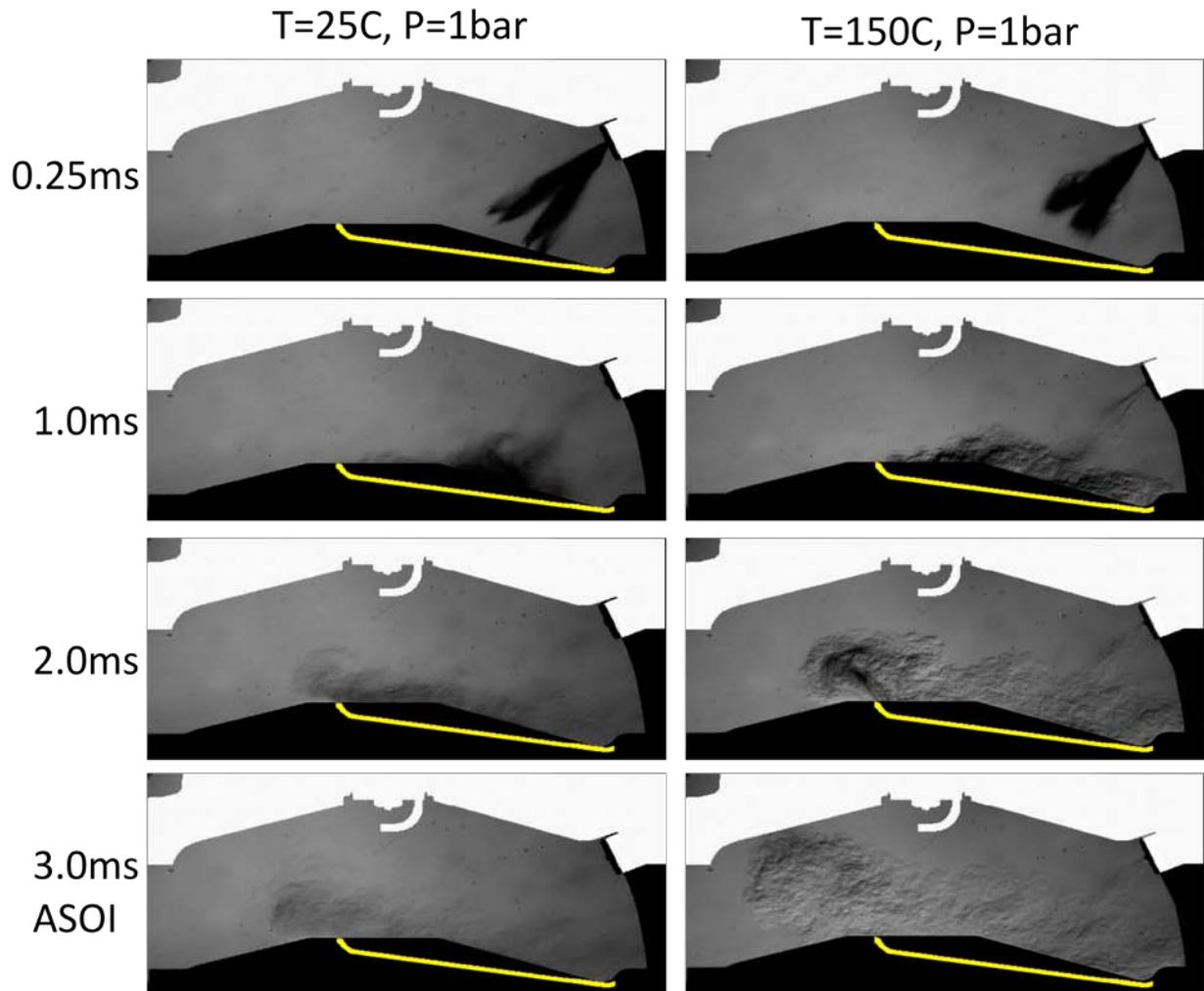


Fig. 4.28 Piston impingement, Injector C, 15mm, 0.5ms injection duration

Before the piston impingement, the spray with higher ambient temperature penetrated slower due to momentum dissipation by phase change as discussed previously. After the spray hit the piston, the spray under high ambient temperature traveled faster than the spray under room temperature. This after-impingement behavior was contrary to the free spray without impingement. It was generally observed that the fuel would wet the piston bowl and produce a thick film of fuel when the piston was relatively cool. However, as the piston surface temperature increased with the air

temperature, the fuel droplets in the spray tip could bounce and redirected along with the curvature of the piston bowl and produce a secondary spray of droplets bullets exiting the bowl (Fig. 4.29). These bounces have massive momentum and will travel across the combustion chamber until they hit the roof. And it results in greater penetration and the spray tip travels further than the combustion system designed. In order to avoid this effect, the spray targeting, the geometry of the piston bowl, and the operating conditions such as the injection timing and pressure must be refined.

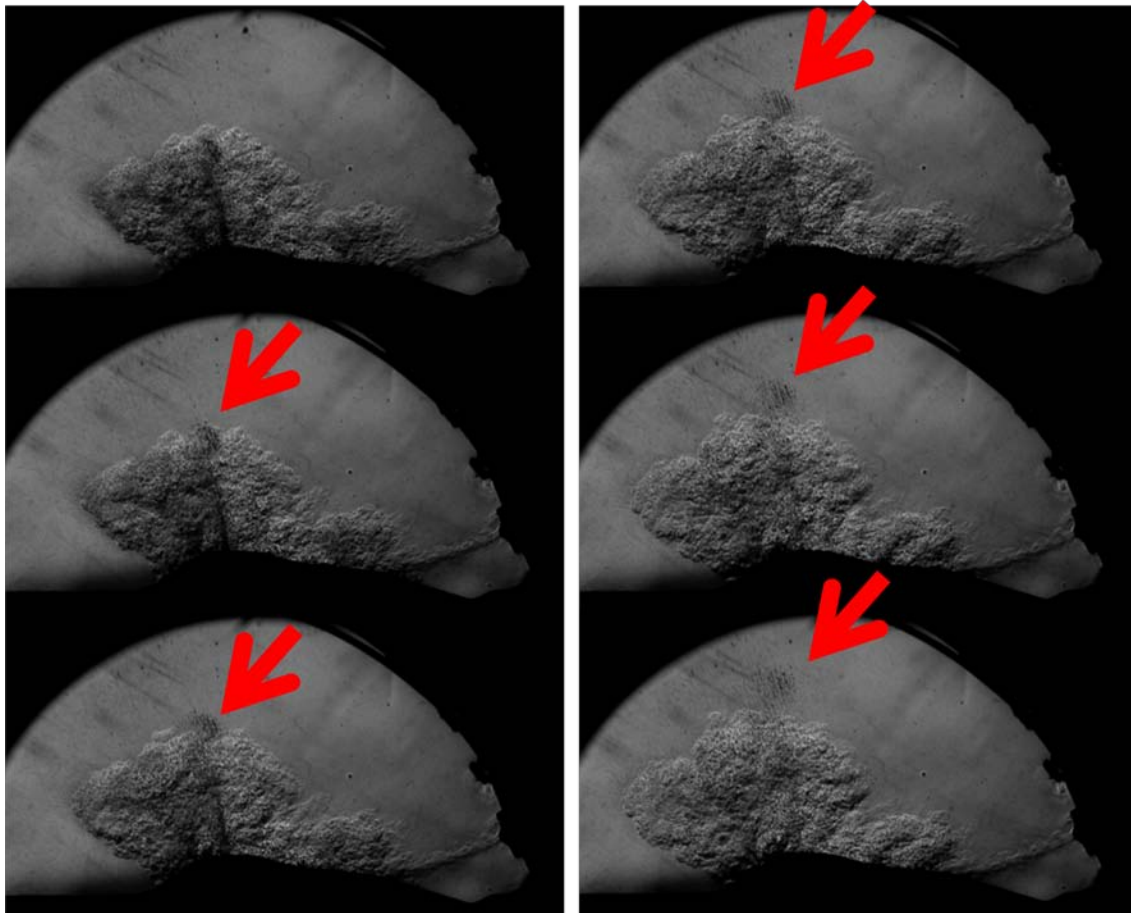


Fig. 4.29 Piston impingement, Injector A, TDC (T=200C P=3bar Duration=0.5ms)

4.4 PDI Spray Testing

Fig. 4.30 and 31 show the typical results of the high-speed Schlieren imaging of PDI spray injection. The intensity change at the middle of the picture is an artifact. The ambient temperature was 200°C. The ambient pressure was 4bar and 1bar respectively. The injection command pulse width (PW) was either 0.3ms which injected approximately 11mg of fuel, or 0.5ms injected 19mg. The time starts counting at the rising edge of the command signal, where the injector driver was triggered. The actual start of injection is before 0.1ms after the triggered signal. Comparing with 0.3ms delay by the multi-hole injectors that are activated by solenoid, piezoelectric injector's fast response is a great advantage especially for multi-pulse operation.

In Fig.4.30, only liquid phase was visible up to 0.5ms with some spikes at the spray front. These strings were reported in Ref [29] as well. At 0.6ms, there was some vapor observed at the vicinity of spikes and the side of "umbrella" where vortices formed. Appearance of vapor in those area is reasonable because the spikes had more surface available than a flat sheet, and the vortex area had better mixing for stronger heat/mass transfer. After the end of the injection at 0.6ms, the liquid spray became like a horizontal band. The body of the liquid fuel cloud maintained its position and continued vaporizing as time elapsed. The process of vaporization was relatively uniform because vaporization due to vortex carried on from the top of the fuel band, and vaporization due to enlarged available surface proceeded from the bottom. The vaporization was completed around 1ms. There was some dark area remained on the right end of the spray, but this must be a projection of very thick cloud of vapor in the direction of the light beam. When the ambient pressure was low as 1bar, less air resistance resulted in

liquid overlapping the vapor phase at the spray front and less vortex formed at the side. In this case, vapor cloud was observed to start forming in the middle of the umbrella at 0.5ms ASOI (Fig. 4.31) by spray liquid film becoming thinner and transparent. Propagation of a liquid band initiated by injector closing was clearly observed with this condition.

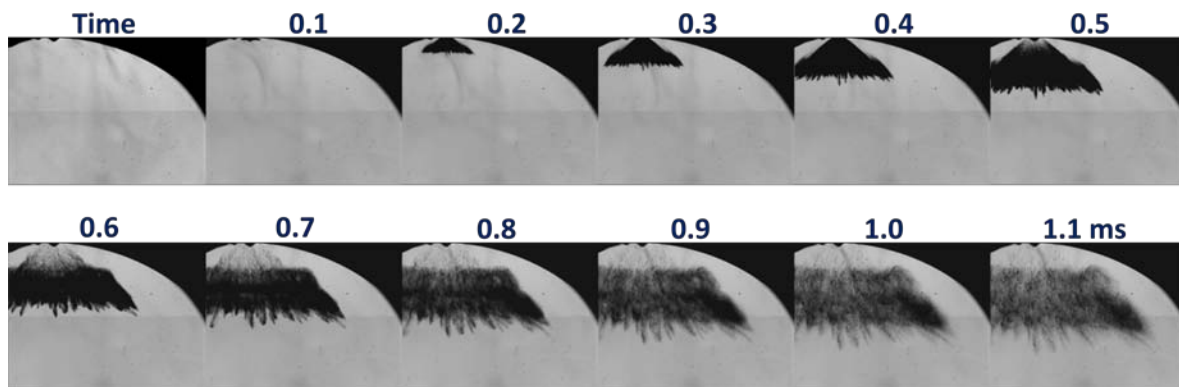


Fig. 4.30 PDI Injection at 200C/4bar, PW=0.3ms

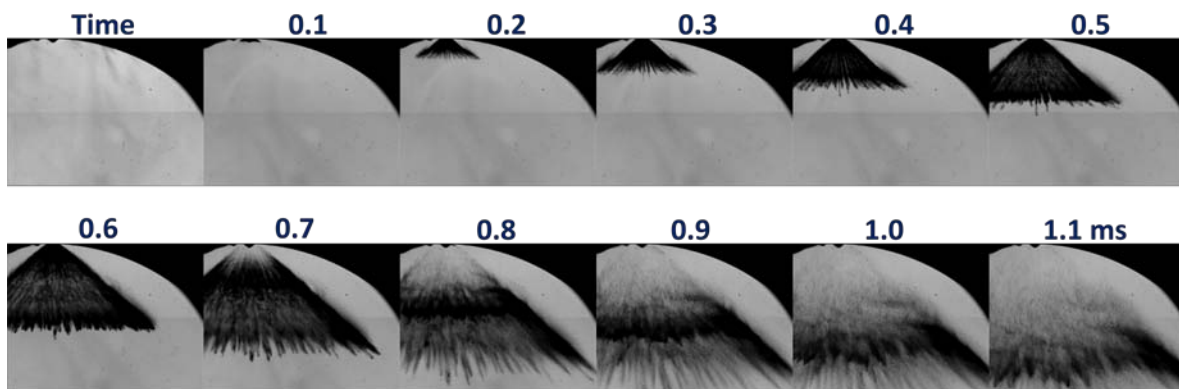


Fig. 4.31 PDI Injection at 200C/1bar, PW=0.5ms

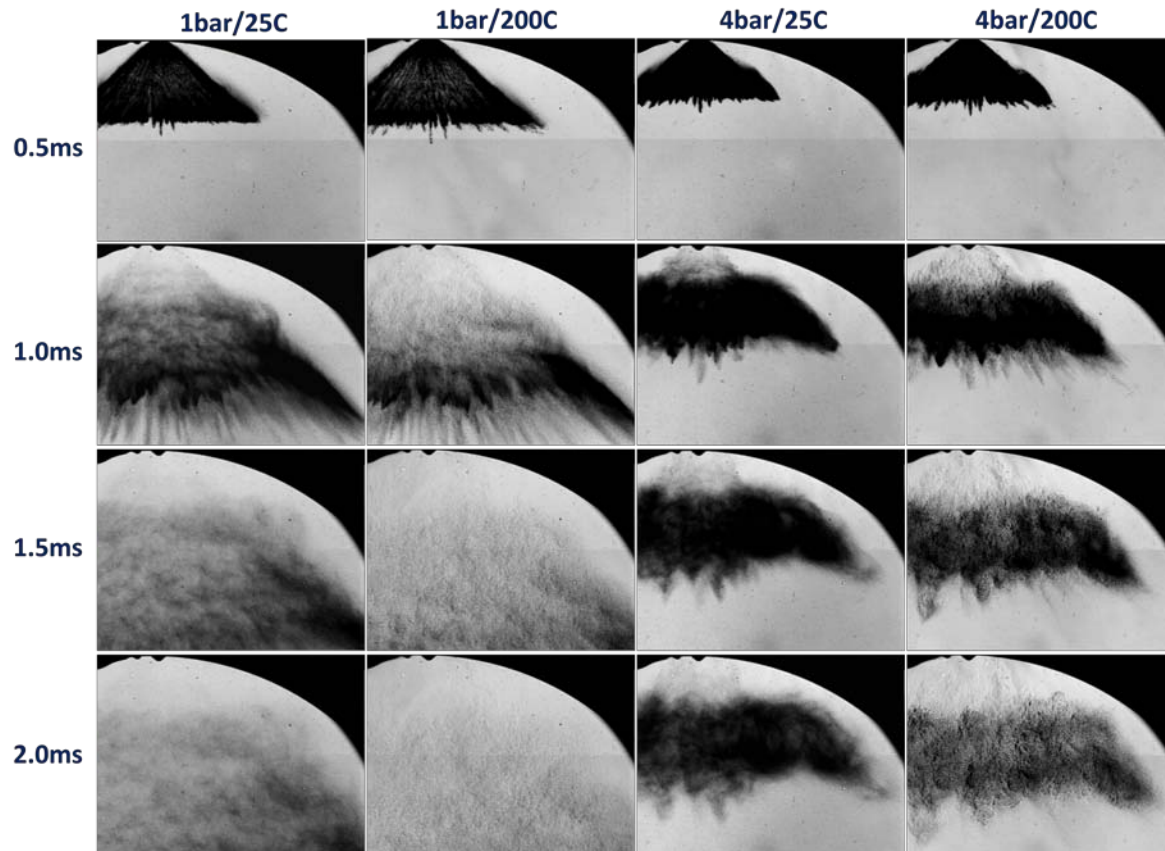


Fig. 4.32 Effect of ambient pressure and temperature

4.4.1 Effect of Ambient Condition

Fig. 4.32 shows the effect of ambient pressure and temperature on the spray structure. At the low ambient pressure, higher ambient temperature enhanced the degree of vaporization obviously, but the spray shape and the position of the mixture seems almost independent on the ambient temperature. After measuring the penetration of the sprays, which is the distance from the fuel exit to the spray front, it was found that the penetrations for varying ambient temperature were identical until 0.6ms as in the top figure in Fig. 4.33. At low temperature, the spray was broken up well but not vaporized as high temperature case was. Examination of Fig. 4.33 revealed that

the penetration curves were nearly straight at the beginning of the injection. After 0.5ms, it seems they started accelerating because of string development. This point can be considered as the primary break up point where shear force breaks the liquid layer of the spray. As Fig. 4.31 shows, the time of liquid layer break up and vapor phase forming was approximately 0.5ms ASOI.

When the injection was taken place in high pressure ambient, considerable suppression of the spray propagation was observed (Fig. 4.32). The mixture stayed at the middle of the picture and formed a fuel belt even at 2.0ms, and the accumulated droplets blocking the optical path resulted in the black cloud for the low temperature case. At the high temperature condition, those fuel cloud was vaporizing and the vapor phase was clearly visualized, while the position and the shape of the cloud seemed not to be much different from the low temperature case. However, there was a clear tendency in terms of penetration as the bottom figure of Fig 4.33 shows. The penetrations at different temperature at 4bar were almost identical at the early stage of injection, but after the spray break up at 0.5ms, higher ambient temperature could yield to longer penetration at the later stage of injection. This is an opposite trend to the result of multi-hole injector. Penetration of multi-hole injector becomes less if the ambient temperature increases because of enhanced vaporization resulting in momentum dissipation. For PDI, the effect of lower air resistance due to lower density of higher temperature air must become dominant. It should be noted that the flow rate of PDI was more than twice as Injector A (PDI:35g/s, Injector A:15.9g/s). Stronger initial momentum of spray was able to overcome the air resistance even after the spray was vaporized. As

same as low ambient pressure case, the point of separation of the penetration curves was around 0.5ms.

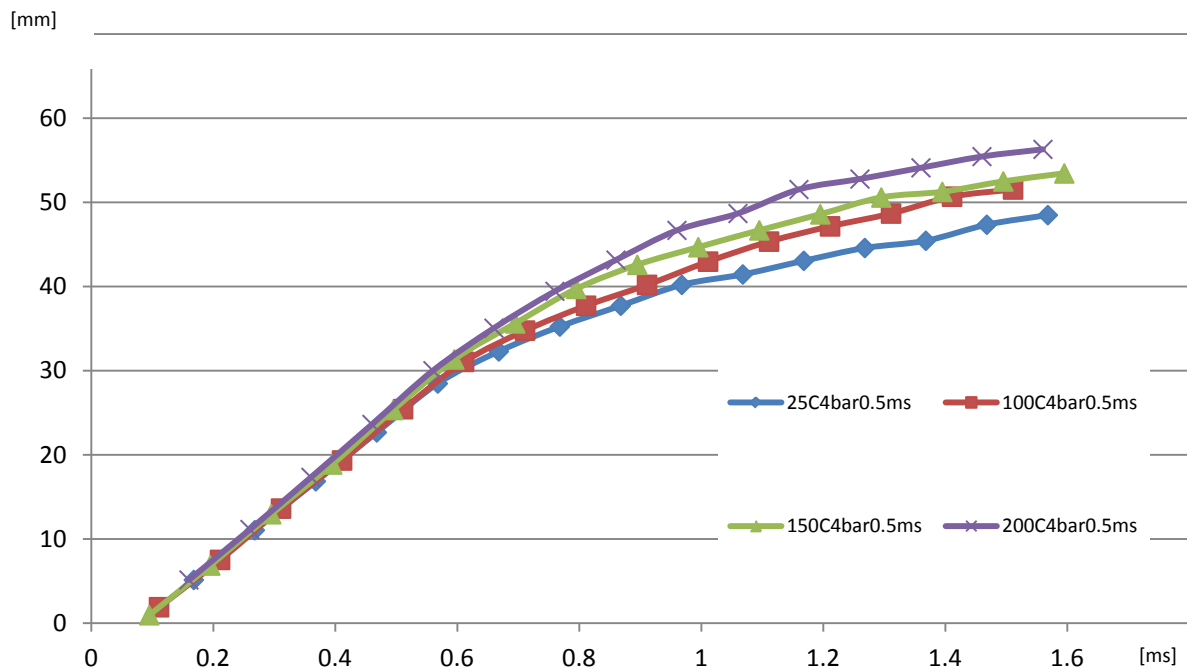
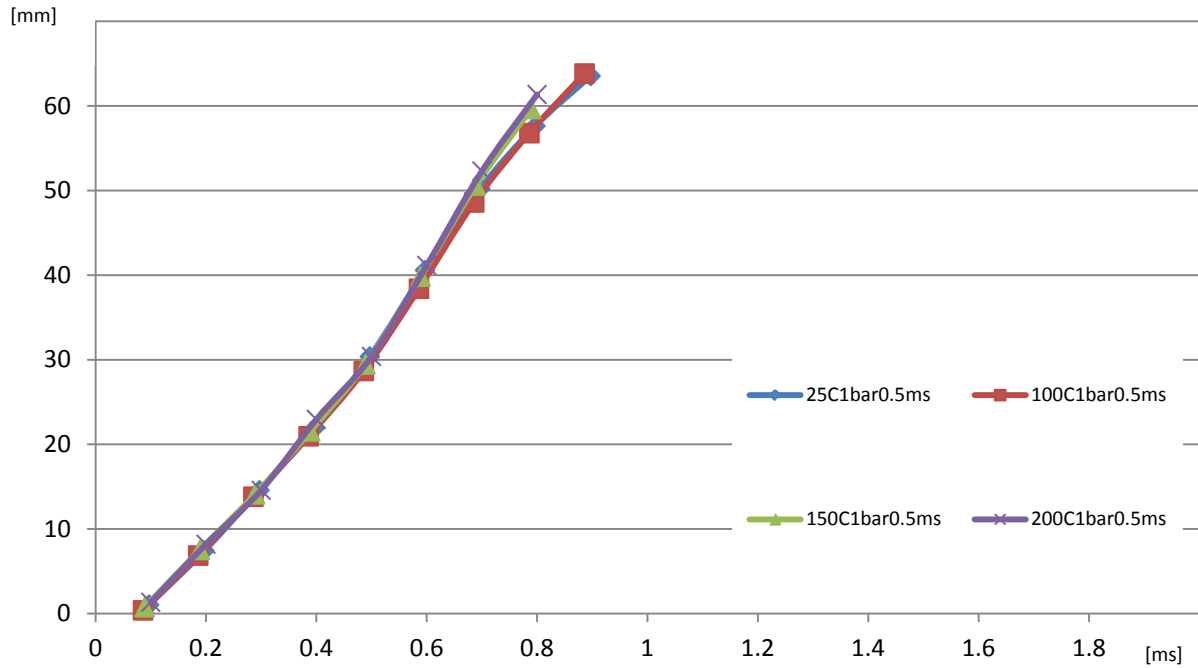


Fig. 4.33 Effect of temperature on penetration curve at 1bar (upper) and 4bar (bottom)

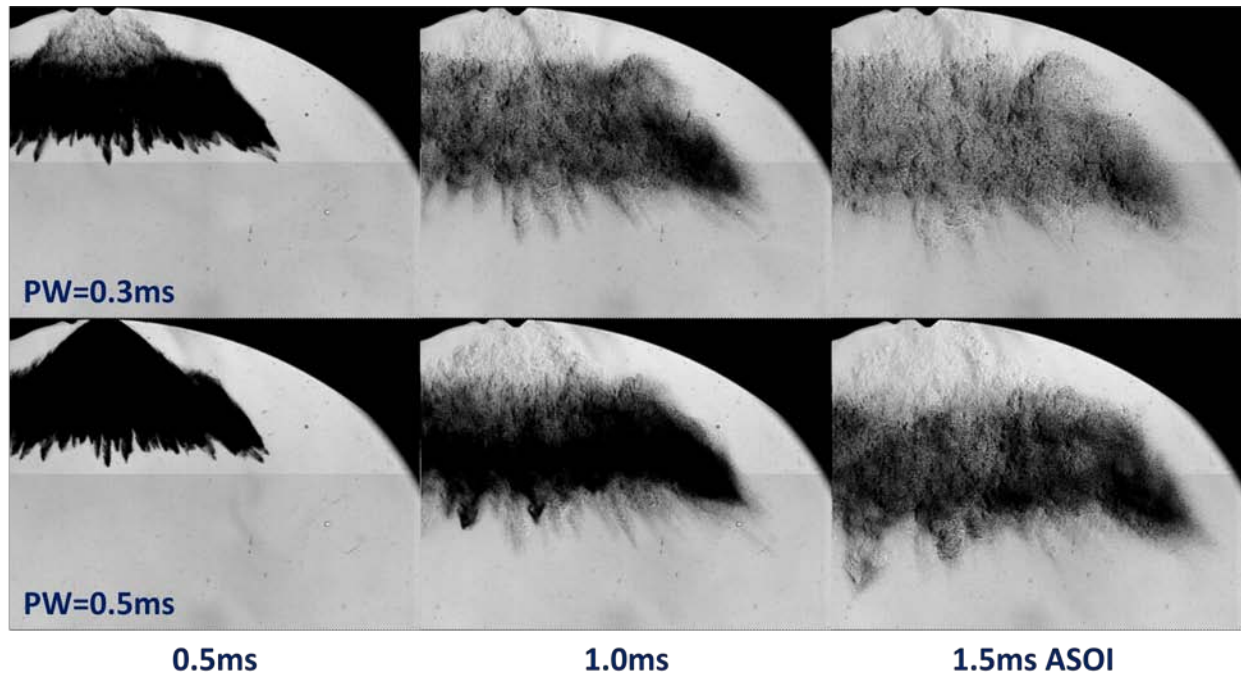


Fig. 4.34 Effect of pulse width (PW) at 200C/4bar ambient condition

4.4.2 Effect of Pulse Width

Fig. 4.34 shows the effect of pulse width (PW) on the spray structure. Since the longer PW provided more fuel injected mass, it took longer time for completing vaporization. Surprisingly, it seems PW did not affect much the position of the mixture cloud and it was confirmed by the penetration curves showed in Fig. 4.35. The penetration curves are independent on the injected mass up to 0.9ms. This can be explained by fast vaporization. The PDI spray consisted of a thin layer of liquid therefore it easily broke because of larger surface available for shear break-up. Once it broke, the liquid droplets turned into vapor quickly and slowed down. Even after breakup, the difference was not significant. This is a very preferred feature for a spray-guided GDI engine because delivery of proper air/fuel mixture near the spark plug is essential. In addition, excess wall wetting can be avoided in wide range of load operation.

4.4.3 Summary

PDI injector's fast response was proved. PDI spray can be characterized by liquid strings in the spray structure and vortices at the side of the umbrella, and vaporization was initiated at those area. The liquid spray broke evenly and formed relatively uniform vapor phase.

Spray penetration was linear and independent on ambient temperature up to 0.5ms. After 0.5ms, higher ambient temperature caused longer penetration at the later stage of injection probably due to lower air resistance. This is an opposite trend to the result of multi-hole injector. In addition, higher chamber pressure suppressed the spray penetration significantly.

It was found that the injection pulse width did not affect much the position of the mixture cloud. It is a preferred feature of PDI injector in real engine operation because delivery of proper air/fuel mixture near the spark plug is essential for a spray-guided GDI engine.

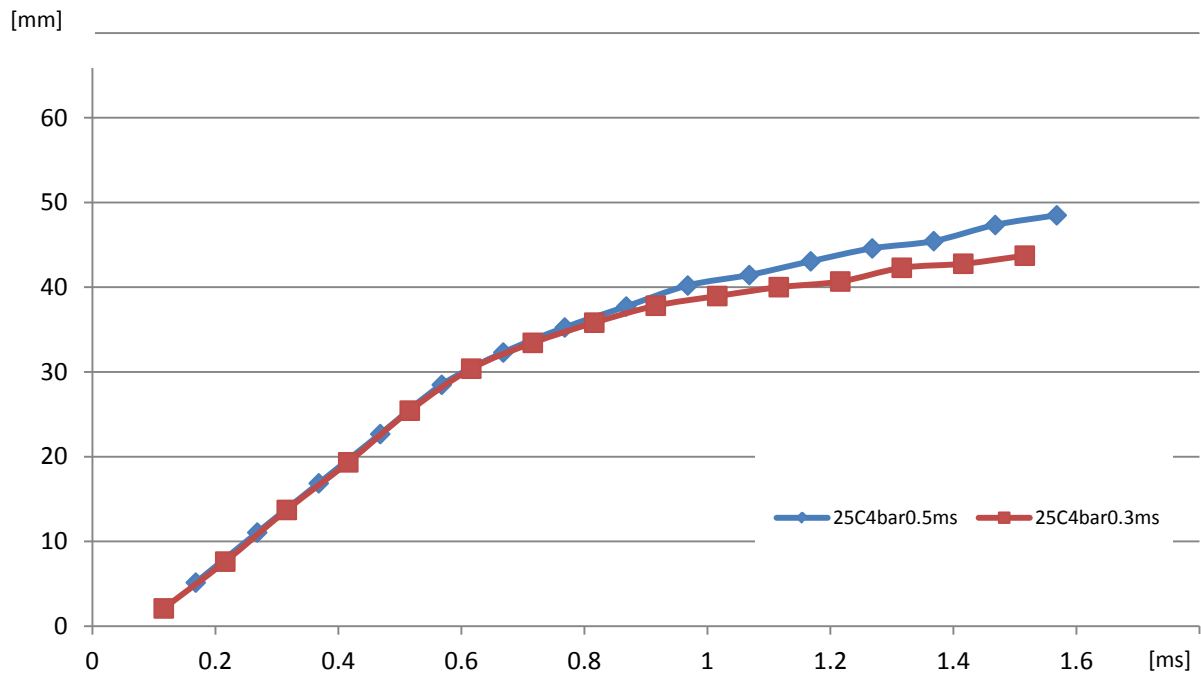
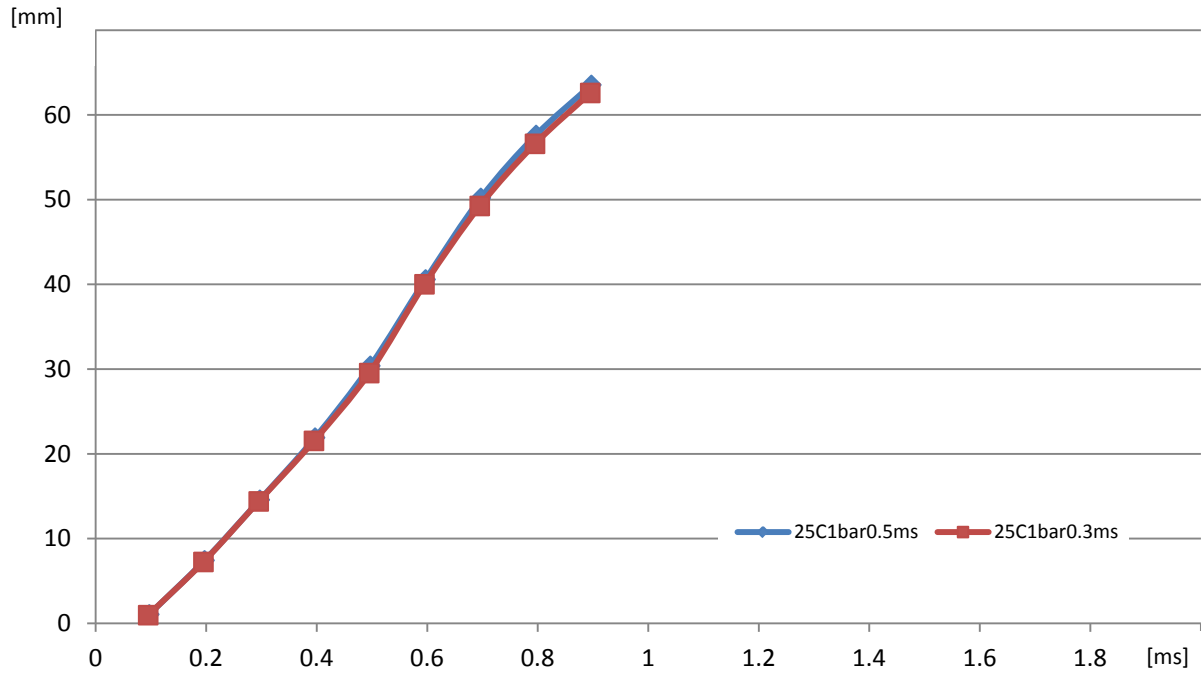


Fig. 4.35 Effect of PW on penetration curve at 25°C of at 1bar (upper) and 4bar (bottom)

CHAPTER 5 “Result of Optical Accessible Engine Testing”

Injector A and B were mounted on the Optical Accessible Engine (OAE) and high-speed visualization of the in-cylinder charge motion was carried out. The testing was conducted for the conventional valve strategy with the production cam, and for the advanced valve strategies with the prototype cams. With the conventional valve configuration, homogeneous and stratified charge mode were tested. With the prototype cams, effect of Early Intake Valve Close (EIVC) and Late Intake Valve Close (LIVC) cams in addition to intake valve deactivation on homogeneous charge motion was examined. Since projection halogen lamps were used for the light sources, only liquid phase of the sprays was visible in the experiment by Mie scattering. The injected fuel was 100% pure ethanol for all the OAE testing because of necessity of minimizing fuel deposit of the window and the liner. It should be noted that no significant difference in the spray shape is expected between E100 and E0 sprays in this particular operating condition, both homogeneous (low temperature and pressure) and stratified (high temperature and pressure), based on the findings in the spray chamber testing section. The OAE was motored at 1000RPM for all the testing conditions. In addition, CFD simulation was carried out for support and deeper understanding of the experimental result.

5.1 CFD Validation

In-cylinder CFD simulations for the spray and mixing in the OAE for both Injector A and B were conducted. An example of the result for Injector B is displayed in Fig. 5.1 and compared with the experimental results for validation. The simulation result shows

the 2D projection images of the particle distributions, with the radius information color coded. The injection quantity was 16mg which was achieved by 0.88ms of the injection command pulse width (PW), and the injection timing was 120 crank angle degrees (CAD) after top dead center (aTDC). The valve strategy was conventional two-valve operation with the production cam. The simulation results at the early stage of injection showed wider spray heads than the experimental results, and the fuel droplets of simulation result last longer than the OAE visualization possibly due to the drop size resolution limit of the Mie scattering visualization which seems to be about 1 μ m. Fig. 5.2 shows images comparison of spray with Injector A at 7.5 and 12.5CAD ASOI with injection at 90CAD for the LIVC deactivation configuration. The injection quantity was 9mg by 0.62ms of the injection command PW. Even though CFD spray over-penetrates for some extent, the agreement of overall spray shape with the experimental result was fair enough to pick up the unique fuel distribution of this condition. Even though further improvement is needed on the CFD configuration such as the breakup and heat/mass transfer models, the overall spray shape and the fuel distribution were comparable with the experimental results in both conventional and advanced valve train configurations.

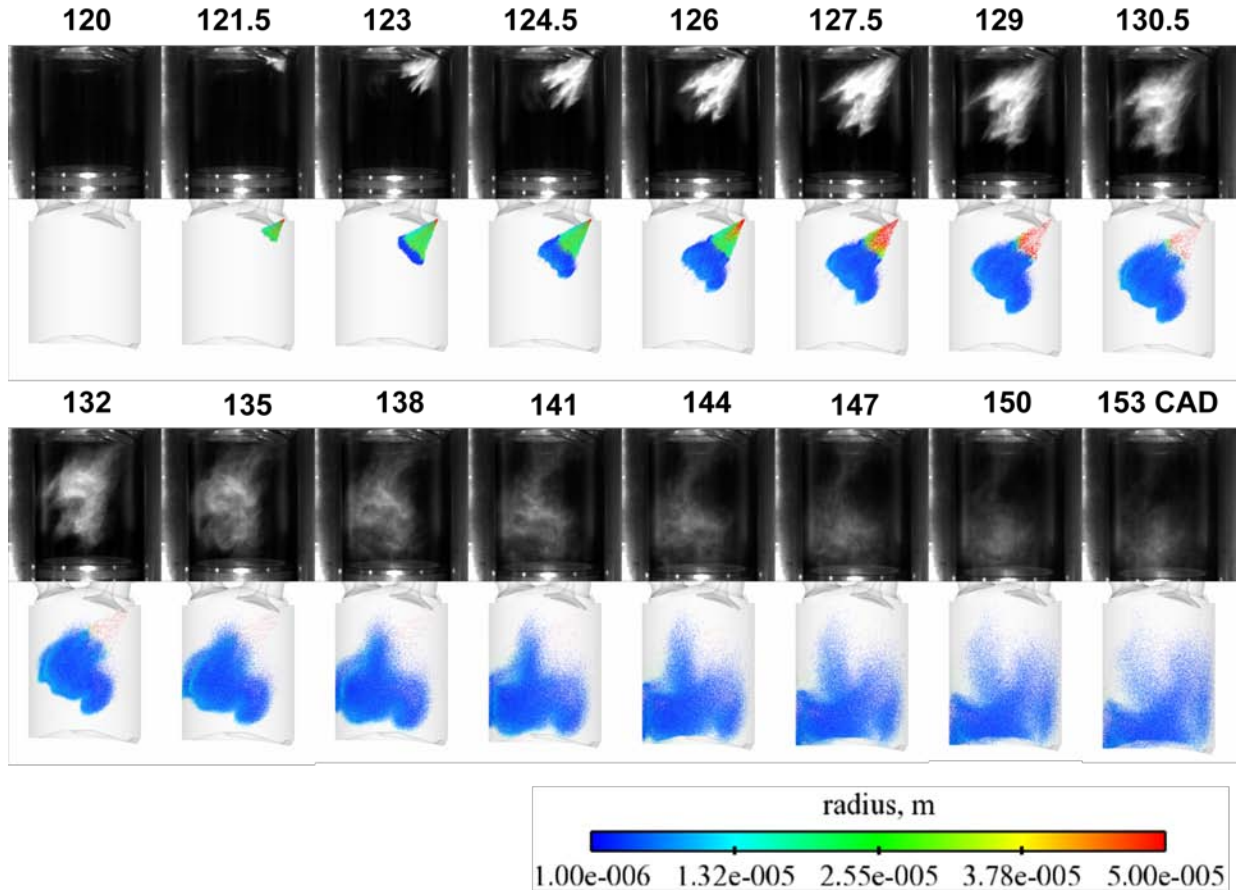


Fig. 5.1 CFD validation of Injector B with injection at 240CAD bTDC with normal valve configuration. Injection quantity was 16mg

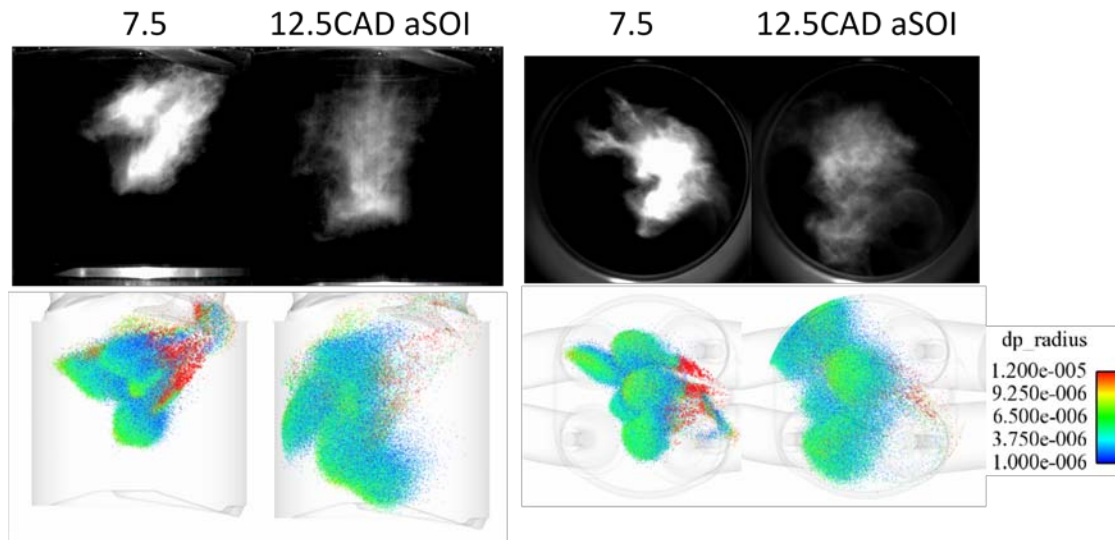


Fig. 5.2 CFD validation of Injector A with injection at 90CAD with LIVC deactivation configuration. Injection quantity was 9mg, side view (left) and bottom view (right)

5.2 Homogeneous Operation

High-speed in-cylinder visualization of homogeneous charge operation was carried out with the conventional valve strategy. Only side view results are discussed here because no swirl motion was observed with this valve setting. The camera speed was set to 8213FPS, which provided time resolution of 0.73CAD at 1000RPM operation. The effect of spray targeting on in-cylinder charge motion was examined first by comparing the spray and mixture behavior of Injector A and B. The injection timing and quantity were fixed at 60CAD aTDC and 32mg respectively. Then injection timing was shifted to 120 and 180CAD aTDC to evaluate the mixture behavior difference if the injection occurred in the middle and at the end of intake stroke. Injector B was used in this testing and the injection quantity was 16mg.

5.2.1 Effect of Injector Nozzle Design

Comparison of two different injectors in terms of mixture formation was conducted and the result image sequence of every 1.5CAD for homogeneous injection is shown in Fig. 5.3. 32mg of ethanol was injected starting at 60CAD aTDC (300CAD before firing TDC). Comparison of two different injectors confirms that the spray of Injector B has more serious piston hitting because the aiming of Injector B was more downward. However, the spray targeting more inclined from the cylinder axis by Injector A hit the cylinder wall at 72CAD. As Fig. 5.3 shows, spray targeting of Injector B was able to avoid the serious side wall wetting while the upper spray of Injector A hit the liner. The side wall hitting can become the source of unburned hydrocarbon and a concern for oil dilution. Although piston impingement can be managed by shifting the injection timing,

the magnitude of side wall wetting depends on geometrical design of the chamber and spray targeting if the injection is limited to single pulse. After the injection, fuel droplets were "tumbled" by the intake air motion. This tumble motion was smoother and stronger with Injector A. The mixture of Injector B behaved stagnated near the piston for an instant after it hit the piston. It seems to have less tumble motion because Injector B was aiming the lower half of the tumble flow which was counter-clockwise and against the direction of the spray. The velocity field simulated by CFD confirmed spray-tumble motion interference. Fig. 5.4 shows the velocity plot on the center plane of the cylinder at the time of injection and it schematically explains the direction of spray is against the direction of tumble. The strong intake air flow traveled across the top of the cylinder and blew down along with the left cylinder wall. Therefore strong counter-clockwise tumble motion was formed at the left half of the cylinder at the time of injection.

The simulation results for the bulk flow dynamic ratios and the total turbulent kinetic energy were plotted in Fig. 5.5. The calculation result without injection is on the figure as well. The dynamic ratios contains two directions of tumble and swirl ratios. The dynamic ratios are defined as the ratios of the three directions of angular speeds of the flow to the angular speed of the crankshaft.

$$\text{Dynamic Ratio} = \frac{\omega_i}{\omega_{crankshaft}}$$

The component of angular speed can be calculated from the angular momentum L_i and the moment of inertia I_i .

$$\omega_i = \frac{L_i}{I_i}$$

The moment of inertia about the z-axis I_3 , for example, for a system of cells can be expressed as:

$$I_3 = \sum_{n=0}^{\text{numcells}} m_n [(x_n - x_{cm})^2 + (y_n - y_{cm})^2]$$

where m_n is the mass of each cell, x_n and y_n are the coordinates of each cell, and x_{cm} and y_{cm} represent the location of the center of the mass, which is considered as the center of rotation. The turbulent kinetic energy is defined by half the trace of the stress tensor. The turbulence can enhance mixing and vaporization through the process of heat/mass convection by turbulent eddies in the flow. It is reasonable that the in-cylinder flow has only one dominant direction (Y) of tumble and almost zero swirl ratio because of the intake port design of the cylinder head. The tumble ratio increased to the peak at around 90CAD aTDC due to intake and piston motion. The curves hit the bottom around BDC, and reached another peak later at 75 CAD before compression TDC, although the second peak was slightly lower due to viscous dissipation. It is found that the both injectors at the early injection timing of 60CAD aTDC counteracted the tumble motion and diminished it to be less the tumble ratio of motoring only. As a result, the tumble ratio curve with the injection stayed lower than the motoring curve all the way. In spite of a sudden jump of turbulent kinetic energy (TKE) at 60CAD imparted by the direct fuel injection into the in-cylinder bulk flow, the total TKE was quickly dissipated. The lower tumble ratios of the cases with injection could not transfer enough energy from the mean flow energy into higher turbulence intensity near the compression TDC, where the turbulent energy is needed the most to speed up combustion. As observed in the in-cylinder visualization, Injector A showed stronger tumble than Injector B because its

spray axis was more aligned with the tumble flow initiated by the intake process in the current combustion chamber geometry. CFD result revealed that the wall film mass of Injector B was almost twice as much as Injector A (Fig. 5.6) because of serious piston impingement. Careful design of spray targeting is recommended to maximize mixing and turbulent energy by strong in-cylinder charge motion and minimize the wall wetting simultaneously.

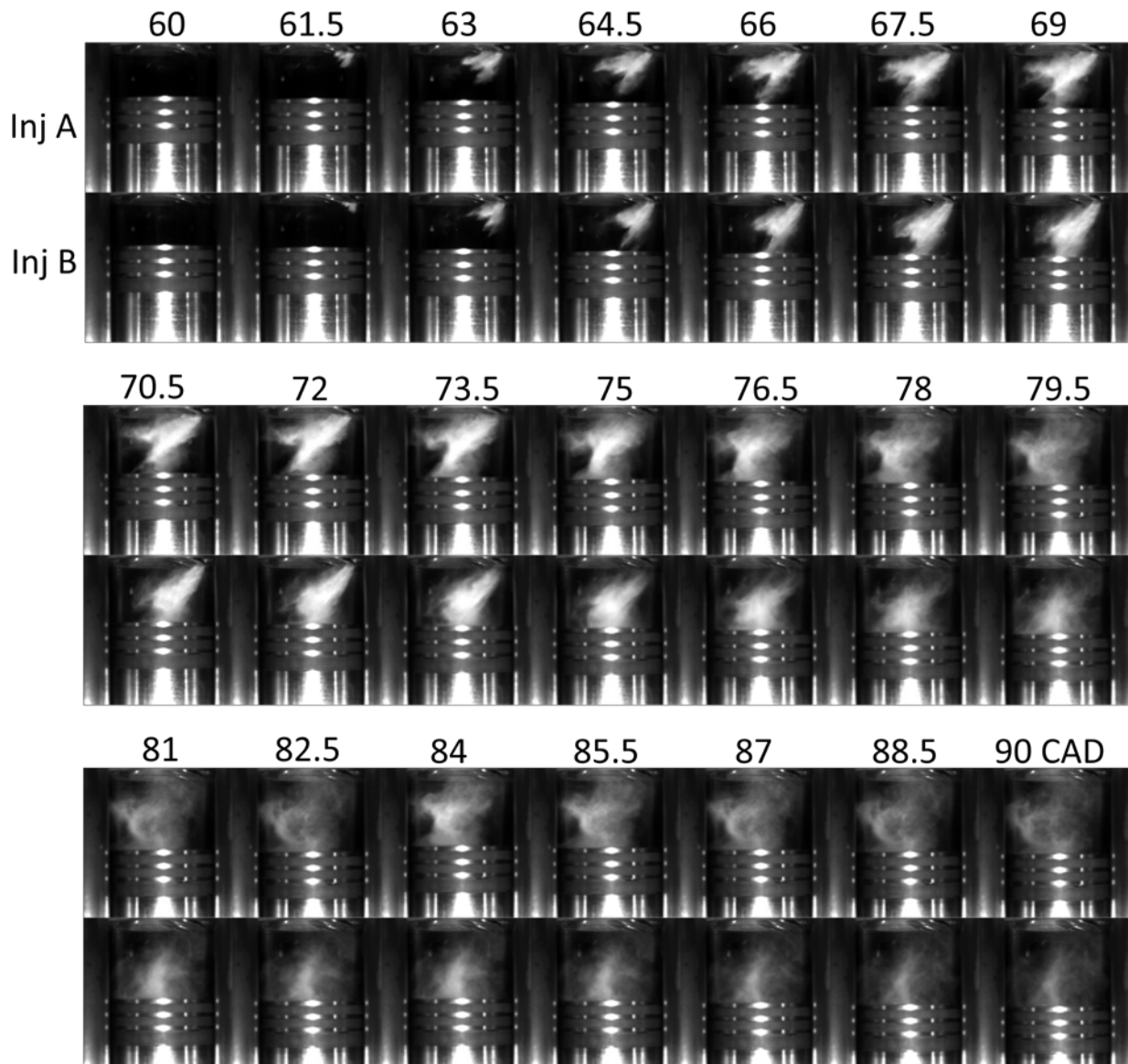


Fig. 5.3 Homogeneous injection at 60deg after intake TDC with different injector

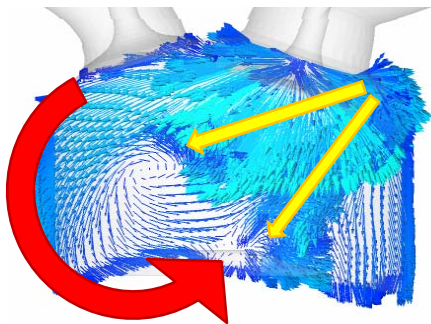


Fig 5.4 Schematic image of spray-tumble motion interaction

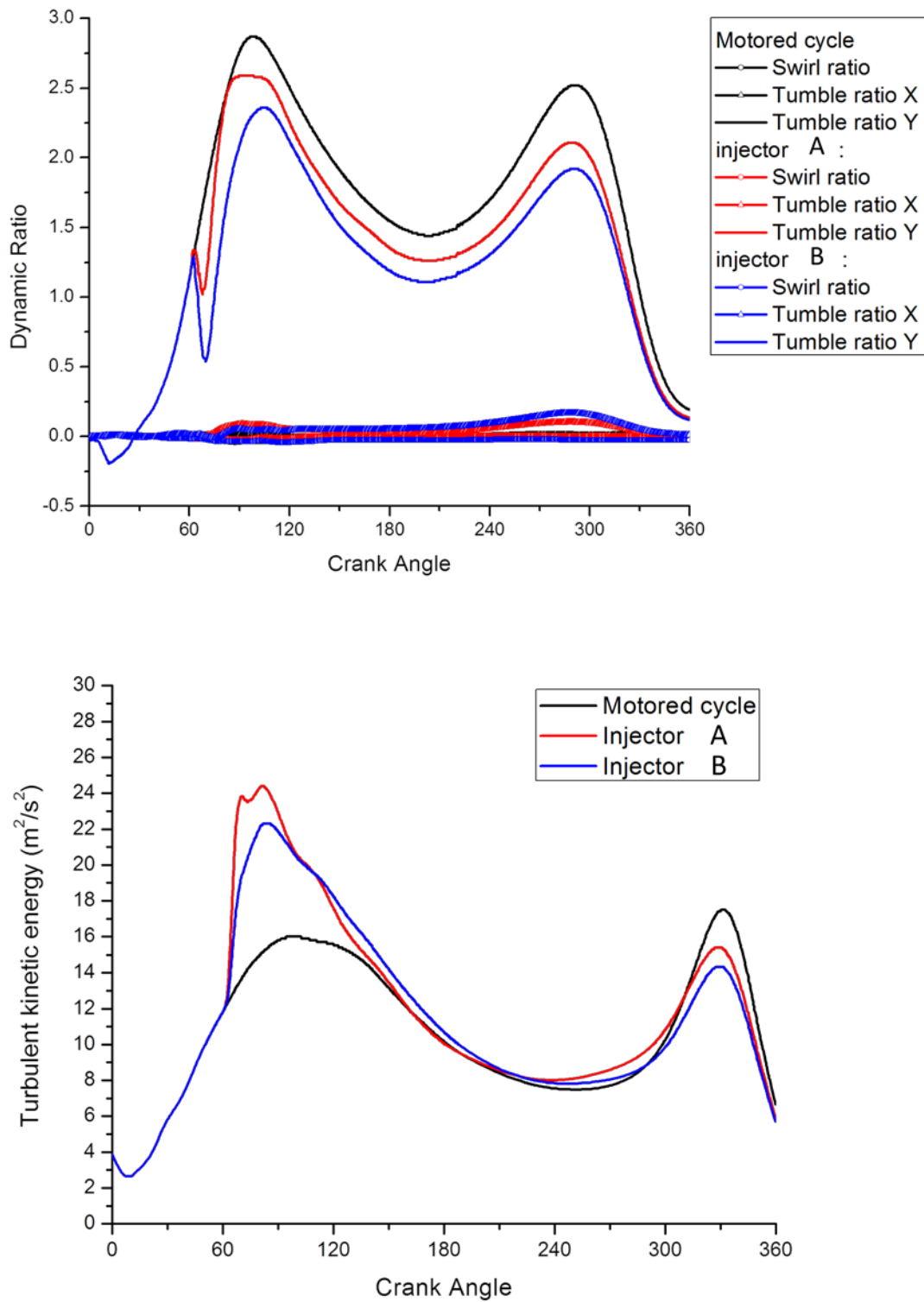


Fig. 5.5 Dynamic ratio and turbulent kinetic energy of homogeneous injection at 60CAD aTDC

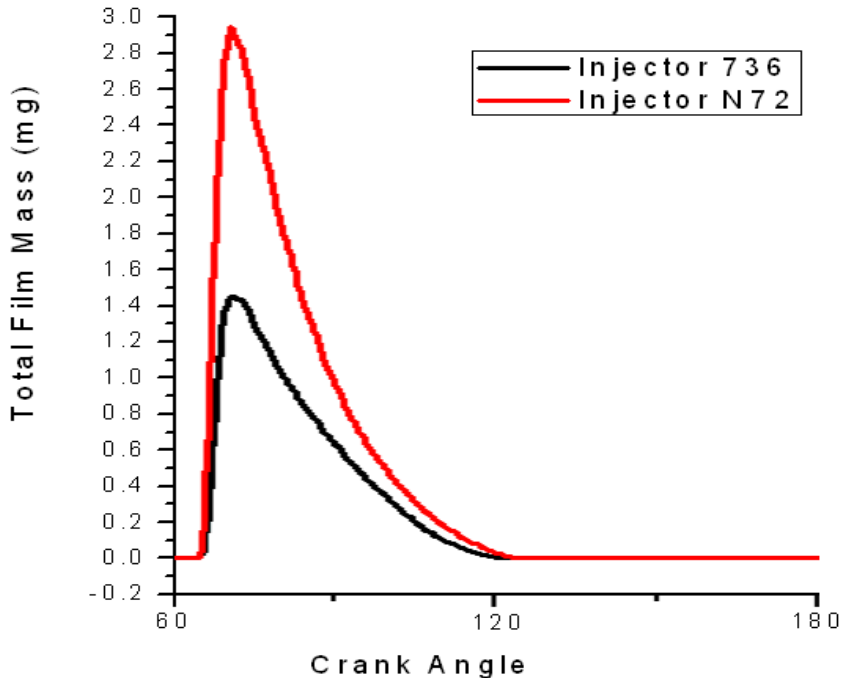


Fig. 5.6 Total wall film mass of homogeneous injection at 60CAD aTDC

5.2.2 Effect of Injection Timing

In order to evaluate the effect of injection timing in a large scale on mixture formation for the homogeneous operation, two other injection timings, 120 and 180CAD aTDC were tested. 16mg of ethanol was injected by Injector B. The result images are shown in Fig. 5.7 for comparison. In the figure, the numbers on the top of the images represent the crank angle elapsed after the start of injection instead of crank angle degree counting from TDC. As pointed out previously, injection at 60CAD resulted in stagnation of fuel cloud near piston because the spray was injected against the direction of tumble. However, spray injection at 120CAD did not show such behavior. The fuel droplets seem smoothly mixed and tumbled with air. The center of the tumble rotation moved down with piston motion thus the spray momentum was no longer against the tumble rotation. Actually, it assisted the air blow down which existed on the left edge of

the cylinder. There was a huge difference between 60CAD and the other two conditions in terms of the piston impingement, too. If the fuel was injected after 120CAD, no impingement was observed, which greatly helps reducing unburned hydrocarbon and soot emission. Between 120 and 180CAD, an obvious difference occurred in mixing after the injection. Fig. 5.8 shows images at 30CAD ASOI for each case. Since 120CAD was on the middle of intake stroke, dynamic in-cylinder flow caused by air induction assisted spray cloud break up and the mixture was carried away to fill up the cylinder more horizontally uniform. The fuel droplets of injection at 120CAD traveled more assisted by the blow down of the intake air, while the fuel of injection at 180CAD stayed in the left half of the chamber yet because of less dynamic in-cylinder flow caused by slower piston movement and closing intake valves. Generally, injection widow is constrained by the soot emission with early injection which is strongly dependent on piston surface wetting, and poor combustion stability with late injection which is dependent on the mixture uniformity. The experimental results were consistent with this respect.

The dynamic ratio and the turbulent kinetic energy calculated by CFD are shown in Fig. 5.9. For the injections of 120 and 180CAD after the intake TDC, no more decrease of the tumble ratio caused by injection was observed. The tumble ratio was enhanced by the fuel injection, as observed by the OAE experiment, and was maintained to be more than the motoring case for the rest of the cycle. Enhanced turbulent energy by stronger in-cylinder motion was also observed at the end of compression stroke. This is where ignition takes place, therefore the late injections are preferred for faster combustion in terms of turbulent energy.

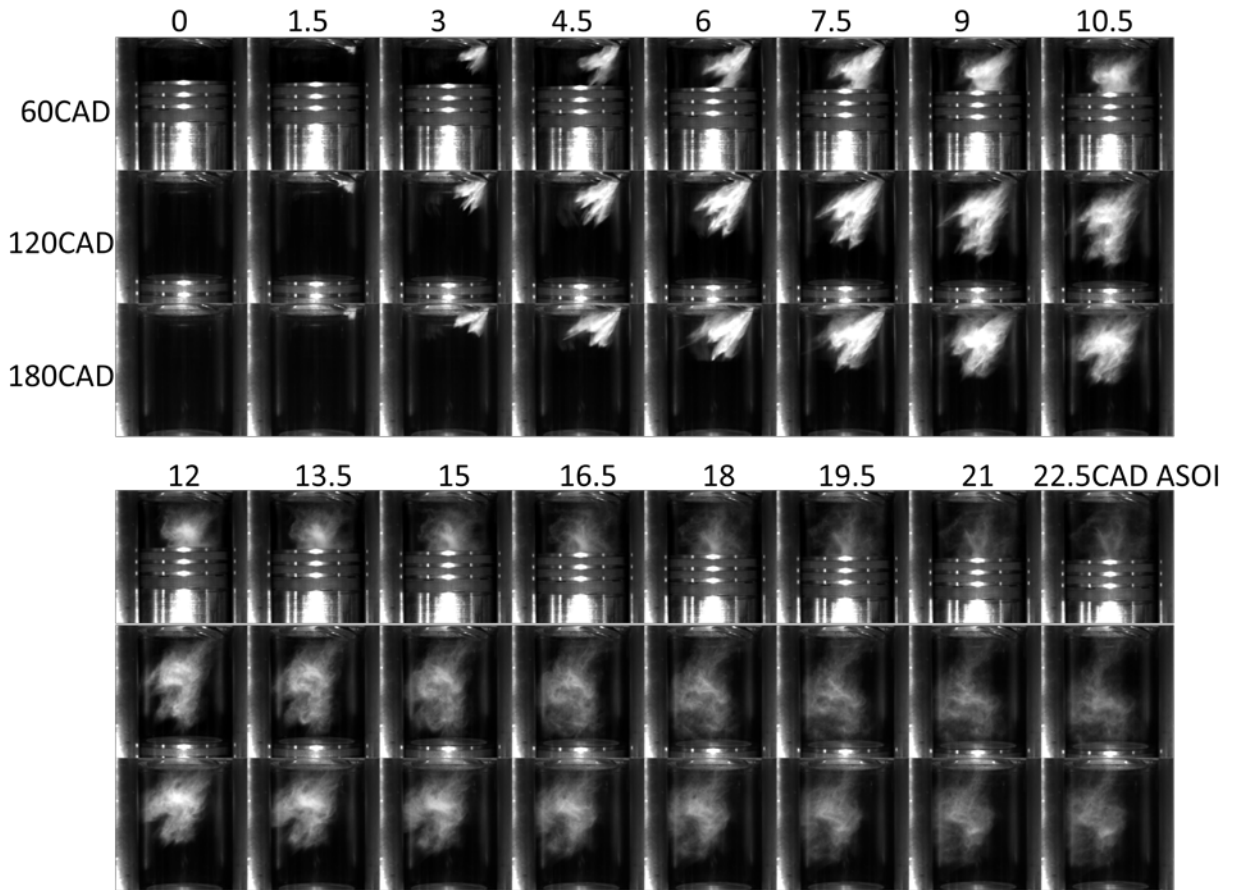


Fig. 5.7 Effect of injection timing on spray and mixing for the homogeneous operation

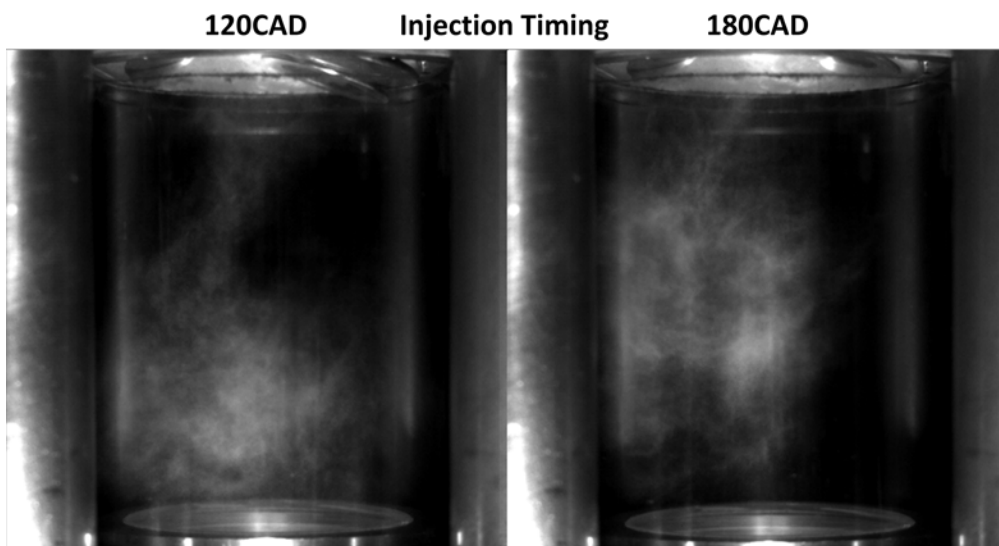


Fig. 5.8 Effect of injection timing on mixing at 30CAD after start of injection

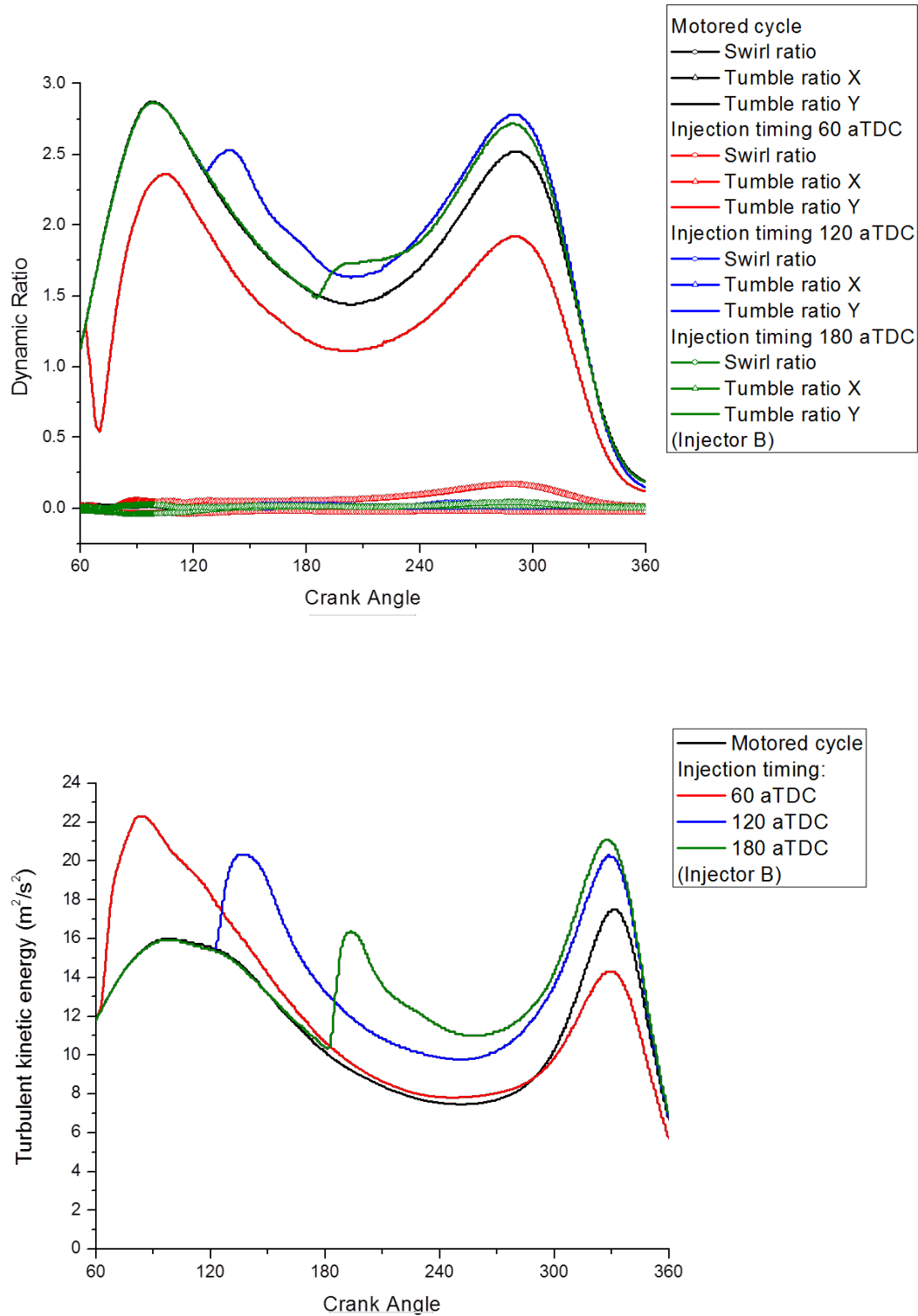


Fig. 5.9 Dynamic ratio and turbulent kinetic energy of homogeneous injection at various timing (Injector B)

Study of Wall Wetting

Figs. 5.10 and 11 show the CFD results of the distribution of the equivalent ratio on the center plane (X-Z) of the cylinder. The injection timing was at 60CAD aTDC. Very rich mixture which equivalence ration was over 9 existed near the piston when the spray hit the surface. Continuous vaporization from the piston surface where spray touched was observed after the fuel impingement, which indicated that a liquid fuel film was formed. The side- and bottom-view of the wetted footprints on the piston at 90CAD aTDC, and the total liquid film mass history as computed by CFD are shown in Fig. 5.12. With the early start of injection at 60CAD, large amount of liquid sticks on the surface due to the relatively shorter injector-piston distance. The maximum wall film amount for Injector B was almost twice as much as Injector A in spite of less liner wetting because of its spray targeting. This piston wetting can be avoided by retarding the injection timing. If the injection timing was set to be later than 120CAD, the maximum film mass is reduced by 62%. Since the spray injected at 120CAD and later was not found to touch the piston, the film mass could be located on the side wall. The time delay from SOI to the rising of the film mass (approximately 12CAD for the cases of SOI at 120 and 180CAD) confirmed it by agreeing with the time of cylinder wall impingement observed in the OAE testing as shown in Fig. 5.7.

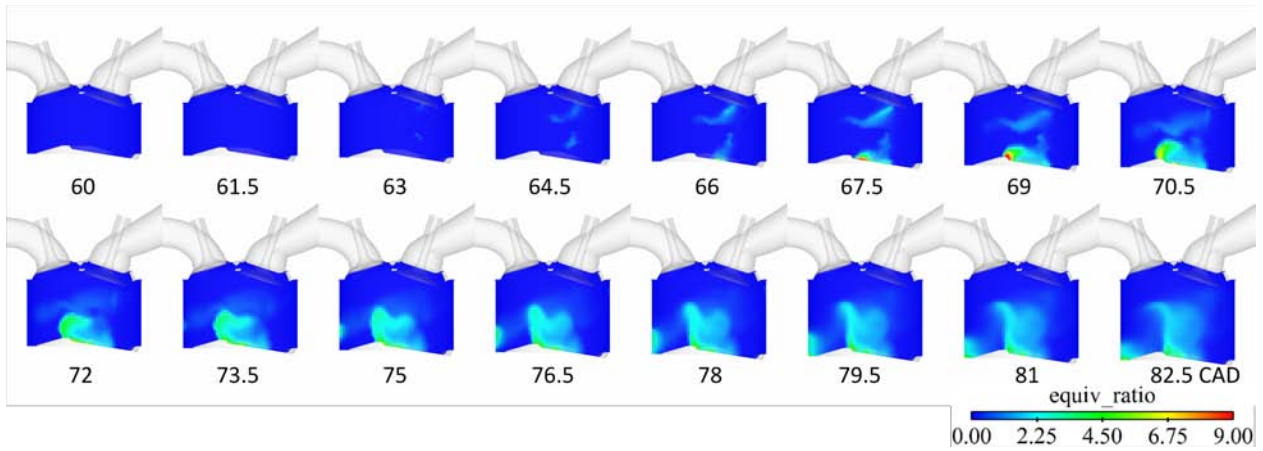


Fig. 5.10 Equivalent ratio distribution of homogeneous injection at 60CAD aTDC with Injector A

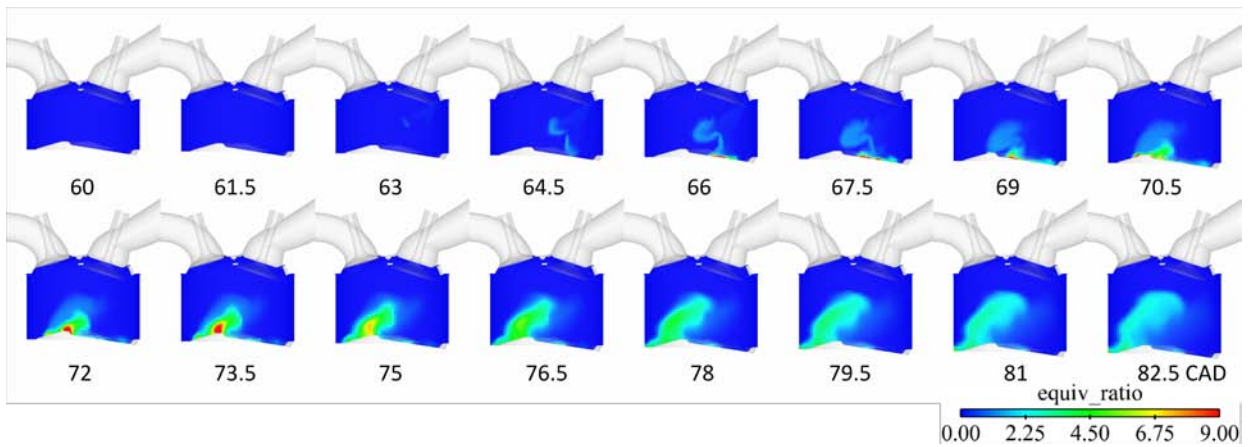


Fig. 5.11 Equivalent ratio distribution of homogeneous injection at 60CAD aTDC with Injector B

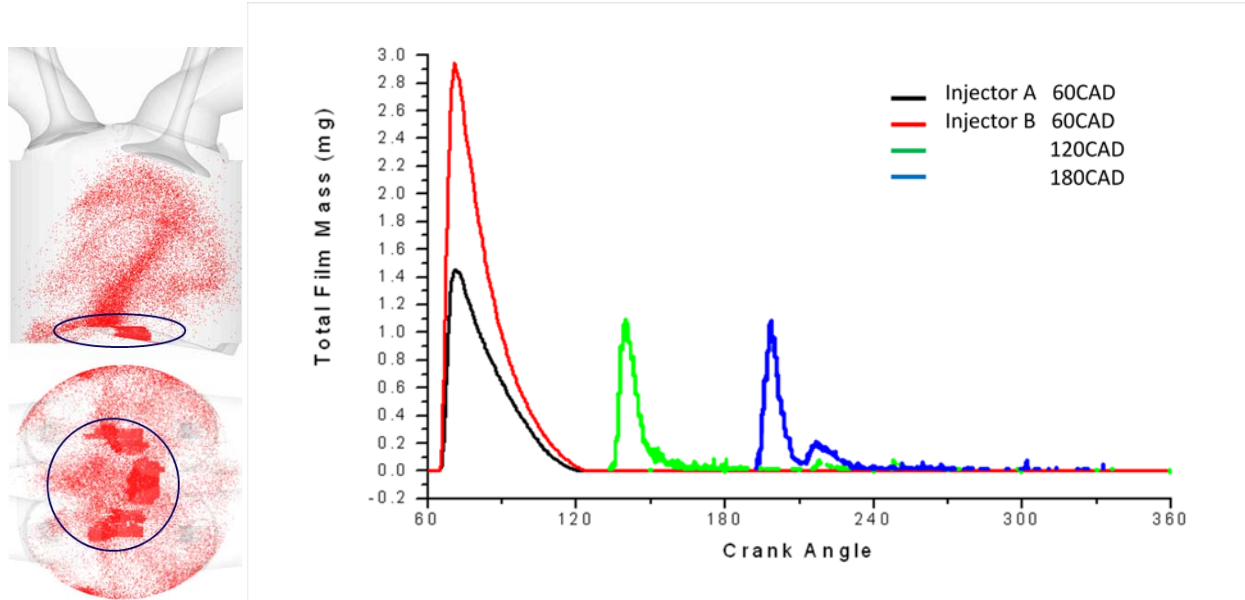


Fig. 5.12 Piston wall wetting footprints and total liquid film mass evolution for homogeneous injection

5.2.3 Summary

High-speed in-cylinder visualization of homogeneous charge operations was carried out with the conventional valve strategy. Spray injection at 60CAD with different injector A and B was tested first. The spray targeting of Injector B, which aimed more downward, resulted in stronger piston impingement with less side wall wetting. Both injection were against the direction of in-cylinder tumble flow and decreased tumble ratio from the motoring curve was observed. Charge motion with Injector A has stronger tumble than Injector B because its spray axis was more aligned with the tumble flow. The lower tumble ratios by injection could not transfer enough energy from the mean flow energy into higher turbulence intensity near the compression TDC.

Spray injection at 120 and 180CAD did not show the stagnation of fuel cloud because the direction of spray momentum was no longer against the direction of tumble

motion. The tumble ratio and the turbulent energy were even increased by later injections. GDI operation with later injection was not suffered by piston impingement but side wall wetting only. Since 120CAD was in the middle of intake stroke, dynamic in-cylinder flow caused by air induction assisted spray cloud break up and the mixture was carried away to fill up the cylinder more horizontally uniform. The fuel cloud of injection at 180CAD stayed in the left half of the chamber even at 30CAD ASOI because of less dynamic in-cylinder flow caused by slower piston movement and closing intake valves.

5.3 Stratified Operation

In-cylinder visualization of stratified charge operation was carried out with the conventional valve strategy with Injection A and B. The injection timing was fixed at 290 aTDC (70deg before compression TDC), and the fuel quantity was 16mg. The camera speed was set to 8213FPS as same as homogeneous operation.

Fig. 5.13 shows the result images of stratified in-cylinder charge visualization. Since the fuel was injected at the middle of compression stroke, higher ambient pressure suppressed the spray propagation shorter and narrower. Promoted vaporization by higher in-cylinder temperature also contributed for shorter spray because only liquid phase of the fuel was visible with Mie-scattering. Comparing with Injector A, the charge motion with Injector B was less dynamic. The fuel cloud of Injector B was seemed stagnated and moved upward only with piston motion. However, horizontal movement of droplets was observed with Injector A. As images at 15CAD after the injection shown in the Fig. 5.14, the spray of Injector B tended to accumulate in the center of the cylinder due to the spray targeting. This is a critical advantage if the

engine is running in stratified mode which needs fuel mixture only near the spark plug. At 296CAD, lower spray hit the piston top. A piston impingement must be managed well in order to optimize the stratified charge formation and to avoid hydrocarbon and soot emissions as discussed previously. Especially for stratified operation, much shorter time between wall impingement and start of combustion strongly affect the engine performance and emission.

The dynamic ratios and the total turbulent kinetic energy of stratified injection at 290CAD aTDC are shown in Fig. 5.15. As observed on the homogeneous injection at 60CAD, both injectors reduced the tumble ratio. This is because of contradiction of the direction of spray and tumble rotation. Although the injections transiently increased the turbulent energy significantly, it became even lower than the motoring case at the critical time of flame development. The injection strategy and the spray targeting should be revised for better burning.

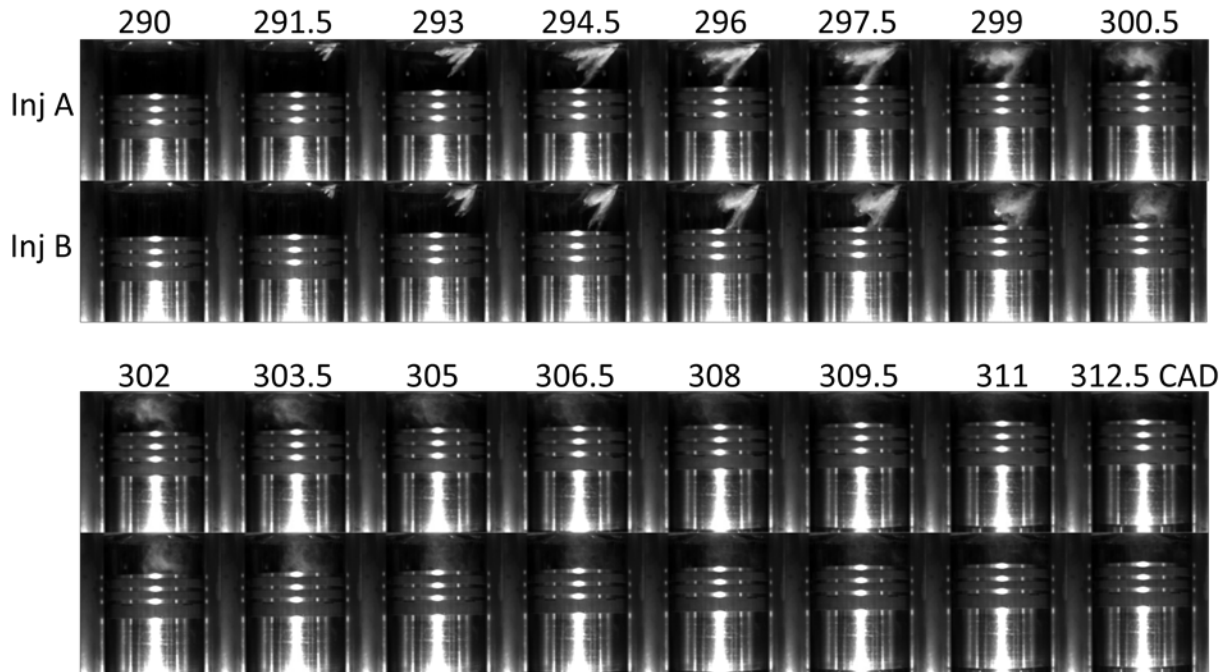


Fig. 5.13 Stratified injection at 70deg before compression TDC

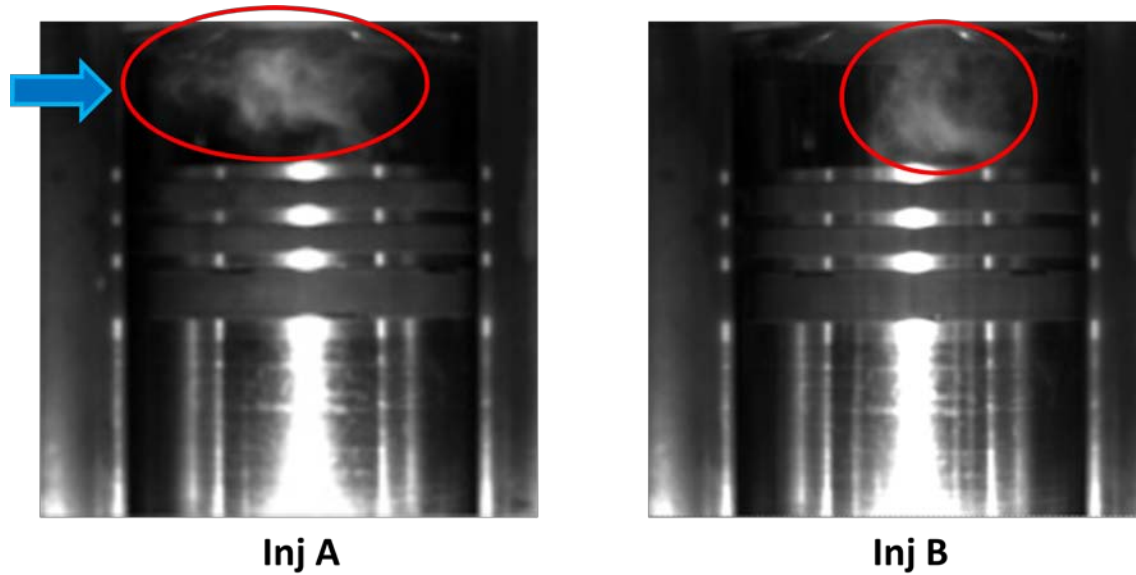


Fig. 5.14 Mixture accumulation of stratified injection at 15CAD ASOI

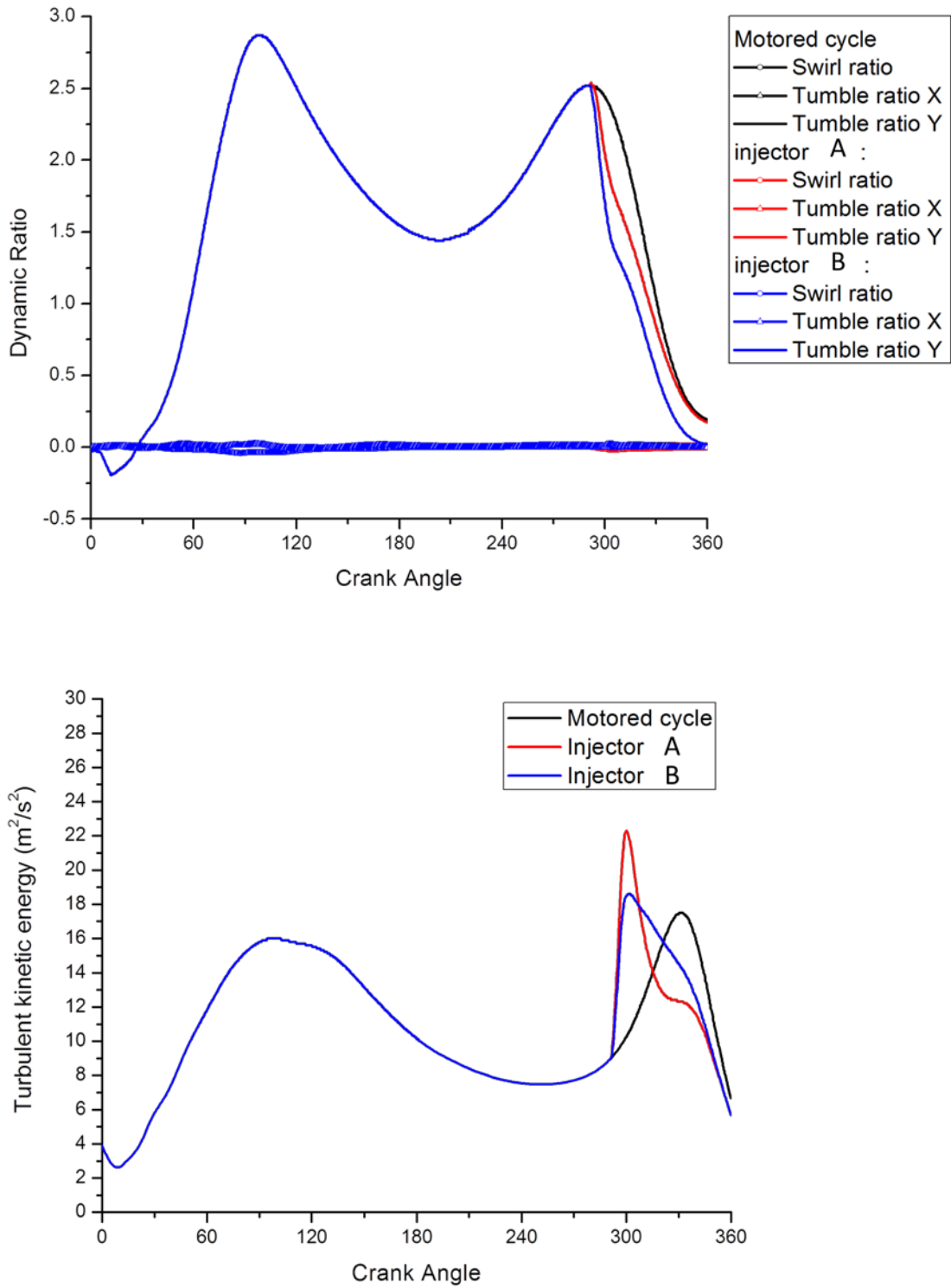


Fig. 5.15 Dynamic ratio and turbulent kinetic energy of stratified injection at 70CAD bTDC

5.4 Effect of Valve Strategy

A study of the effect of advanced valvetrain strategy on in-cylinder charge motion was conducted with the optical engine. Three methods for the advanced valvetrain, Early Intake Valve Close (EIVC), Later Intake Valve Close (LIVC), and valve deactivation are discussed. And for each valve strategy, injection timing sweep testing was conducted from 30CAD to 110CAD aTDC. Injector A was used and the injection amount is fixed at 9.2mg (0.62ms for the command PW) for all the testing in this section. The camera speed was set to 7207FPS, which provided time resolution of 0.83CAD at 1000RPM operation.

Visualization of the in-cylinder spray and its interaction with the intake flow for the two-valve EIVC configuration with the injection timing at 70CAD aTDC is presented in Fig. 5.16 as an example. The top row of the image shows the side view perpendicular to the injector axis. The bottom row shows the view through the piston window. The injector is placed on the upper right corner of the images in the side view, and it is located at the center of the right side in the bottom view. The locations of the intake and exhaust valves are on the right and left half of the images respectively as marked in the figure. The images were processed by adjusting the intensity for better display.

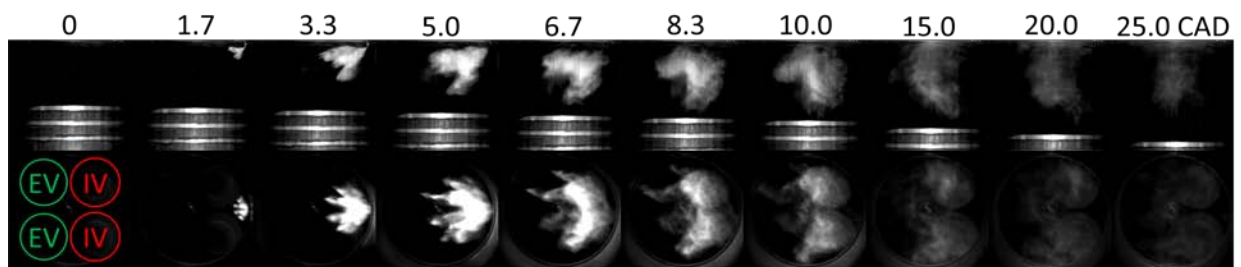


Fig. 5.16 In-cylinder visualization of side and bottom views with the injection timing at 70CAD aTDC. Two-valve EIVC configuration

5.4.1 Two-valve EIVC Result

The typical in-cylinder visualization result of side and bottom views with two-valve EIVC configuration is shown in Fig. 5.16. The injection timing was at 70CAD aTDC. Through the bottom view, a symmetric spray cloud respect to the X-Z plane was captured indicating there was no swirl motion. It was observed in the side view that some of the fuel droplets moved upward after 5CAD from the start of injection (SOI) due to entrainment by the intake air jet even though the spray aimed downwards with the angle of 67deg between the injector axis and the cylinder axis. The bottom part of the spray appears to graze the piston surface, but the resulting emission is supposed to be negligible because of its small amount of fuel depositing on the piston which will be vaporized by the time of combustion.

By the metal engine testing, it was found that the amount of soot and unburned hydrocarbon in emission was increased by advancing the injection timing (Chapter 2.3 and Fig. 2.1). This increase in emission was supposed to be the result of piston wetting, and it was confirmed by OAE (Fig. 5.17). Comparing with 70CAD injection in Fig. 5.16, stronger spray hitting on the piston surface was observed when the injection timing was 50CAD. And by advancing the injection timing another 20CAD, the spray impinged on the piston became to be bounced and redirected towards the cylinder wall and the chamber roof. In the optical engine, most of the fuel hit the piston stuck on the surface as liquid film because of low surface temperature. Comparison in the Fig. 5.17 clearly shows the amount of droplets in the air was much smaller with 30CAD injection after impingement. As discussed in Chapter 4.3, spray bounce at the piston surface is more critical for higher wall temperature condition, which can be produced in a real metal

engine. The resultant side wall wetting by spray bounce has a potential to become another source of emissions other than wetting of the piston.

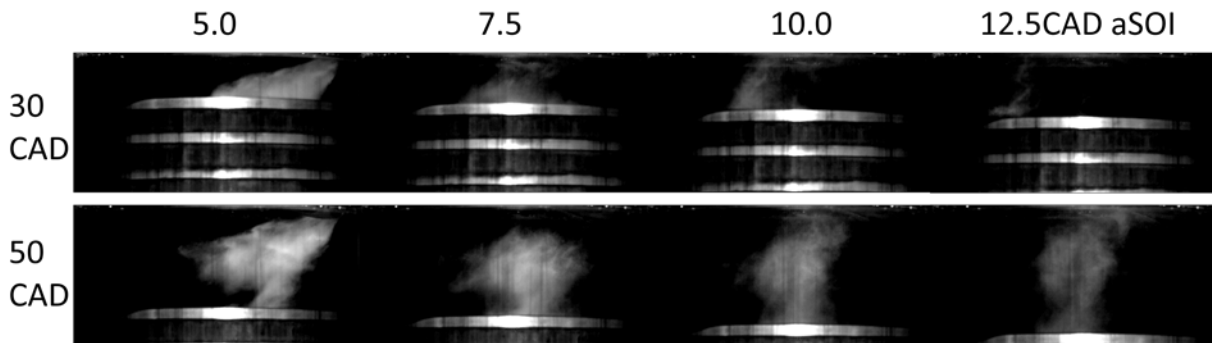


Fig. 5.17 Piston/side wall impingement by early injections at 30/50CAD aTDC with two-valves EIVC

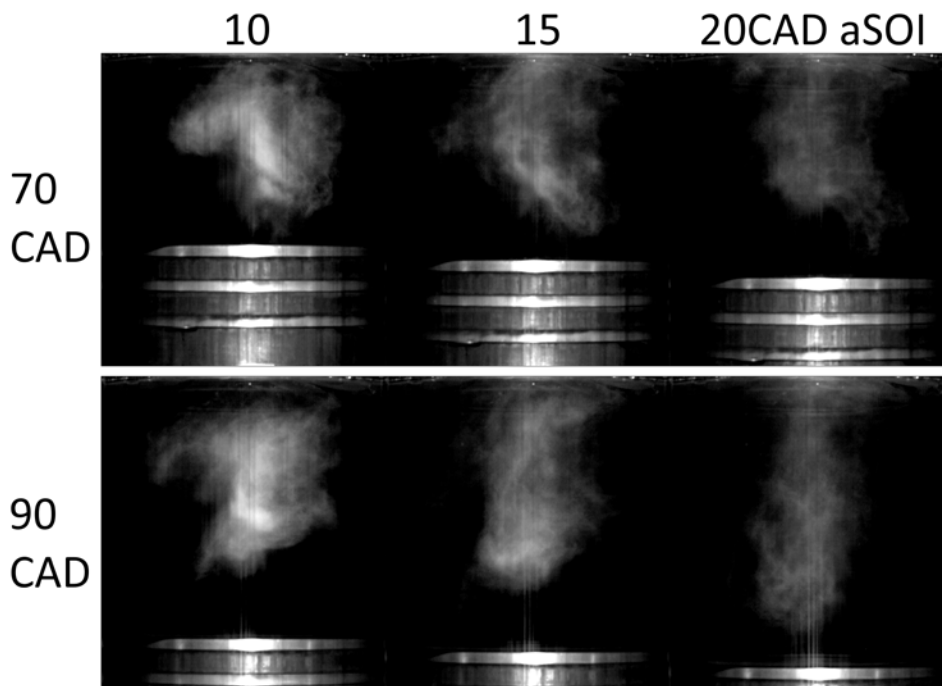


Fig. 5.18 Spray stretch by later injections at 70/90CAD aTDC with two-valves EIVC

According to the metal engine testing, the other side of the injection window was limited by unstable combustion. It can be explained by shorter time for mixture preparation if the injection takes place later. In addition, lower cylinder temperature by over-expansion of EIVC configuration around BDC disturbed fuel vaporization. OAE testing observed that the fuel cloud of later injections were stretched as shown in Fig. 5.18. Upper part of the fuel cloud was pulled by incoming inlet air jet, and lower part was carried away by the tumble flow.

5.4.2 Deactivated EIVC Result

The in-cylinder visualization result with one of the intake valves deactivated is shown in Fig. 5.19. Only the bottom right intake valve was active in the bottom view. Injection timing was 70CAD bTDC. The charge flow and the spray structure developed differently from the two-valve condition. Fig. 5.20 displays superimposed images of the two- and the one-valve EIVC conditions with color enhanced, red for two-valve and green for one-valve. It should be noted that a certain pixel turns to yellow if it has the same intensity for those two conditions. It was observed that the swirl motion induced by a single operating valve broke the symmetry of the spray in the bottom view. The upper half of the deactivation spray extended for more distribution, while the lower half of the spray did not penetrate further as the upper half did. It seemed that the spray was deflected by a counter-clock wise swirl motion, but the total in-cylinder charge motion produced by deactivation was a combination of swirl and tumble that was difficult to resolve. After some time elapsed, the complex flow converged and the direction of the swirl motion was revealed to be clock wise. It is found by the side view that the upward

motion of the injected fuel by the inlet air was stronger for the deactivation mode because of the halved inlet area. The image comparison at 20CAD ASOI showed that the fuel cloud of deactivation (green) was almost torn out at the middle of the cylinder by stronger entrainment.

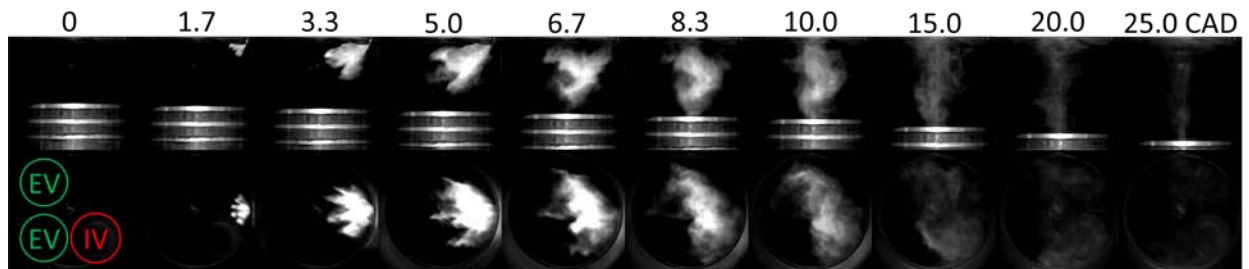


Fig. 5.19 In-cylinder visualization of side and bottom views with the injection timing at 70CAD aTDC. One-valve EIVC configuration

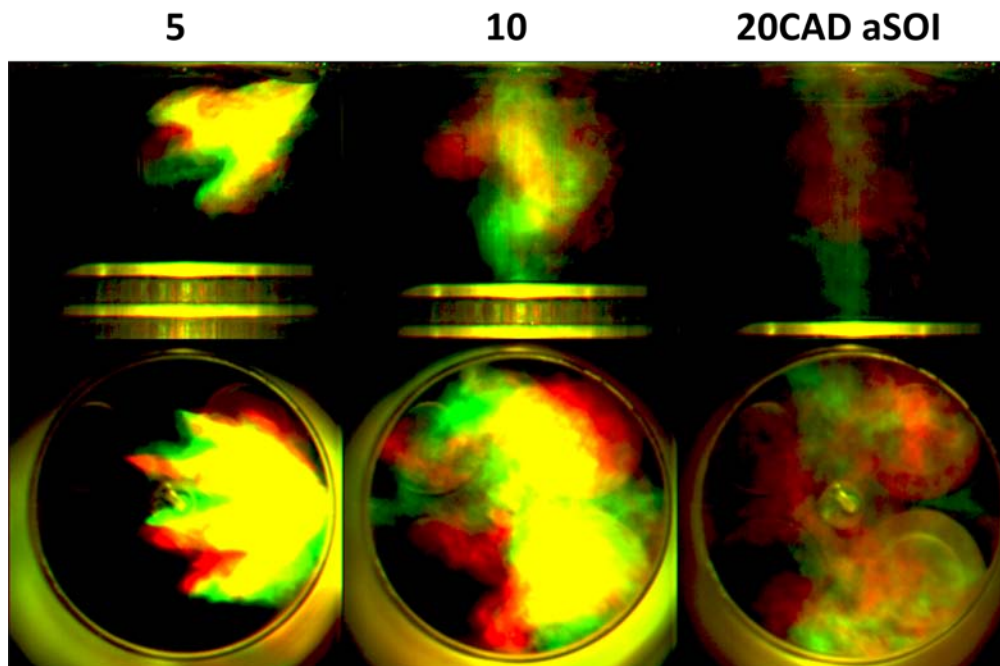


Fig. 5.20 Two-(red) and one-valve(green) comparison for EIVC with injection at 70CAD

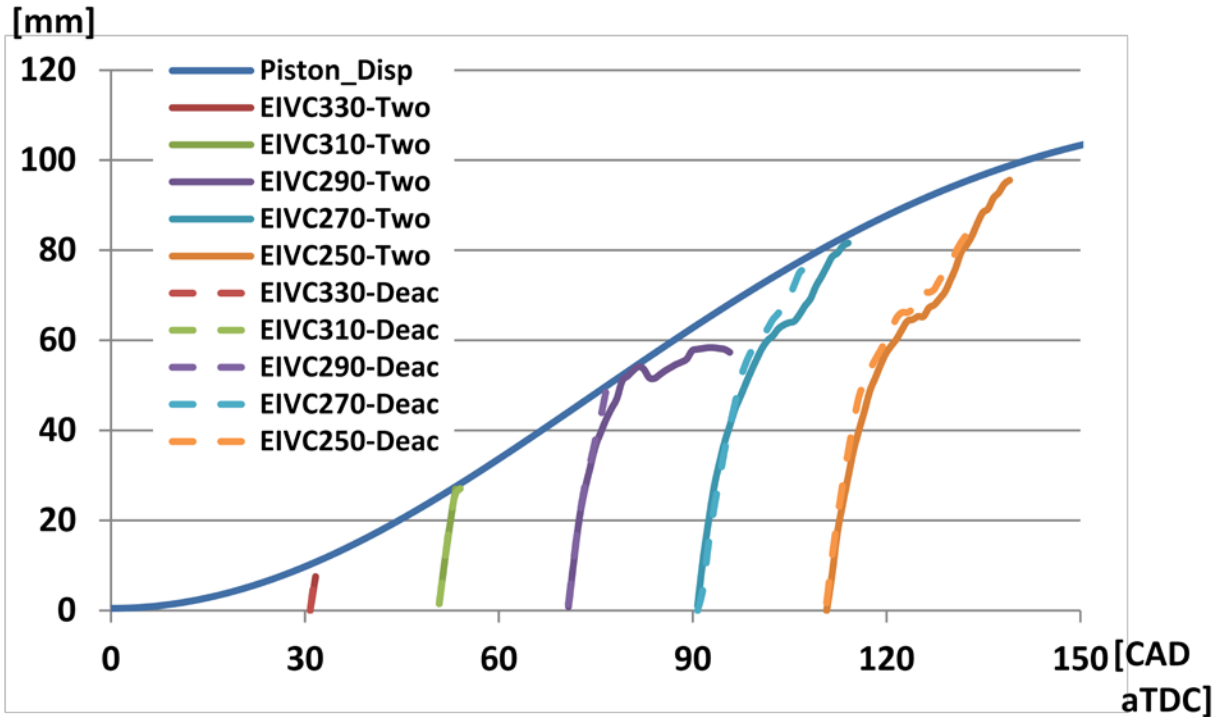


Fig.5.21 EIVC penetration curves for injection timing sweep from 30-110CAD aTDC intake (330-250CAD bTDC firing)

More stretched fuel cloud after the injection is another noticeable difference for the deactivation configuration. Fig. 5.21 shows the penetration curve of the EIVC conditions with both two- and one-valve. Penetration was defined as the vertical component of the measured distance from the injector tip to the lowest position of the fuel cloud in the side view images. The piston displacement curve was plotted on the figure as well. With the injection timing before 70CAD (290CAD bTDC), the sprays hit the piston surface with strong momentum. After 70CAD, the spray tip reached the piston surface but the impingement was very weak. The sprays penetrated by their initial momentum and then they were carried away by the in-cylinder air flow. This is why the penetrations have two stages for the two-valve cases. When one intake valve was deactivated, this “sweep” by charge motion was stronger and the spray clouds were

stretched even more. Lower in-cylinder pressure at the time of injection by over-expansion of deactivation must contribute to extend the penetration.

Fig. 5.21 also implies strong piston impingement with injection at 330CAD for both two- and one-valve. However the metal engine testing result showed extended range of nearly zero soot emission with valve deactivation. False color comparison of those conditions in Fig. 5.22 found out that the most of the fuel cloud of deactivation (Green) stayed away from the piston surface after the impingement because of stronger inlet air entrainment. Stronger in-cylinder flow must promote vaporization of the deposit fuel by forced convection. This explains why deactivation can widen the injection window to the earlier side which is limited by the soot emission.

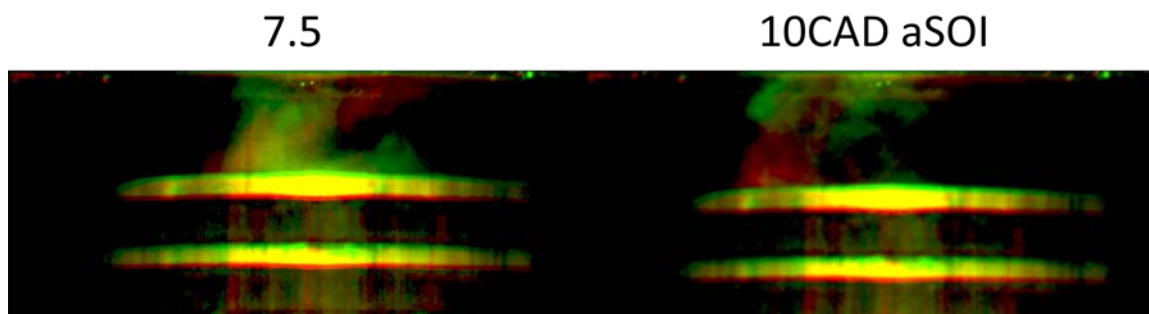


Fig. 5.22 Two-(red) and one-valve(green) comparison for EIVC with injection at 330CAD

It was observed that the intake flow of the valve deactivation configuration deflected the spray and entrained it into the higher velocity air flow. The increased mixing and bulk motion by deactivation increased the rate of vaporization. The fractions of the fuel cloud area respect to the total image area calculated from the bottom view results are plotted in Fig. 5.23 for the injection timing from 50-110 CAD after TDC (310-250CAD bTDC firing). If the injection timing was too early, 30CAD for example, piston

impingement was severe and fuel disappearance by vaporization and depositing on the surface could be indistinguishable. The spray injected at 50CAD had less peak area than other conditions because it had spray droplets disappearance by weak piston impingement. After the peak, faster vaporization of the deactivation case was clearly observed. As the injection retarded, there was no piston interference and the spray was injected into stronger intake air flow, more benefit of valve deactivation in terms of faster vaporization was found. Even for the 110CAD injection, where the intake valve was half closed and the weakened air flow resulted in the slowest vaporization for the two-valve, vaporization of the one-valve operation was fast as 70/90CAD injection.

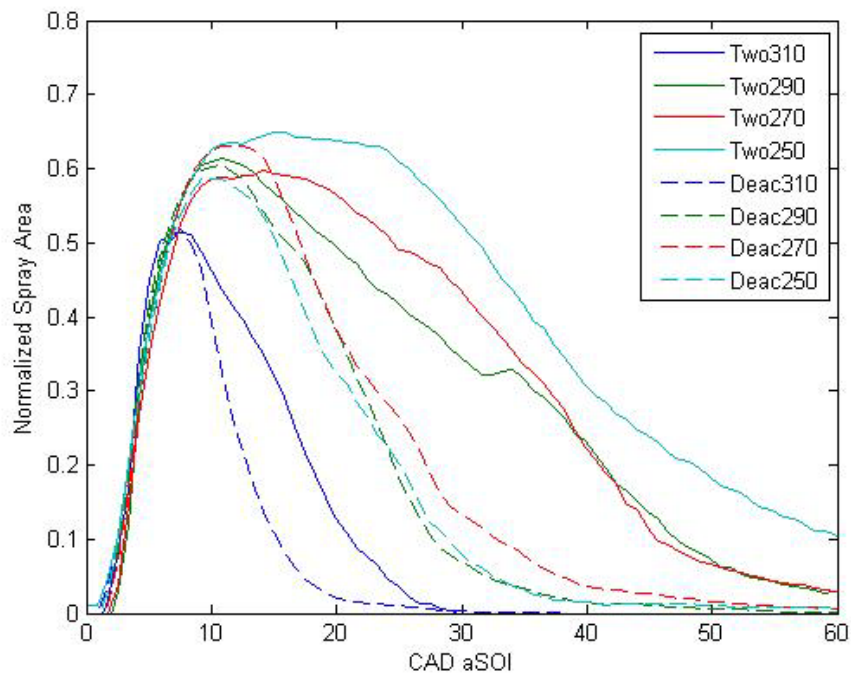


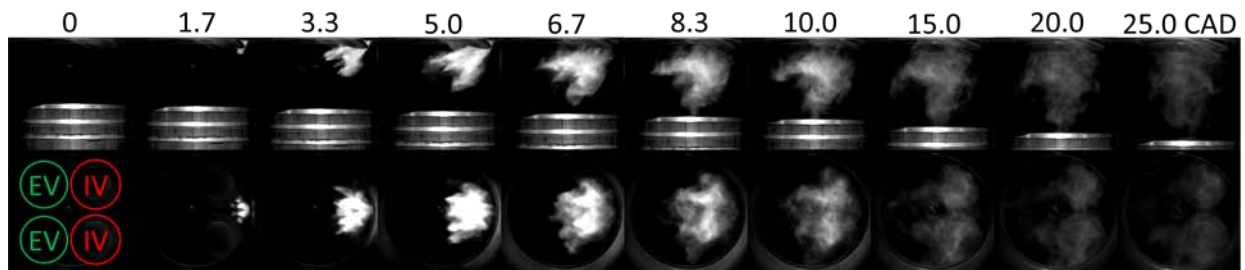
Fig. 5.23 Normalized spray area from bottom view, EIVC conditions

5.4.3 LIVC Result

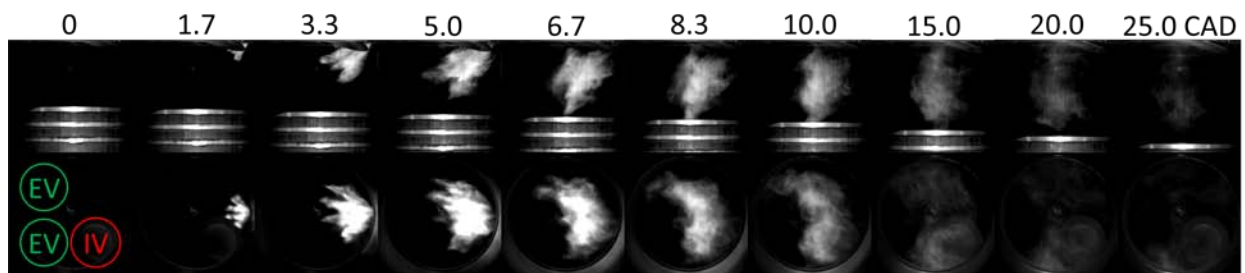
Fig. 5.24(a) shows the visualization result of the two-valve LIVC condition with 70CAD injection timing. Fig. 5.25(a) is the false color comparison of EIVC (red) and LIVC (green) with injection at 70CAD. The plume numbers were defined as printed on the figure for clarification of the discussion. The shape of the fuel cloud of LIVC at 5CAD aSOI in the bottom view had less penetration due to the interference of the spray with the intake valves. Plume 1 and 6 were bent by the valves and collapsed each other to form a fuel cloud propagating in between. The effect of the valve interference remained at 20CAD aSOI in a wedged shape of the fuel cloud. The injection or valve strategy must be revised to avoid unnecessary valve wetting. Through the side view, it was observed that the fuel cloud tended to depart and be isolated from the chamber roof space. It indicated that the initial spray momentum directing downward overcame the drag force of intake jet entrainment. This isolation was more obvious for later injections at 90 and 110CAD (Fig. 5.25(b)). Fig. 5.25(b) also shows the image comparison at 20CAD aSOI with 50CAD injection. A large amount of fuel stayed near piston in a liquid phase with LIVC, while the most of EIVC cloud was already disappeared. It is reasonable to consider that the high lift valves of LIVC result in less dynamic air intake flow for poor mixing and vaporization.

Normalized spray area of the two-valve LIVC condition was calculated from the bottom view results and plotted with the two-valve EIVC result in Fig. 5.26. LIVC with 50CAD (310 CAD bTDC firing) injection shows slower vaporization rate than EIVC as pointed out by the previous paragraph. It should be noted that piston hitting instead of valve hitting with 50CAD injection reduced the peak spray area. Later three LIVC

conditions show smaller spray area than EIVC at the beginning of the injection by the valve hitting effect allowing only 4 plumes penetrate normally. The slope of the curves indicates slower vaporization rates of LIVC for all the conditions.

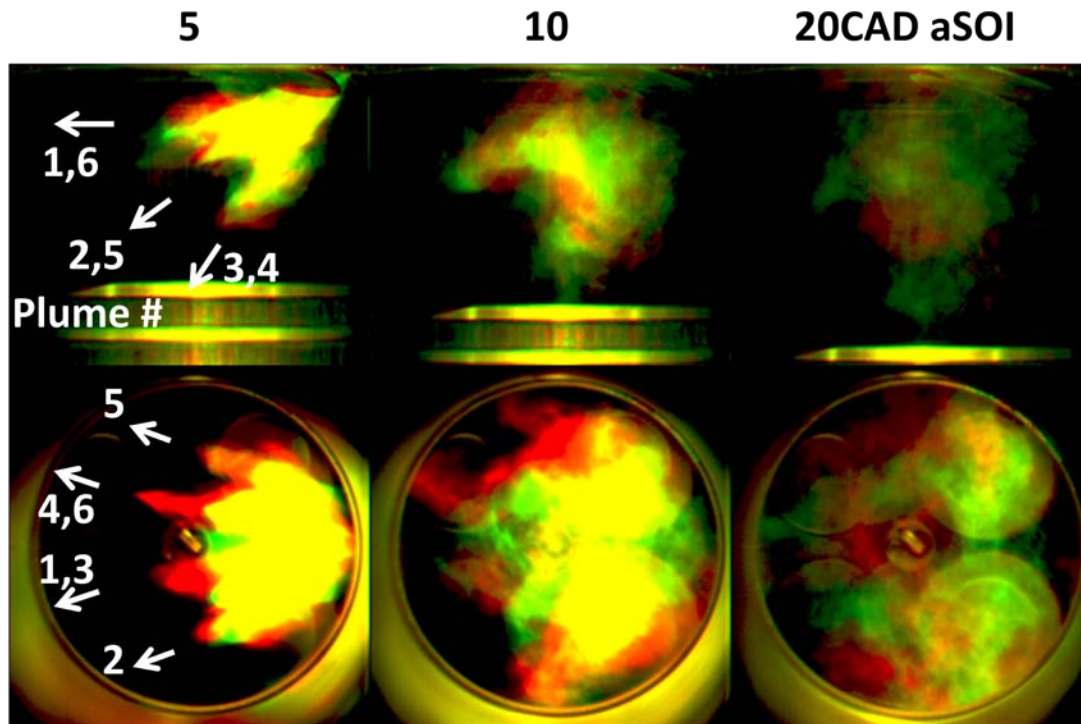


(a) LIVC, two intake valves

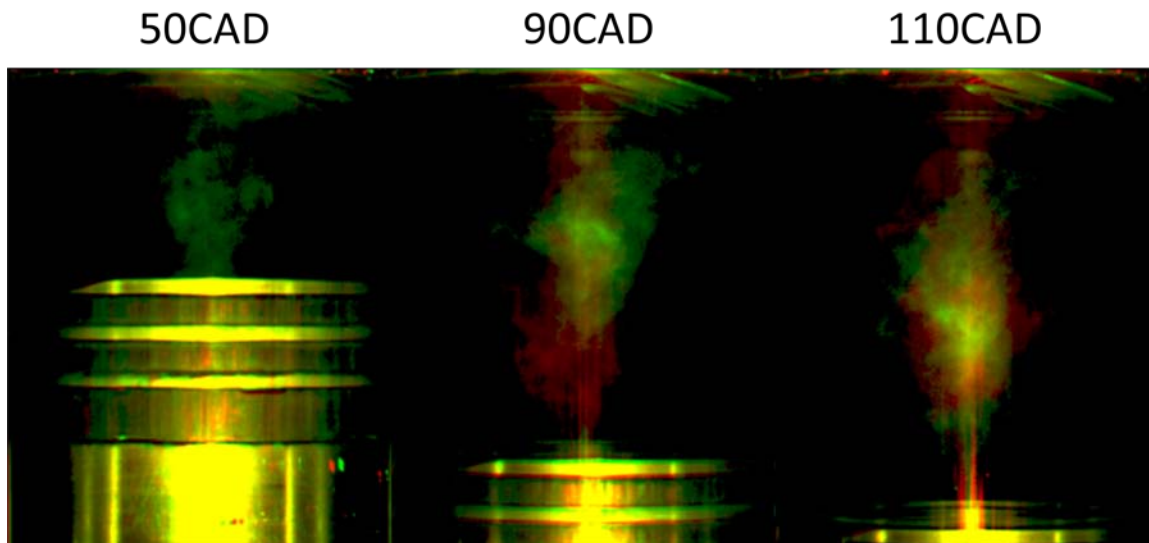


(b) LIVC, deactivation

Fig. 5.24 In-cylinder visualization of side and bottom views with the injection timing at 70CAD aTDC. LIVC configuration



(a) Injection at 70CAD with plume number



(b) 20CAD aSOI with injection at 50/90/110CAD

Fig. 5.25 EIVC(red) and LIVC(green) comparison for two-valve with injection at 70CAD

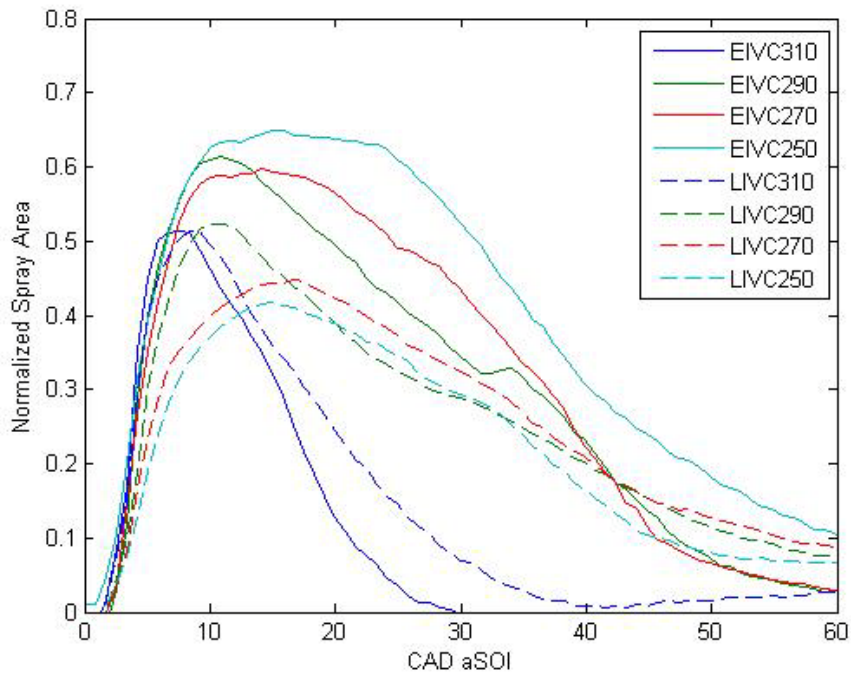


Fig. 5.26 Normalized spray area from bottom view, two-valve conditions

The visualization results of LIVC with one valve deactivated is shown in Fig. 5.24(b). Compared with the two-valve LIVC, the same tendency in the deactivation benefit was observed as EIVC (Fig. 5.27). The penetration of the lower half of the spray was suppressed and asymmetric cloud was observed by the bottom view. The degree of asymmetry was even extended due to penetration of plume 6 without interference with the intake valve which is not open. Then clockwise swirl rotated the fuel for temporary symmetric at 20CAD ASOI. The side view shows strong fuel droplets entrainment by intake air flow of deactivation. And the early injection at 30CAD shows fuel “lift off” from the piston surface. Faster vaporization by deactivation can be observed by LIVC too (Fig. 5.28). The peak spray area of deactivation was higher because of the less effect of the valve interference.

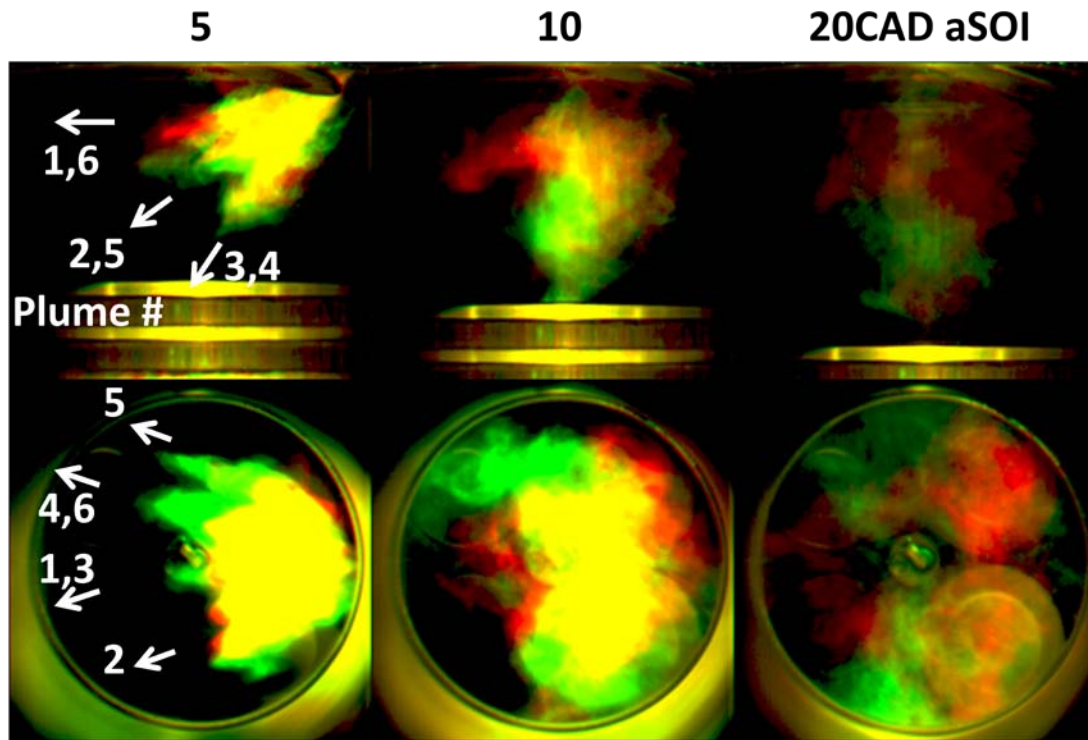


Fig. 5.27 Two-(red) and one-valve(green) comparison for LIVC with injection at 70CAD

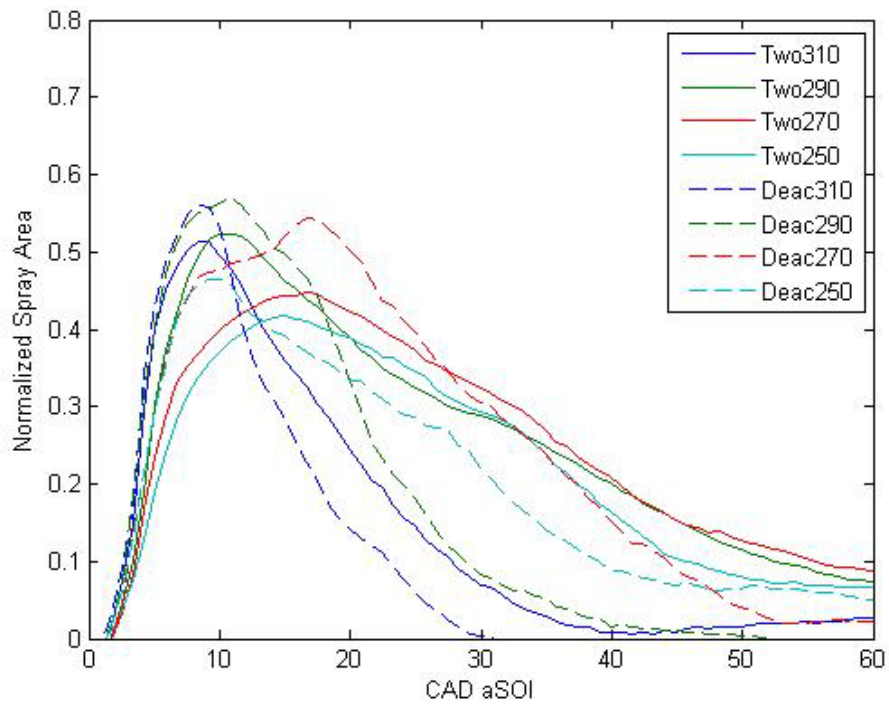


Fig. 5.28 Normalized spray area from bottom view, LIVC conditions

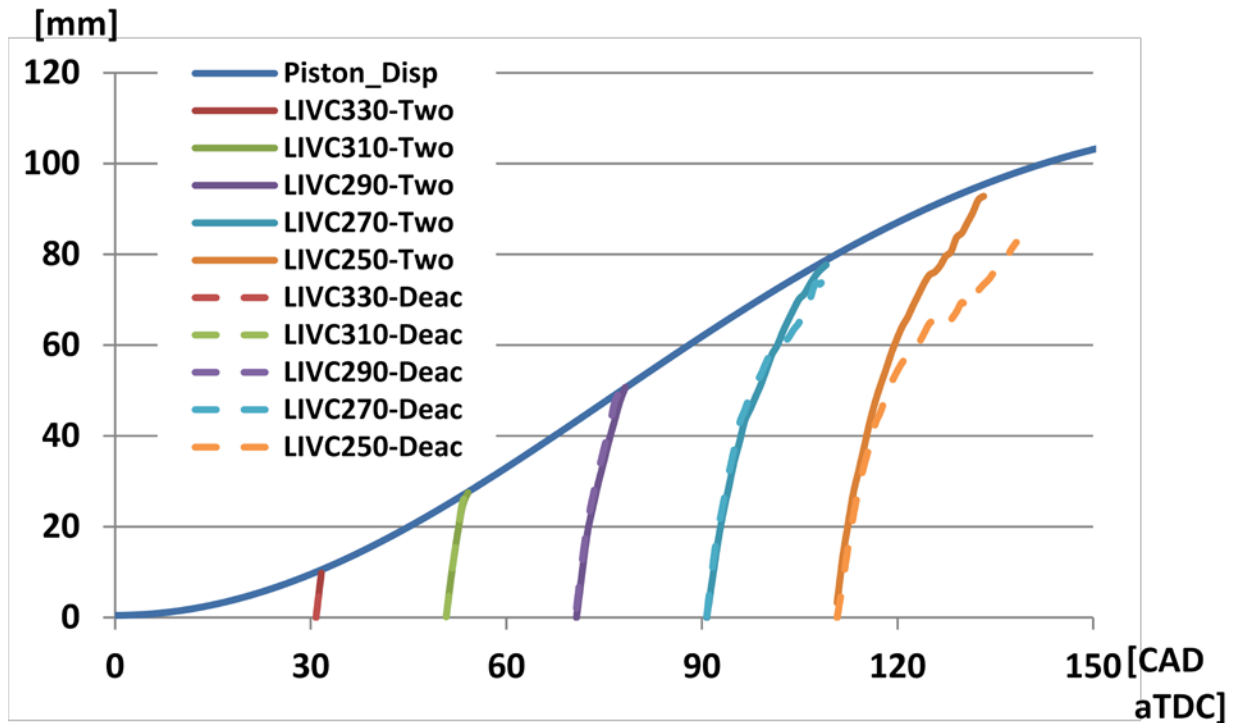


Fig. 5.29 LIVC penetration curves for injection timing sweep from 30-110CAD aTDC intake (330-250CAD bTDC firing)

However, the deactivated LIVC clouds were not stretched downward after the injection as EIVC with one-valve operation did. Fig. 5.29 shows penetration comparison of the two- and the one-valve LIVC. The pairs of penetration with the injection at 30-70CAD aTDC (330-290CAD bTDC firing) were nearly identical. But later two conditions of deactivation show slower penetration than two-valve cases, which is the opposite result of EIVC. It is recalled that the greater penetration by deactivation of EIVC was caused by over-expansion. High lift of LIVC did not produce over-expansion, and the reduced penetration by deactivation of LIVC can be explained simply by enhanced mixing promoting vaporization of the fuel.

False color comparison was made for the two deactivation cases in Fig. 5.30. There was not much difference in the over-all spray shape, but fuel cloud separation

from the combustion roof seen at 20CAD ASOI indicating weak air entrainment by LIVC could be recalled. Slower fuel disappearance by LIVC could be observed also. By the spray area comparison (Fig. 5.31), vaporization of the one-valve LIVC was confirmed to be slower than the one-valve EIVC configuration because of slower air intake flow coming through the big valve opening gap.

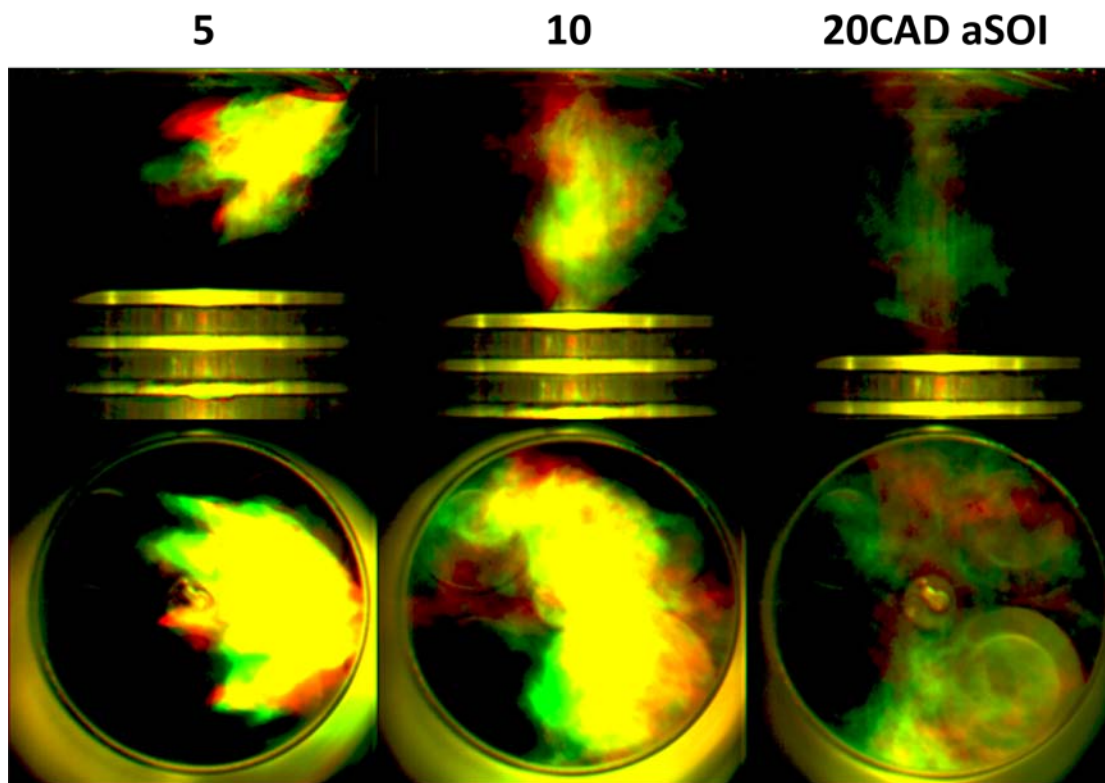


Fig. 5.30 EIVC (red) and LIVC (green) comparison for deactivation with injection at 70CAD

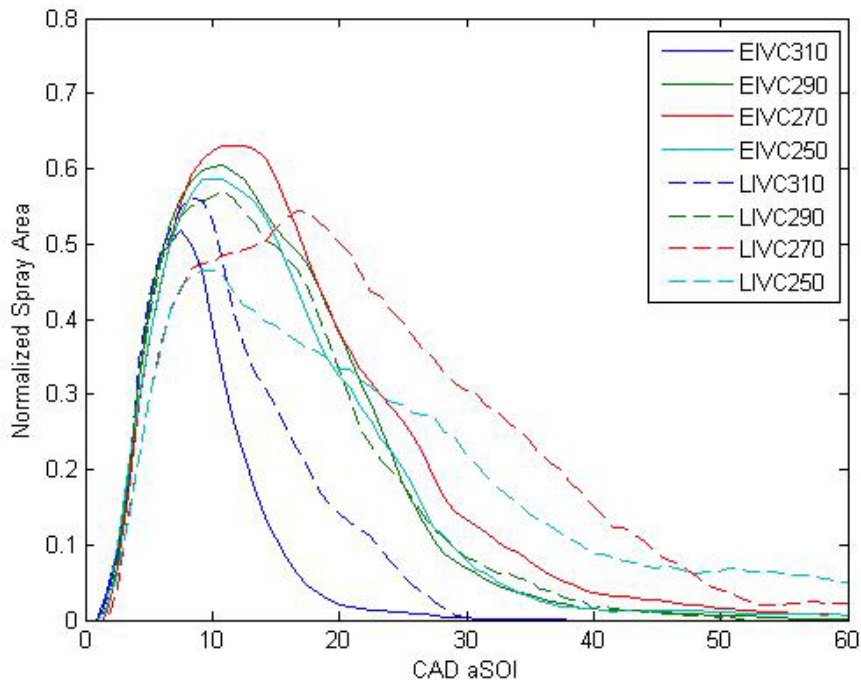


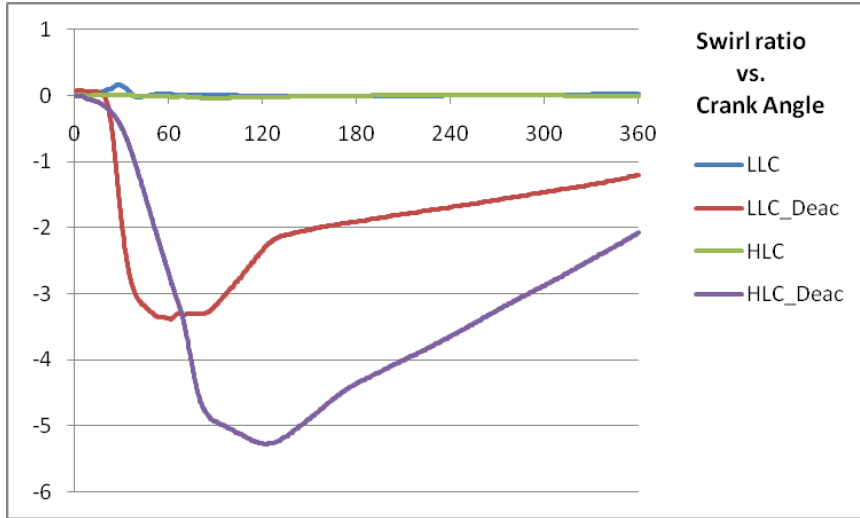
Fig. 5.31 Normalized spray area from bottom view, deactivation conditions

5.4.4 Simulation Result

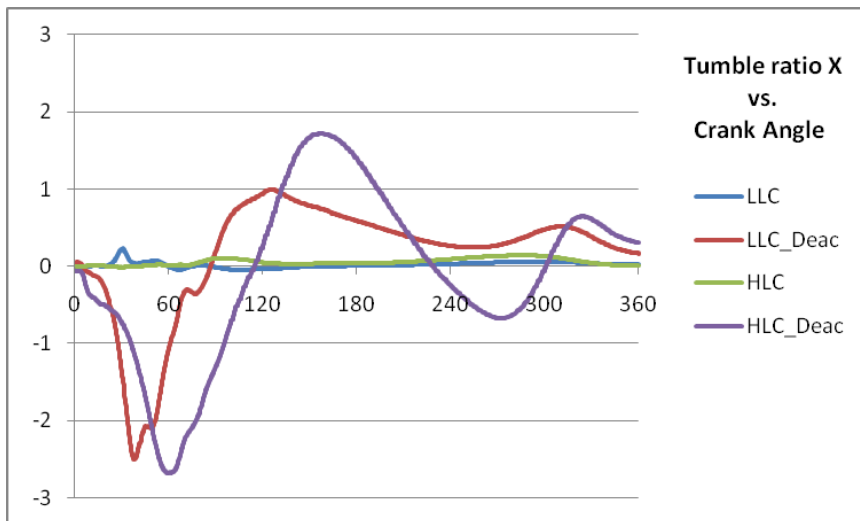
CFD simulation results of the dynamic ratios, which consists of swirl ratio and two directions (X and Y) of tumble ratios, are plotted in Fig. 5.32. The flow was tumble dominated when both intake valves were active, initially with a reverse tumble followed by a forward tumble around the Y-axis. For the two-valve operation, the tumble ratio Y of LIVC (HLC) was much greater than EIVC (LLC) except the period up to 60CAD, where EIVC produced negative tumble in larger magnitude. When a valve was deactivated, swirl and a cross tumble around the X-axis became significant and the initial reverse tumble was reduced to negligible level. The tumble Y of deactivation cases during compression stroke was a reverse tumble. Valve deactivation produced complex in-cylinder charge motion which consisted all three motions. The use of LIVC

promoted more vigorous charge motion through the compression stroke since the valve closes significantly after BDC. Even though LIVC produced overall stronger charge motion, dynamic ratios of EIVC developed faster at the beginning of the intake stroke, where early injection took place.

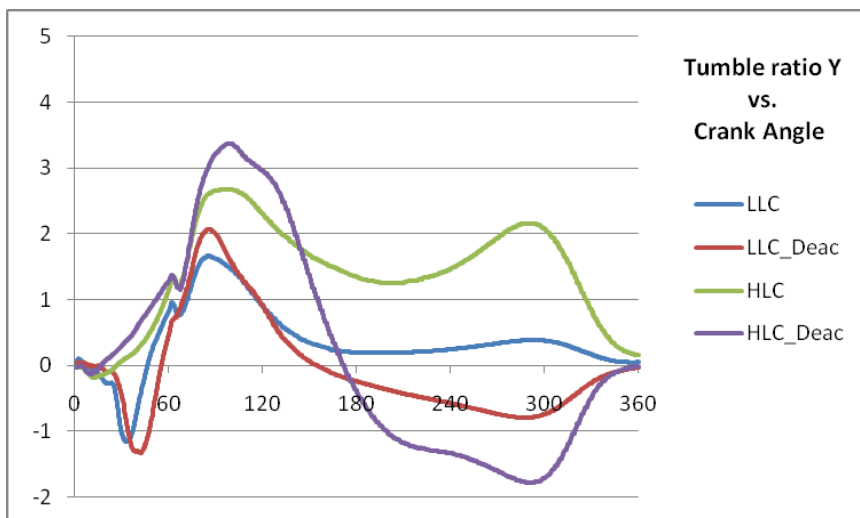
The stronger inlet air flow of EIVC resulted in higher mass averaged turbulent kinetic energy (TKE) in that period of possible injection window (Fig. 5.33). The curves of EIVC configurations (LLC) have two peaks in which the first peak was due to intake flow and the second was designated to injection at 60CAD. The highest TKE by LIVC cams happened later than 60CAD and overlaid by injection. Especially for the deactivation mode, the peak TKE was 9 times stronger than the two-valve LIVC case. This very dynamic in-cylinder flow must enhance the break-up and mixing of the spray. Actually the order of the cam configuration in stronger TKE at the time of injection (one-valve EIVC > one-valve LIVC > two-valve EIVC > two-valve LIVC) was consistent with the order in vaporization rate obtained by OAE testing. And the strong turbulent contributed to less wall wetting even for the early injection. CFD confirmed that more turbulent resulted in less liquid film on the wall as shown in Fig. 5.34. As experimental section pointed out, a greater amount of film mass of two-valve LIVC (HLC) can be the results of valve wetting. Although the EIVC contributed for more turbulent flow at the time of mixing, TKE at the time of combustion was less than LIVC cases. Because of its high valve lift, LIVC was compatible with high load operation. Stronger turbulence at the end of compression is a benefit at high speed operation, where faster combustion is required.



(a) Swirl ratio



(b) Tumble ratio X



(c) Tumble ratio Y

Fig. 5.32 Dynamic ratios with injection at 60CAD

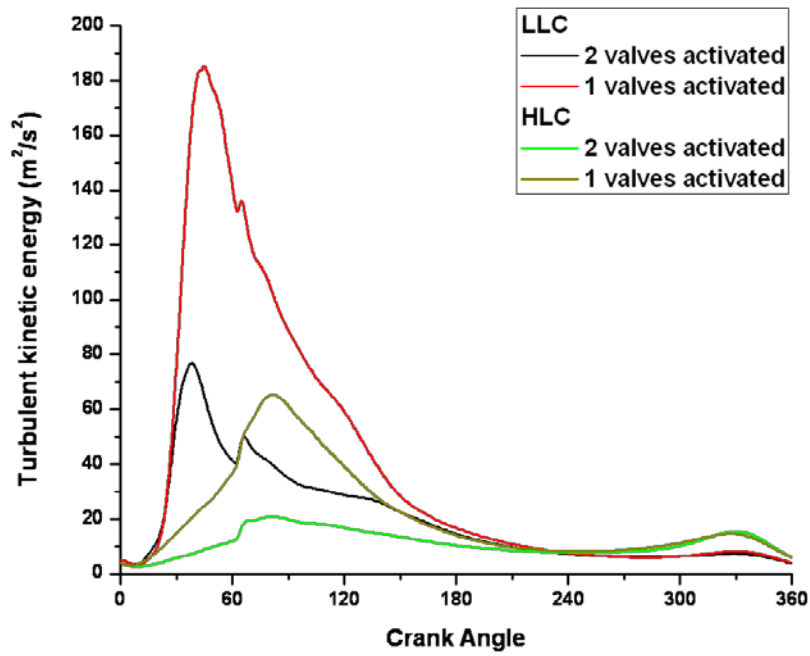


Fig. 5.33 Mass averaged turbulent kinetic energy with injection at 60CAD

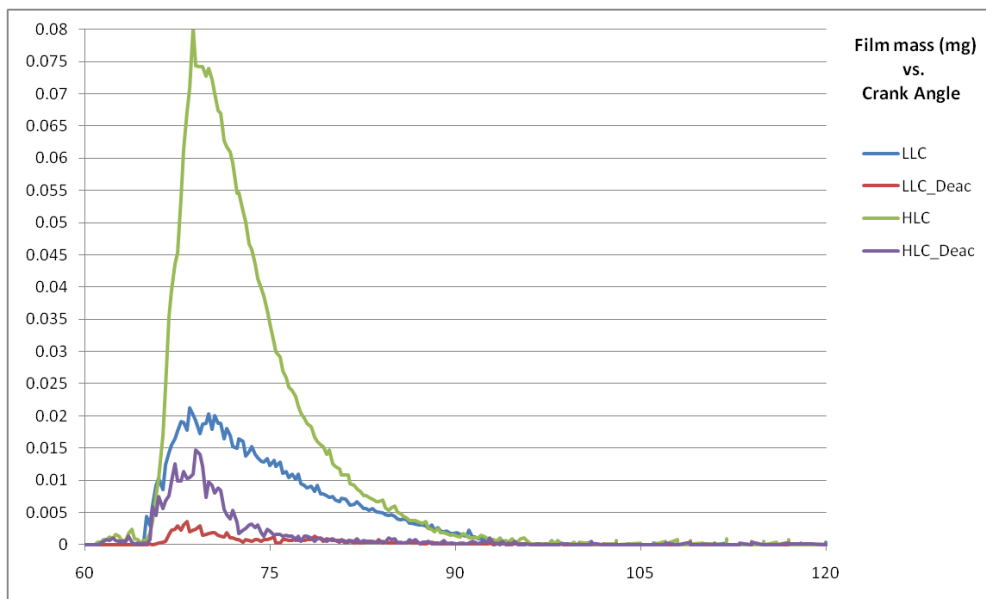


Fig. 5.34 Total liquid film mass on the wall

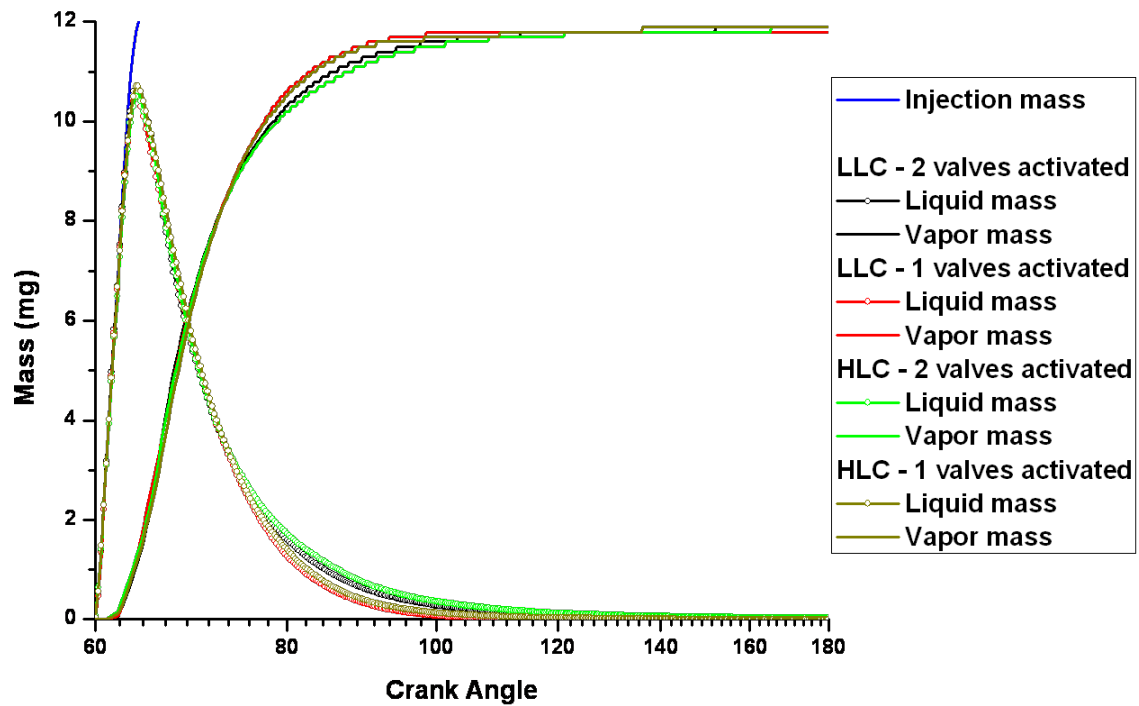


Fig. 5.35 Liquid/vapor fuel mass inside cylinder

Fig. 5.35 is the comparison in liquid/vapor fuel mass history inside the cylinder. It is found that the vapor curve of the deactivation cases developed faster than the two-valve cases. And comparing EIVC and LIVC, vaporization of EIVC cases was slightly faster. This order is consistent with the TKE level at 60-120CAD, which proved that turbulent is critically related to enhancement of vaporization.

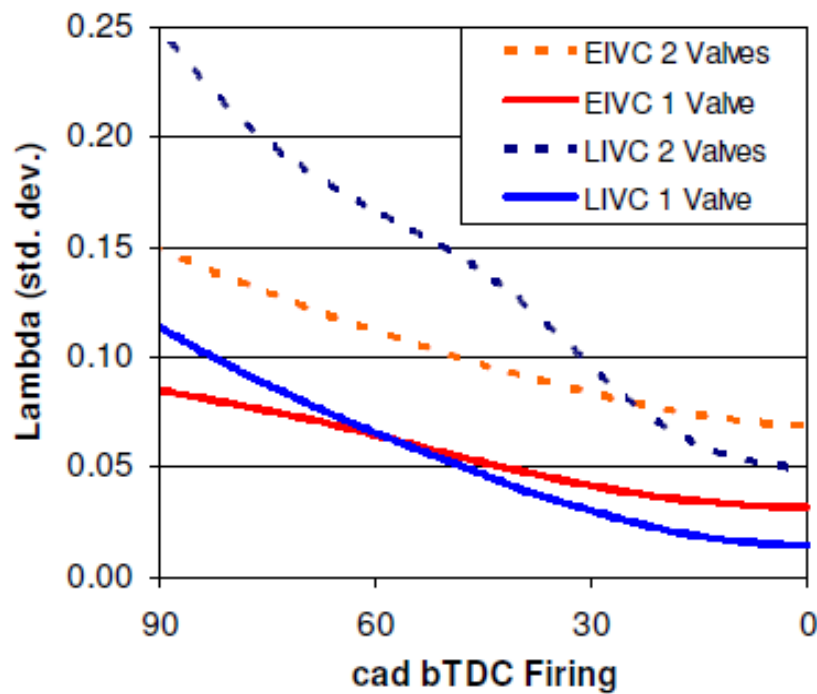


Fig. 5.36 Standard deviation of lambda

To evaluate the effectiveness of advanced valvetrain strategies on homogeneity and mixing, the standard deviation of lambda was evaluated and is shown in Figure 5.36. Valve deactivation reduced the variation of local air/fuel ratio for both strategies due to enhanced mixing by stronger turbulence at the time of spray injection during early intake stroke. At the time appropriate for ignition and combustion, the stronger turbulence of LIVC strategies resulted in more fast-decreasing lambda variation providing more homogeneous mixture for better combustion stability.

When operating with valve deactivation at high loads and low speeds on the fired engine, it was observed that the tendency to knock increased when a valve was deactivated. The CFD results were evaluated for the bulk gas temperature and the results are presented in Figure 5.37. The figure shows the in-cylinder gas temperature

during the intake and compression stroke. The effect of charge cooling coincided with the injection events at 300 and 280CAD bTDC (60 and 80CAD aTDC). An increase in the gas temperature by increased heat transfer from the cylinder surface was obtained late in the intake stroke and during compression that resulted in higher gas temperatures near the end of compression. This will result in higher end-gas temperatures that can increase knock for sensitive fuels.

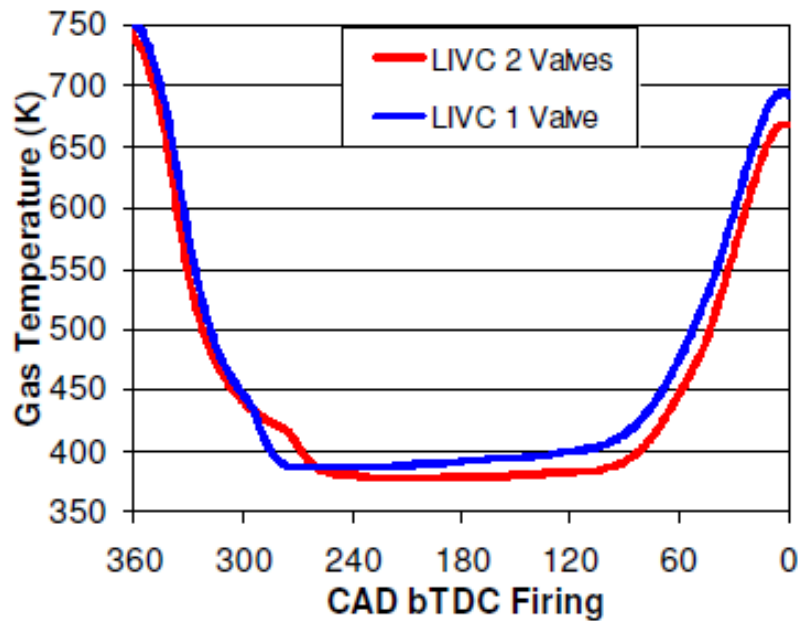


Fig. 5.37 In-cylinder gas temperatures of LIVC configuration

5.4.5 Summary

A study of the effect of advanced valvetrain strategy on in-cylinder charge motion was conducted with the optical engine. Three methods for the advanced valvetrain, EIVC, LIVC, and valve deactivation were discussed. With two-valve EIVC operation, a symmetric spray cloud respect to the X-Z plane was captured indicating there was no

swirl motion. Some of the fuel droplets moved upward after 5CAD ASOI due to entrainment by the strong intake air jet produced by low valve lift of the EIVC cam. Strong piston impingement and subsequent chamber wall wetting was observed with the early injection timing where the metal engine produced more soot. For later injections, lower cylinder temperature by over-expansion of EIVC configuration around BDC disturbed fuel vaporization and combustion stability in addition to shorter mixture preparation time. OAE testing observed that the fuel cloud of later injections were stretched vertically by the air blow down.

Deactivation of one of the intake valves produced swirl charge motion in the cylinder which was mixed with tumble. Valve deactivation deflected the spray and entrained it into the higher velocity air flow which can be produced by halved valve opening gap. Stronger tumble rotational flow and lower cylinder pressure at the time of injection obviously stretched the fuel cloud downward more than two-valve operation. Soot emission by the early injection could be reduced by valve deactivation because of “lift off” of the fuel cloud from the piston surface. The enhanced mixing and bulk motion also increased the rate of vaporization.

High lifting valve of LIVC produced slower inlet air velocity and less fuel cloud entrainment. The less dynamic in-cylinder charge motion resulted in slower mixing and vaporization than EIVC. The same tendency in the deactivation benefit was observed as EIVC. Therefore LIVC with deactivation was able to compensate the negative aspects of LIVC in terms of mixing and vaporization by higher inlet air velocity resulting improved charge motion. However, fuel cloud stretch of later injection was not observed because of increased in-cylinder pressure. High lift of LIVC caused spray-valve

interference therefore the injection and valve strategy must be revised to avoid unnecessary surface wetting.

Multi-dimensional CFD was carried out to support the optical engine work. CFD confirmed that the in-cylinder flow was tumble dominated, initially with a reverse tumble followed by a forward tumble around the Y-axis when both valves were active. Valve deactivation generated swirl and a cross tumble around the X-axis, and produced complex in-cylinder charge motion which consisted all three motions. The use of LIVC promoted more vigorous charge motion through the compression stroke, but dynamic ratios of EIVC developed faster at the beginning of the intake stroke. The stronger inlet air flow of EIVC resulted in higher mass averaged turbulent kinetic energy (TKE). The order of the cam configuration in stronger TKE was consistent with the order in vaporization rate which was proven in both experimental and simulation. And CFD also confirmed that the strong turbulent contributed to less wall wetting even for the early injection. Although the EIVC contributed for more turbulent flow at the time of mixing, LIVC could accelerate the flame speed due to higher turbulence level at the time of combustion. Evaluation of the standard deviation of lambda revealed that valve deactivation reduced the variation of local air/fuel ratio for both EIVC and LIVC strategies. And the more vigorous charge motion of the LIVC strategy provided a more uniform mixture for better combustion stability. Stronger charge motion by deactivation enhanced heat transfer from the cylinder surface and increased end-gas temperature for increased knock tendency.

CHAPTER 6 “Conclusion”

6.1 Summary of the Work

Chamber Testing

High speed spray visualization in a spray chamber was conducted for a study of spray development. By Schlieren visualization technique, the effect of different conditions including ambient conditions (temperature, pressure) and injection conditions (fuel type, fuel temperature, nozzle design) on spray formation is discussed in both qualitative and quantitative methods. Three fuels of E100, E50, and gasoline (E0) were tested with GDI injectors to evaluate the effect of ethanol composition in the fuel. The spray behavior after piston impingement is examined briefly. Piezoelectric Direct Injector (PDI) was tested with pure ethanol to evaluate the effect of ambient condition and pulse width on the spray structure. Following points were drawn as conclusions.

- Schlieren visualization was very effective method to observe the vapor phase of the fuel spray as well as the dense core.
- The 2-stage thresholding image processing method was developed to discriminate both liquid and vapor phases together from a Schlieren image.
- High ambient temperature promoted vaporization and vaporized fuel dissipated its momentum for less penetration. High ambient pressure suppressed the spray development and made the effect of temperature negligible.
- When fuel was injected and exposed to flash boiling condition, the effect of flash boiling could changed the spray shape drastically by plume collapse.

- Gasoline spray showed faster vaporization and more flash boiling effect than the ethanol spray at the early stage of injection because of higher saturation pressure of lighter components of hydrocarbons. Decelerating and vaporization of the gasoline spray after the injection was also slower than ethanol spray because the heavier components remained in liquid.
- When the ambient pressure was increased to prevent flash boiling, the spray behavior became nearly identical for all fuels.
- When the energy content of injected fuel was fixed, gasoline spray had faster complete vaporization due to flash boiling and less injection quantity. The spatial distribution of E0 fuel was poorer than ethanol spray because of spray collapse and less quantity.
- The position of the centroid of spray indicated the same tendency as spray penetration and can be a substitute.
- There are no significant difference in the spray angle for all the testing.
- Multi-component gasoline spray was found to be less sensitive to fuel temperature in the range that ethanol spray experienced flash boiling because of multiple boiling point corresponding to each component.
- The penetration was comparable with Injector A and B at the early stage of injection even though Injector B was designed for larger flow rate. At later part of injection, Injector B showed further penetration.
- Plume distribution of Injector B caused strong side spray bending. Even though the spray targeting of Injector B was narrower, it could resist against spray collapse by flash boiling.

- The comparison of Injector A and C confirmed that the spray of a multi-hole injector with smaller L/D penetrated faster and wider during the injection.
- Injector A had wider spray cone angle with wider spray targeting angle, and this enlarged the available surface of the sprays to accelerate the vaporization faster.
- The piston impingement testing showed that the spray under high ambient temperature traveled faster than the spray under room temperature after the spray hit the piston. Poorly refined injector spray targeting and piston bowl geometry may cause a secondary spray of droplets bullets exiting the bowl.
- PDI spray can be characterized by liquid strings in the spray structure and vortices at the side of the umbrella, and vaporization was initiated at those area. The liquid spray broke evenly and formed relatively uniform vapor phase.
- PDI spray penetration was linear and independent on ambient temperature at the beginning of injection. As time elapsed, higher ambient temperature caused longer penetration at the later stage of injection.
- Higher chamber pressure suppressed the PDI spray penetration significantly.
- The injection pulse width did not affect much the position of the PDI mixture cloud

OAE Testing

High-speed visualization of the in-cylinder charge motion was carried out using an optical accessible engine (OAE). The testing was conducted for the conventional valve strategy with the production cam, and for the advanced valve strategies with the prototype cams. With the conventional valve configuration, homogeneous and stratified

charge mode were tested with the two different type of injectors. With the prototype cams, effect of Early Intake Valve Close (EIVC) and Late Intake Valve Close (LIVC) cams in addition to intake valve deactivation on homogeneous charge motion was examined. Multi-dimensional CFD was carried out to support the optical engine work. Following points were drawn as conclusion.

- The in-cylinder spray simulation results by CFD agreed fairly well with the optical engine results.
- The spray targeting of Injector B, which aimed more downward, resulted in stronger piston impingement with less side wall wetting. The fuel droplets tended to accumulate in the center of the cylinder due to the spray targeting.
- Injection at 60CAD aTDC was against the direction of in-cylinder tumble flow, and decreased tumble ratio and turbulent energy from the motoring state. Charge motion with Injector A had stronger tumble than Injector B because its spray axis was more aligned with the tumble flow.
- Later injections at 120 and 180CAD increased tumble ratio and turbulent kinetic energy (TKE). No piston wetting was observed by later injections.
- Since 120CAD was in the middle of intake stroke, dynamic in-cylinder flow caused by stronger air induction carried the fuel droplets away to fill up the cylinder more horizontally uniform than the other conditions.
- For stratified injection mode, higher ambient pressure suppressed the spray propagation shorter and narrower. Promoted vaporization by higher in-cylinder temperature also contributed for limited spray distribution.

- The dynamic ratio and the total turbulent kinetic energy of stratified injection at 290CAD aTDC were also decreased by injection because of contradiction of the direction of spray and tumble rotation.
- In-cylinder flow was tumble dominated when both valves were active. Deactivation of one of the intake valves produced swirl charge motion in the cylinder which was mixed with tumble.
- Strong piston impingement and subsequent combustion chamber wall wetting was observed with early injection. Soot emission by the early injection could be reduced by valve deactivation because of in-cylinder turbulent and “lift off” of the fuel cloud from the piston surface.
- Stronger tumble rotational flow and lower cylinder pressure at the time of later injection by EIVC obviously stretched the fuel cloud downward. Lower cylinder temperature by over-expansion of EIVC configuration around BDC disturbed fuel vaporization and combustion stability.
- High lifting valve of LIVC produced less dynamic in-cylinder charge motion at early intake stroke resulted in slower mixing and vaporization. The use of LIVC promoted more vigorous charge motion through the compression stroke, but dynamic ratios of EIVC developed faster at the beginning of the intake stroke.
- LIVC with deactivation showed the same benefit as EIVC, and it was able to compensate the negative aspects of LIVC in terms of mixing and vaporization.
- The stronger inlet air flow of EIVC resulted in higher TKE and enhanced vaporization rate which was proven in both experiment and simulation.

- LIVC could accelerate the flame speed due to higher turbulence level at the time of combustion.
- Valve deactivation reduced the variation of local air/fuel ratio. And the more vigorous charge motion of the LIVC strategy provided a more uniform mixture for better combustion stability
- Stronger charge motion by deactivation enhanced heat transfer from the cylinder surface and increased end-gas temperature for increased knock tendency.

6.2 Recommendation and Future Work

6.2.1 Recommendation

It is recommended to take the effect of flash boiling into consideration of engine design. To utilize instant vaporization by flash boiling without suffering by plume collapse can improve GDI engine operation. The spray collapse by flash boiling can be managed by fuel temperature or design of injector nozzle in addition to injection pressure.

When designing a flex-fuel GDI engine, spray comparison must be made with fixed energy content. Since the injection volume is increased with high ethanol ratio, the injection strategy must be revised to minimize wall wetting. For example, injection timing shift or multiple injection to reduce the penetration are required. The difference in the phase change characteristics of gasoline and ethanol, especially the effect of multiple component in gasoline, should be considered.

Injection timing under homogeneous GDI operation must be determined based not only on piston impingement and time for vaporization, but also on interaction with in-

cylinder flow. Use of EIVC/LIVC cam strategies and VVA for active control of valve strategy are suggested for Miller cycle engines. Use of valve deactivation at low load to reduce the possibility of soot emission and unstable combustion in addition to fuel consumption is recommended. LIVC is suitable for high speed/load operation due to its high valve lift and resultant greater turbulence at the end of compression, and combination of deactivation with LIVC can improve mixing and BSFC.

Finally, careful design of spray targeting is recommended to maximize mixing and turbulent energy by strong in-cylinder charge motion and to minimize the wall wetting simultaneously.

6.2.2 Future Work

- Use of strong and uniform light source is recommended to improve the Schlieren image quality.
- Study of microscopic imaging at the exit of injector hole may bring deeper understanding of spray characteristics.
- Piston impingement should be studied more because it is the main source of soot formation, and may be not avoidable especially for stratified operation.
- Further improvement is needed on the CFD configuration such as the breakup and heat/mass transfer models.
- CFD simulation should be run for the high speed operation because OAE operation is limited to low speed..
- Study of spray bending must be performed more by CFD. Internal flow dynamics in the sac or uneven air entrainment could be the key factor.

This research focuses of mixture preparation. Diagnostics of combustion is the next step required to understand deeply the topics discussed in this dissertation. Preliminary testing of combustion visualization has been already done, and the following section introduce the progress.

Preliminary Testing of Combustion Visualization

The OAE was modified for a combustion visualization testing. In order to achieve stable combustion, the OAE must be warmed up and supplied with hot air. The quartz cylinder was replaced with a stainless steel liner with built-in water jacket which can heat the temperature of the liner and the cylinder head to 80°C. The new liner was equipped with two parallel sapphire optical windows for Schlieren visualization of combustion. The capability of full-stroke visualization was given up, but it was possible to shorten the optical piston for less vibration and higher speed operation. The electric circulation heater which used in the chamber testing was utilized to heat up the intake air. Intake air diluting system by pressurized nitrogen was installed at the upstream of the heater for simulating EGR. O₂ sensors were mounted at both the upstream and downstream of the OAE to record the oxygen concentration. The intake manifold was replaced with a customized coupling where manifold absolute pressure (MAP) and intake air temperature were monitored.

The preliminary testing of combustion visualization was performed with the engine speed at 600RPM. The production cam was used with one intake valve deactivated. 22.3mg of pure gasoline was injected at 60CAD aTDC intake which was supposed to form near stoichiometric mixture. The intake air temperature was 108°C

and water temperature was 80°C. The fake EGR system was turned off. The ignition timing was set to 45CAD bTDC firing.

The measured cylinder pressure curve was plotted in Fig. 6.1 along with the injection and ignition signals. The pressure curve was typical for a gasoline engine. The peak pressure of motoring curve was less than the previous settings discussed in the main body of this dissertation, indicating the effective compression ratio was reduced to approximately 7.1, because of the dead volume at the optical windows on the combustion chamber. The peak pressure of the fired case was 35.6bar at 7.2CAD aTDC. Calculated Indicated Mean Effective Pressure (IMEP) was 4.6bar.

The resultant images of the preliminary combustion visualization testing are shown in Fig. 6.2. Since the right intake valve was deactivated, the direction of swirl must be clockwise as discovered in the OAE section. After the spark was discharged at 45CAD bTDC, there was an ignition delay which was approximately 6.7ms (24CAD). During that time, the area of reacting air/fuel mixture was transferred to right bottom of the image by in-cylinder swirl. That was where the blue flame propagation was initiated. The blue flame traveled across the cylinder bore with increasing intensity. After the blue flame, there was yellow cloud formed at all over the cylinder probably indicating soot formation. Large bright yellow dots started forming near TDC pointed out that there was large liquid droplets remained.

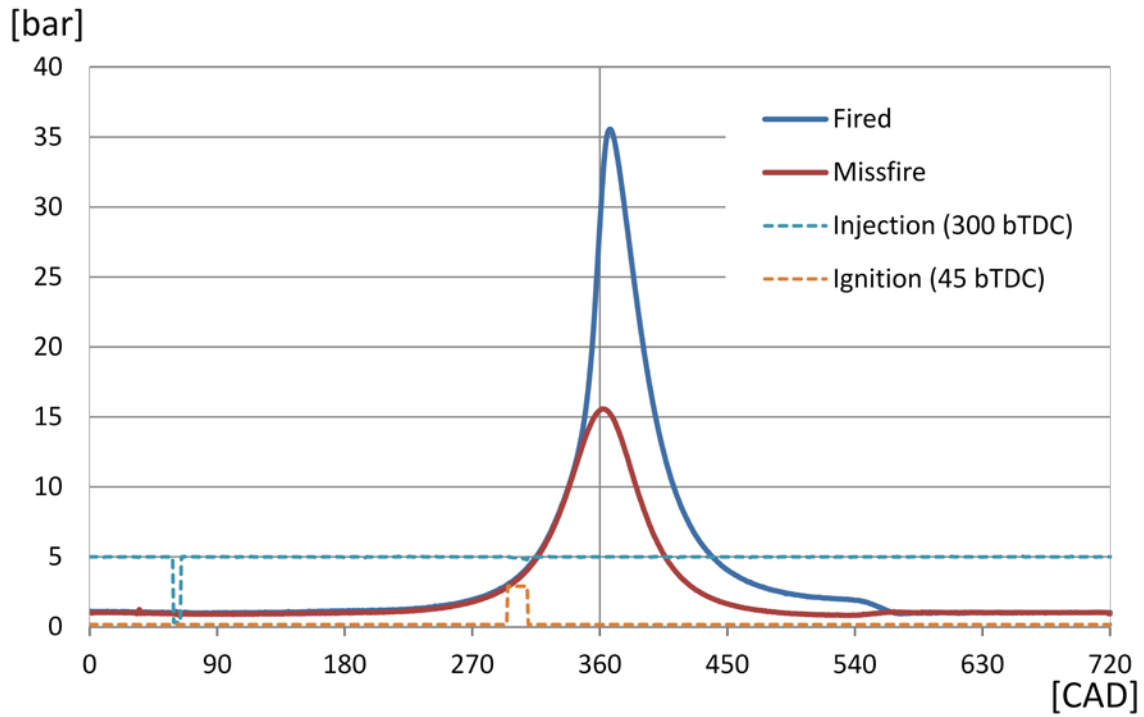


Fig. 6.1 Cylinder pressure curve of the preliminary combustion visualization testing

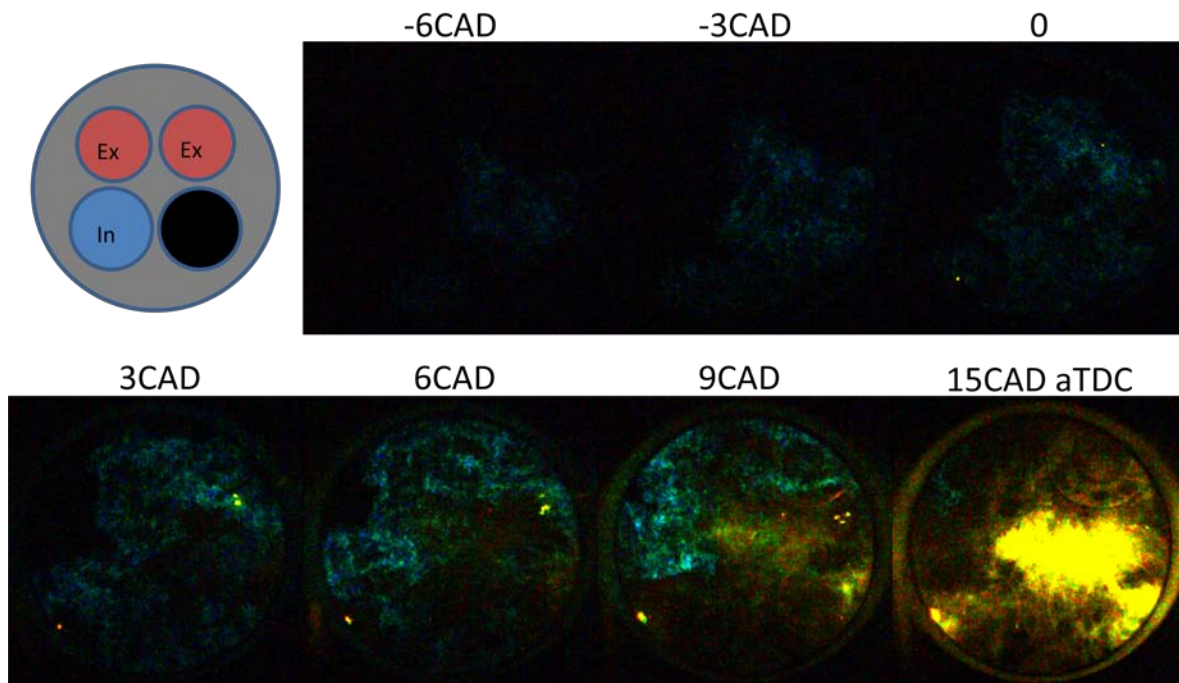


Fig. 6.2 Visualization result of the preliminary combustion visualization testing

Effect of operating conditions discussed in this dissertation on combustion quality should be studied in the future work. Especially the effect of fuel composition and the valve deactivation are interesting. Detail study of cylinder pressure and heat release curve is necessary to understand the combustion deeply. In addition, improvement of the resultant image is required. Using an image intensifier will help increase the image quality at the data acquisition. To improve the post image processing method is recommended as well.

REFERENCES

1. Zhao, F., M.-C. Lai, and D.L. Harrington, *Automotive spark-ignited direct-injection gasoline engines*. Progress in Energy and Combustion Science, 1999. **25**: p. 437-562.
2. Kim, H., et al., *Correlating Port Fuel Injection to Wetted Fuel Footprints on Combustion Chamber Walls and UBHC in Engine Start Processes*. SAE Technical Paper 2003-01-3240, 2003.
3. Sadakane, S., et al., *Development of a New V-6 High Performance Stoichiometric Gasoline Direct Injection Engine*. SAE Technical Paper 2005-01-1152, 2005.
4. Kirwan, J.E., et al., *3-Cylinder Turbocharged Gasoline Direct Injection: A High Value Solution for Low CO₂ and NO_x Emissions*. SAE Technical Paper 2010-01-0590, 2010.
5. Park, J., et al., *Visualization and Analysis of the Impingement Processes of a Narrow-Cone DI Gasoline Spray*. SAE Technical Paper 2001-01-2023, 2001.
6. Mittal, M., et al., *A Study of Fuel Impingement Analysis on In-Cylinder Surfaces in a Direct-Injection Spark-Ignition Engine with Gasoline and Ethanol-Gasoline Blended Fuels*. SAE Technical Paper 2010-01-2153, 2010.
7. Gold, M., et al., *Application of Optical Techniques to the Study of Mixture Preparation in Direct Injection Gasoline Engines and Validation of a CFD Model*. SAE Technical Paper 2000-01-0538, 2000.

8. Kuwahara, K., K. Ueda, and H. Ando, *Mixing Control Strategy for Engine Performance Improvement in a Gasoline Direct Injection Engine*. SAE Technical Paper 980518, 1998.
9. Hung, D.L.S., et al., *A High Speed Flow Visualization Study of Fuel Spray Pattern Effect on Mixture Formation in a Low Pressure Direct Injection Gasoline Engine*. SAE Technical Paper 2007-01-1411, 2007.
10. Yamamoto, S., D. Tanaka, and K. Sato, *Keys to Understanding Spray-guided Combustion of a Narrow-spacing Gasoline Direct Injection SI Engine with a Centrally Mounted Multi-hole Injector*. SAE Technical Paper 2009-01-1497, 2009.
11. Arcoumanis, C. and T. Kamimoto, *Flow and Combustion in Reciprocating Engines* 2009, Berlin: Springer.
12. Iwamoto, Y., et al., *Development of Gasoline Direct Injection Engine*. SAE Technical Paper 970541, 1997.
13. Kanda, M., et al., *Application of a New Combustion Concept to Direct Injection Gasoline Engine*. SAE Technical Paper 2000-01-0531, 2000.
14. Tagaki, Y., et al., *Simultaneous Attainment of Low Fuel Consumption, High output Power and Low Exhaust Emissions in Direct Injection SI Engines*. SAE Technical Paper 980149, 1998.
15. Ortmann, R., et al., *Methods and Analysis of Fuel Injection, Mixture Preparation and Charge Stratification in Different Direct Injected SI Engines*. SAE Technical Paper 2001-01-0970, 2001.
16. Chang, W.-S., Y.-N. Kim, and J.-K. Kong, *Design and Development of a Spray-guided Gasoline DI Engine*. SAE Technical Paper 2007-01-3531, 2007.

17. Zhao, F.-Q., et al., *Spray Dynamics of High Pressure Fuel Injectors for DI Gasoline Engines*. SAE Technical Paper 961925, 1996.
18. Kubo, M., A. Sakakida, and A. Iiyama, *Technique for Analyzing Swirl Injectors of Direct-injection Gasoline Engines*. SAE Technical Paper 2001-01-0964, 2001.
19. Kang, K.K., et al., *The Fuel Spray Structure of High Pressure Direct Swirl Injector for Gasoline Injection System*. SAE Technical Paper 2004-01-0541, 2004.
20. Honda, T., et al., *A Study of Mixture Formation and Combustion for Spray Guided DISI*. SAE Technical Paper 2004-01-0046, 2004.
21. Mitroglou, N., et al., *Spray Structure Generated by Multi-Hole Injectors for Gasoline Direct-Injection Engines*. SAE Technical Paper 2007-01-1417, 2007.
22. Skogsberg, M., et al., *Effects of Injector Parameters on Mixture Formation for Multi-Hole Nozzles in A Spray-Guided Gasoline DI Engine*. SAE Technical Paper 2005-01-0097, 2005.
23. Dahlander, P. and R. Lindgren, *Multi-hole Injectors for DISI Engines: Nozzle Hole Configuration Influence on Spray Formation*. SAE Technical Paper 2008-01-0136, 2008.
24. Hiroyasu, H. and M. Arai, *Structures of Fuel Spray in Diesel Engines*. SAE Technical Paper 900475, 1990.
25. Montgomery, D.T., et al., *Effect of Injector Nozzle Hole Size and Number on Spray Characteristics and the Performance of a Heavy Duty D.I. Diesel Engine*. SAE Technical Paper 962002, 1996.
26. Arregle, J., J.V. Pastor, and S. Ruiz, *The Influence of Injection Parameters on Diesel Spray Characteristics*. SAE Technical Paper 1999-01-0200, 1999.

27. Siebers, D.L., *Liquid-Phase Fuel Penetration in Diesel Sprays*. SAE Technical Paper 980809, 1998.
28. Bergstrand, P. and I. Denbratt, *Diesel Combustion with Reduced Nozzle Orifice Diameter*. SAE Technical Paper 2001-01-2010, 2001.
29. Martin, D., et al., *Experimental Investigation of the Interaction of Multiple GDI Injections using Laser Diagnostics*. SAE Technical Paper 2010-01-0596, 2010.
30. Skogsberg, M., P. Dahlander, and I. Denbratt, *Spray Shape and Atomization Quality of an Outward-Opening Piezo Gasoline DI Injector*. SAE Technical Paper 2007-01-1409, 2007.
31. Ferguson, C.R. and A.T. Kirkpatrick, *Internal Combustion Engines: Applied Thermosciences*. Second Edition ed2001, New York: John Wiley & Sons.
32. Sellnau, M., et al., *2-step Variable Valve Actuation: System Optimization and Integration on an SI Engine*. SAE Paper 2007-01-0040, 2007.
33. Cleary, D. and G. Silvas, *Unthrottled Engine Operation with Variable Intake Valve Lift, Duration, and Timing*. SAE Paper 2007-01-1282, 2007.
34. Kamo, R., et al., *Emissions Comparisons of an Insulated Turbocharged Multi-Cylinder Miller Cycle Diesel Engine*. SAE Technical Paper 980888, 1998.
35. Moore, W., et al., *Charge Motion Benefits of Valve Deactivation to Reduce Fuel Consumption and Emissions in an GDI, VVA Engine*. SAE Paper 2011-01-1221, 2011.
36. Moore, W., *Engine Efficiency Improvements Enabled by Ethanol Fuels, in an GDI, VVA Flex Fuel Engine*. SAE Paper 11PLF-0277, 2011.

37. Marriott, C.D., et al., *Development of a Naturally Aspirated Spark Ignition Direct-Injection Flex-Fuel Engine*. SAE Technical Paper 2008-01-0319, 2008.
38. Andersson, M. and J. Wärnberg, *Application of laser-induced fluorescence for imaging sprays of model fuels emulating gasoline and gasoline/ethanol blends*. ICLASS 2009, 11th Triennial International Annual Conference on Liquid Atomization and Spray Systems, 2009.
39. Taniguchi, S., K. Yoshida, and Y. Tsukasaki, *Feasibility Study of Ethanol Applications to A Direct Injection Gasoline Engine*. SAE Technical Paper 2007-01-2037, 2007.
40. Christie, M.J., N. Fortino, and H. Yilmaz, *Parameter Optimization of a Turbo Charged Direct Injection Flex Fuel SI Engine*. SAE Technical Paper 2009-01-0238, 2009.
41. Kapus, P.E., et al., *Ethanol Direct Injection on Turbocharged SI Engines – Potential and Challenges*. SAE Technical Paper 2007-01-1408, 2007.
42. Kar, K., et al., *Measurement of Vapor Pressures and Enthalpies of Vaporization of Gasoline and Ethanol Blends and Their Effects on Mixture Preparation in an SI Engine*. SAE Technical Paper 2008-01-0317, 2008.
43. Syed, I.Z., et al., *Numerical Investigation of Laminar Flame Speed of Gasoline-Ethanol/Air Mixtures with Varying Pressure, Temperature and Dilution*. SAE Technical Paper 2010-01-0620, 2010.
44. Francqueville, L.d., *Effects of Ethanol Addition in RON 95 Gasoline on GDI Stratified Combustion*. SAE Technical Paper 2011-24-0055, 2011.

45. Wallner, T. and S.A. Miers, *Combustion Behavior of Gasoline and Gasoline/Ethanol Blends in a Modern Direct-Injection 4-Cylinder Engine*. SAE Technical Paper 2008-01-0077, 2008.
46. Nagaoka, M. and K. Kawamura, *A Deforming Droplet Model for Fuel Spray in Direct-Injection Gasoline Engines*. SAE Technical Paper 2001-01-1225, 2001.
47. Chryssakis, C., D.N. Assanis, and C. Bae, *Development and Validation of a Comprehensive CFD Model of Diesel Spray Atomization Accounting for High Weber Numbers*. SAE Technical Paper 2006-01-1546, 2006.
48. Zeng, W., et al., *Characterization of Methanol and Ethanol Sprays from Different DI Injectors by Using Mie-scattering and Laser Induced Fluorescence at Potential Engine Cold-start Conditions*. SAE Technical Paper 2010-01-0602, 2010.
49. Powell, J.W. and C.-f.F. Lee, *An Investigation of Multiple Scattering in a Hollow-Cone Spray*. SAE Technical Paper 2007-01-0648, 2007.
50. Uhl, M., et al., *Time Resolved Spray Characterisation in a Common Rail Direct-Injection Production Type Diesel Engine Using Combined Mie/LIF Laser Diagnostics*. SAE Technical Paper 2003-01-1040, 2003.
51. Adam, A., et al., *Analysis of Droplets Evaporation Process of Diesel Spray at Ignition Delay Period using Dual Nano-sprark Shadowgraph Photography Method*. SAE Technical Paper 2009-32-0017, 2009.
52. Pickett, L.M., S. Kook, and T.C. Williams, *Visualization of Diesel Spray Penetration, Cool-Flame, Ignition, High-Temperature Combustion, and Soot Formation Using High-Speed Imaging*. SAE Technical Paper 2009-01-0658, 2009.

53. Arnaud, E., et al., *A Fluid Motion Estimator for Schlieren Image Velocimetry*. ECCV 2006, Lecture Notes in Computer Science, 2006. **3951**: p. 198-210.
54. Pastor, J.V., et al., *Evaporating Diesel Spray Visualization using a Double-pass Shadowgraphy/Schlieren imaging*. SAE Technical Paper 2007-24-0026, 2007.
55. Koyanagi, K., et al., *Optimizing Common Rail-Injection by Optical Diagnostics in a Transparent Production Type Diesel Engine*. SAE Technical Paper 1999-01-3646, 1999.
56. Senda, J., et al., *Experimental Analysis on Soot Formation Process in DI Diesel Combustion Chamber by Use of Optical Diagnostics*. SAE Technical Paper 2002-01-0893, 2002.
57. Henle, A., et al., *Homogeneous Operating Strategies in a DI Diesel Engine With Pent-Roof Combustion Chamber and Tumble Charge Motion: Studies on a Single-Cylinder Test-Engine and an Optical Access Engine*. SAE Technical Paper 2005-01-0181, 2005.
58. Colban, W.F., et al., *A Detailed Comparison of Emissions and Combustion Performance Between Optical and Metal Single-Cylinder Diesel Engines at Low Temperature Combustion Conditions*. SAE Paper 2008-01-1066, 2008.
59. Kashdan, J.T. and B. Thirouard, *A Comparison of Combustion and Emissions Behaviour in Optical and Metal Single-Cylinder Diesel Engines*. SAE Paper 2009-01-1963, 2009.
60. Hori, T., et al., *Large Eddy Simulation of Non-Evaporative and Evaporative Diesel Spray in Constant Volume Vessel by Use of KIVALES*. SAE Technical Paper 2006-01-3334, 2006.

61. Yi, Y. and C.M. DeMinco, *Numerical Investigation of Mixture Preparation in a GDI Engine*. SAE Technical Paper 2006-01-3375, 2006.
62. Joh, M., et al., *Numerical Prediction and Validation of Fuel Spray Behavior in a Gasoline Direct-Injection Engine*. SAE Technical Paper 2001-01-3668, 2001.
63. Dukowicz, J.K., *A Particle-Fluid Numerical Model for Liquid Sprays*. J. Comp. Physics, 1980. **35**: p. 229-253.
64. O'Rourke, P.J. and A.A. Amsden, *The TAB Method for Numerical Calculation of Spray Droplet Breakup*. SAE Technical Paper 872089, 1987.
65. Ricart, L.M., R.D. Reitz, and J. Deck, *Comparisons of Diesel Spray Liquid Penetration and Vapor Fuel Distribution With In-Cylinder Optical Measurements*. Transactions of the ASME, 2000. **122**: p. 588-595.
66. Weber, J., P. Spiekermann, and N. Peters, *Model Calibration for Spray Penetration and Mixture Formation in a High Pressure Fuel Spray Using a Micro-Genetic Algorithm and Optical Data*. SAE Technical Paper 2005-01-2099, 2005.
67. Reitz, R.D., *Modeling Atomization Processes in High-Pressure Vaporizing Sprays*. Atomization and Spray Technology, 1987. **3**.
68. Park, S.H., et al., *A study on the fuel injection and atomization characteristics of soybean oil methyl ester (SME)*. International Journal of Heat and Fluid Flow, 2009. **30**: p. 108-116.
69. Schmidt, D.P. and C.J. Rutland, *A New Droplet Collision Algorithm*. Journal of Computational Physics, 2000. **164**.

70. Park, J.S., et al., *Visualization and Measurement of a Narrow-Cone DI Gasoline Spray for the Impingement Analysis*. International Journal of Automotive Technology, 2004. **5**: p. 221-238.
71. Otsu, N., *A Threshold Selection Method from Gray Level Histograms*. IEEE Transactions of Systems Management and Cybernetics, 1979. **9**: p. 62-69.
72. Richards, K.J., P.K. Senecal, and E. Pomraning, *CONVERGE™ (Version 1.3)*2008, Middleton, WI: Convergent Science, Inc.
73. Liu, A.B., D.K. Mather, and R.D. Reitz, *Modeling the Effects of Drop Drag and Breakup on Fuel Sprays*. SAE Technical Paper 930072, 1993.
74. Reitz, R.D. and F.V. Bracco, *Mechanisms of Breakup of Round Liquid Jets*. Encyclopedia of Fluid Mechanics 1986, Houston, TX: Gulf Pub.
75. Han, Z. and R.D. Reitz, *Turbulence Modeling of Internal Combustion Engines Using RNG $k-\epsilon$ Models*. Combust. Sci. and Tech, 1995. **106**.
76. National Institute of Standard and Technology (NIST). 2011; Available from: <http://webbook.nist.gov>.

ABSTRACT**SPRAY CHARACTERIZATION OF FLEX-FUEL GASOLINE DI INJECTORS
AND SPRAY INTERACTION WITH CHARGE MOTION
IN A VARIABLE VALVE ACTUATION ENGINE**

by

ATSUSHI MATSUMOTO**May 2012****Advisor:** Dr. Ming-Chia Lai**Major:** Mechanical Engineering**Degree:** Doctor of Philosophy

The objective of this study is to understand the characteristics of GDI sprays and behavior of in-cylinder charge motion in a GDI engine which is equipped with variable valve actuation. High speed spray visualization in a spray chamber was conducted for a study of spray development. By Schlieren visualization technique, the effect of different conditions including ambient conditions (temperature, pressure) and injection conditions (fuel type, fuel temperature, nozzle design) on spray formation was discussed in both qualitative and quantitative methods. High-speed visualization of the in-cylinder charge motion was carried out as well using an optical accessible engine. The testing was conducted for the conventional valve strategy with the production cam, and for the advanced valve strategies with the prototype cams. Multi-dimensional CFD was carried out to support the optical engine work.

By the experiments, Schlieren visualization was found to be very effective method to observe the vapor phase of the fuel spray, and the 2-stage thresholding image processing method was developed to process Schlieren images. Evaluation of the spray images revealed that the effect of flash boiling could change the spray shape

drastically by plume collapse. Significance of flash boiling depended not only on ambient condition, but on injection condition and a combination of other effects including fuel properties and nozzle design. The optical engine testing revealed that the interaction of spray and in-cylinder flow, especially contradiction of the direction of spray momentum and tumble rotation, was a key factor for mixture formation. Stronger inlet air flow by low-lift cam resulted in higher turbulent energy and enhanced vaporization rate which was proven in both experiment and simulation. Deactivation of one of the intake valves produced swirl charge motion in the cylinder which was mixed with tumble. Soot emission caused by piston impingement of the early injection could be reduced by valve deactivation. The use of high-lift long-duration cam promoted more vigorous charge motion and thus higher turbulence at the end of compression stroke, but dynamic ratios of low-lift short-duration cam developed faster.

AUTOBIOGRAPHICAL STATEMENT

ATSUSHI MATSUMOTO

Atsushi Matsumoto was born in 1982 in Osaka, Japan. He received Bachelor's degree in Mechanical Engineering from Kobe University in 2004. When he was a senior, he joined the Multi-phase Flow Lab and worked for his thesis entitled "Visualization and Measurement of Two-phase Flow in a Rod Bundle using Neutron Radiography". In 2005, he enrolled the College of Engineering of Wayne State University (WSU) as a Master's student. After his achievement of Master's degree in 2006, he continued his research at WSU as a Ph.D. student. His research interests are gasoline/diesel injector analysis, and in-cylinder charge and combustion diagnostics.

Major Publications:

- Interactions of Multi-hole DI Gasoline Sprays with Charge Motion and their Implications to Flexible Valve-trained Engine Performance. *JSAE Paper 20119344*, September 2011
- Spray Characterization of Ethanol Gasoline Blends and Comparison to a CFD Model for a Gasoline Direct Injector. *SAE International Journal of Engines August 2010*, 3:402-425
- Direct Injection Multi-hole Spray and Mixing Characterization of Ethanol Gasoline Blends in Engine. *ILASS Americas, 22nd Annual Conference on Liquid Atomization and Spray Systems, Cincinnati, OH, May 2010*
- Characterization of Diesel Common Rail Spray Behavior for Single- and Double-hole Nozzles. *SAE International Journal of Engines April 2009*, 1:1144-1156